

Julius-Maximilians Universität Würzburg



**Generierung und Charakterisierung von
Stromal Interaction Molecule 2 (STIM2)-
defizienten Mäusen**

**Generation and Characterization of Stromal
Interaction Molecule 2 (STIM2)-deficient Mice**

Doctoral thesis for a doctoral degree at the Graduate
School of Life Sciences, Section Biomedicine

submitted by

Alejandro Berna Erro

from

Alicante, Spain

Würzburg, 2009

Submitted on:

Office stamp

Members of the *Promotionskomitee*:

Chairperson: Prof. Dr. Thomas Hünig

Primary Supervisor: Prof. Dr. Bernhard Nieswandt

Supervisor (Second): Prof. Dr. Thomas Dandekar

Supervisor (Third): Prof. Dr. Ulrich Walter

Date of Public Defence:

Date of Receipt of Certificates:

PERSONAL DEDICATION

The fact that I am here writing this thesis is the result of a great effort done by other people, long time ago, that has nothing to be with research. I would like to dedicate this work to them:

To my most beloved people:

My parents Rafael Berna and Juana Maria Erro. They emigrated to France and learned what is working hard. They worked in the mountains under the stars, in the forests and agriculture fields. They have glamorized many dirty floors and offices. They faced many barriers and many different works to seek for a prosper times. They helped and they have been helped many times by nice people. They transmitted me their life values.

I would like to include my parents as the additional formal authors of this thesis, doctors honoris causa of the other life sciences.

My sister Ana Cristina and her little family: Because is MY sister and a very nice person, what else I could say. Also to her daughters, my couple little nieces Claudia and Abril, that will become great persons in the future, for pride of my sister.

I would like to dedicate my thesis to all members of my broad family for been such nice persons, specially my beloved grandmother Carmen.

I also would like to mention a very important person, my teacher in "La Colonia Santa Isabel" school, Don José for his excellent didactic skills and for his enthusiasm to Natural Sciences, which we share. I want to express him my grateful for listen to me, culture my curiosity for the nature and for his effort preventing that it do not die.

El hecho de que esté aquí escribiendo la tesis es el resultado de un gran esfuerzo hecho, hace tiempo, por otras personas que no tienen nada que ver con la investigación. Quiero dedicar este trabajo:

A la gente que más quiero:

Mis padres Rafael Berna y Juana María Erro. Migraron a Francia y aprendieron lo que es trabajar duro. Trabajaron en las montañas bajo las estrellas, en los bosques y en los campos de cultivo. Embellecieron muchos suelos y oficinas. Afrontaron mucha barreras y trabajos en busca de tiempos más prósperos. Han ayudado y han sido ayudados muchas veces por buenas gentes. Ellos me transmitieron sus valores.

Quiero incluir a mis padres como adicional autores formales de esta tesis, "doctores honoris causa" de las otras ciencias de la vida.

Mi hermana Ana Cristina y su pequeña familia. Porque es MY hermana y es una buena persona, que más podría decir. También quiero dedicar mi tesis a sus

hijas, mi parejita de sobrinas Claudia y Abril, que se convertirá en grandes personas en el futuro para orgullo de mi hermana.

Quisiera dedicar mi tesis doctoral a todos los miembros de mi extensa familia por ser así de buenas personas, especialmente a mi querida abuela Carmen.

También me gustaría dedicar mi tesis doctoral y mencionar a una persona muy importante, mi profesor de E.G.B. en La Colonia Santa Isabel Don José, por su excelente didáctica y por su entusiasmo por las ciencias naturales, el cual compartimos. Me gustará expresarle mi gratitud por escucharme, cultivar mi curiosidad por la naturaleza y no dejar que se perdiera.

Die Tatsache, dass ich hier meine Dissertation schreiben konnte, habe ich der großen Mühe vieler Menschen, die nichts mit Forschung zu tun haben, zu verdanken.

Ich möchte folgenden Personen meine Arbeit widmen:

Meinen Eltern, Rafael Berna und Juana María Erro. Sie wanderten nach Frankreich aus und lernten dort, was harte Arbeit bedeutet. Sie arbeiteten auf den Bergen unter den Sternen, in den Wäldern und auf den Feldern. Sie brachten viele Böden und Büros in einen schöneren Zustand. Sie überwandten viele Hindernisse und übten viele Jobs auf der Suche nach glücklicheren Zeiten aus. Sie halfen vielen und ihnen wurde von vielen großzügigen Menschen geholfen. Sie übertrugen mir ihre Werte. Ich möchte meine Eltern als weitere förmliche Autoren meiner Arbeit einschließen, Ehrendoktoren anderer Wissenschaften des Lebens.

Meiner Schwester Ana Cristina und ihrer kleinen Familie, weil sie MEINE Schwester und ein sehr guter Mensch ist. Außerdem möchte ich diese Arbeit ihren Töchtern widmen, meinen Nichten Claudia und Abril, die zu großartigen Menschen werden werden und auf die meine Schwester sehr stolz sein kann.

Ich möchte meiner Arbeit allen Mitgliedern meiner grosse Familie widmen, weil sie alle freundliche und gute Menschen sind.

Auch möchte ich meine Doktorarbeit einem weiteren wichtigen Menschen widmen, den ich hier auch erwähnen möchte: Meinem E. G. B. Lehrer, Don José, in La Colonia Santa Isabel-Schule für seine hervorragende Didaktik und seinen Enthusiasmus für die Naturwissenschaften, den ich mit ihm ebenso teile. Ich möchte ihm hiermit meine Dankbarkeit dafür äußern, dass er mir zuhörte, meine Neugier für die Natur weckte, die noch immer ungebrochen ist.

1.	SUMMARY (Zusammenfassung)	7
1.1.	English	7
1.2.	Deutsch	8
1.3.	Abbreviations	10
2.	INTRODUCTION	14
2.1.	Ca²⁺ signaling in eukaryotic cells	16
2.1.1.	IP ₃ dependent signaling	17
2.1.2.	Intracellular Ca ²⁺ stores and stored Ca ²⁺ release	18
2.1.3.	Store-Operated-Ca ²⁺ (SOC) channels	19
2.2.	Stromal Interaction Molecule 2 (STIM2)	21
2.2.1.	Domain architecture	22
2.2.1.1.	EF-hand-SAM region	23
2.2.1.2.	C-terminal region	24
2.2.2.	STIM2 function	24
2.3.	Platelets	25
2.3.1.	Platelet activation pathways	26
2.3.2.	Platelet activation and Ca ²⁺ homeostasis	28
2.4.	Lymphocytes T, mast cells, macrophages and Ca²⁺ signaling	31
2.4.1.	T cell activation pathways and Ca ²⁺ signaling	32
2.4.2.	Mast cell activation pathways and Ca ²⁺ signaling	33
2.4.3.	Macrophage activation pathways and Ca ²⁺ signaling	35
2.4.4.	Ca ²⁺ -dependent effector signaling in cells of the immune system	36
2.5.	Neurons and Ca²⁺ signaling	36
2.6.	Aim of the work	38

3.	MATERIALS	39
3.1.	Reagents	39
1.1.1.	Chemicals	39
1.1.2.	Buffers	41
1.1.3.	Plasmids	44
1.1.4.	Bacteria	44
1.1.5.	Oligonucleotides	44
3.1.1.	Antibodies	45
4.	METHODS	47
4.1.	Western blot	47
4.2.	Knockout mice generation	47
4.2.1.	Isolation of BAC clones containing the <i>Stim2</i> gene	48
4.2.2.	Isolation of plasmid DNA from BAC clones	48
4.2.3.	Isolation of DNA from agarose gels	48
4.2.4.	Colony hybridization	48
4.2.5.	Isolation of plasmid DNA from competent bacteria	49
4.2.6.	Long term PCR amplification	49
4.2.7.	Culture of embryonic stem (ES) cells	49
4.2.8.	DNA electroporation in ES cells	49
4.2.9.	Positive selection of electroporated ES cells	50
4.2.10.	Freezing ES clones	50
4.2.11.	ES cell genotyping	50
4.3.	Bone marrow mice generation	50
4.4.	Mouse DNA isolation	51
4.5.	Mouse genotyping	51
4.5.1.	PCR genotyping	51
4.5.2.	Southern blot	51
4.6.	Histology	52
4.7.	Blood analysis	52
4.8.	Platelet analysis	53

4.8.1.	Platelet isolation	53
4.8.2.	Platelet counting	53
4.8.3.	Flow cytometry	53
4.8.4.	Platelet life span experiments	54
4.8.5.	Intracellular Ca ²⁺ measurements	54
4.8.6.	Aggregometry experiments	55
4.8.7.	Tyrosine phosphorylation assay	55
4.8.8.	Flow chamber assay	56
4.8.9.	Spreading assay	56
4.8.10.	<i>In vivo</i> experiments	56
4.8.10.1.	Tail bleeding time experiments	56
4.8.10.2.	Intravital microscopy of thrombus formation in FeCl ₃ injured mesenteric arterioles	57
4.9.	Isolation and analysis of cells of the immune system	57
4.9.1.	Isolation of cells of the immune system	57
4.9.2.	Cellularity assessment in primary and secondary lymphoid organs	58
4.9.3.	Intracellular Ca ²⁺ measurements in cells of the immune system	58
4.9.4.	<i>In vivo</i> anaphylaxia experiments	59
4.9.5.	Induction of Immune thrombocytopenia purpura (ITP) in mice	59
4.9.6.	Flow cytometry in cells of the immune system	59
4.9.7.	Antibody isotype titer determination in mouse serum	60
4.9.8.	Keyhole limpet hemocyanin (KLH) immunizations	60
4.9.9.	Induction and evaluation of experimental autoimmune encephalomyelitis (EAE)	60
4.9.10.	Immunohistochemistry	61
4.10.	Isolation and analysis of neuronal tissue	61
4.10.1.	Isolation and culture of neurons	61
4.10.2.	Brain slice preparation and culture	62

4.10.3.	Immunocyto- and immunohistochemistry in neurons	63
4.10.4.	Ca ²⁺ imaging	63
4.10.5.	tMCAO model	64
4.10.6.	Stroke assessment by MRI	64
4.11.	Statistical analysis	65
5.	RESULTS	66
5.1.	STIM2 is expressed in most organs in mouse and is the main isoform in brain	66
5.2.	<i>Stim2</i> gene isolation and generation of a <i>Stim2</i> knockout mouse	67
5.3.	<i>Stim2</i> ^{-/-} mice are viable and fertile, but adults die spontaneously	69
5.4.	<i>Stim2</i> ^{-/-} females are not able to feed their offspring	73
5.5.	Analysis of STIM2-deficient platelets	77
5.5.1.	STIM2-deficient platelets are normal in number, size and surface glycoprotein expression and display a normal life span <i>in vivo</i>	77
5.5.2.	Unaltered Ca ²⁺ homeostasis in STIM2-deficient platelets	79
5.5.3.	Normal function of <i>Stim2</i> -deficient platelets <i>in vitro</i>	80
5.5.4.	Tyrosine phosphorylation assay	84
5.5.5.	Normal spreading and thrombus formation of <i>Stim2</i> ^{-/-} platelets <i>ex vivo</i>	85
5.5.6.	Normal function of <i>Stim2</i> ^{-/-} platelets in murine <i>in vivo</i> models	86
5.6.	Analysis of STIM2 deficiency in immune cells	88
5.6.1.	The effect of STIM2 deletion on the innate immune system: Mast cells	88
5.6.1.1.	<i>Stim2</i> deletion does not alter Ca ²⁺ homeostasis and SOCE in mast cells	88

5.6.1.2.	<i>Stim2</i> ^{-/-} mice are protected against IgE-mediated anaphylaxis independently of mast cells	90
5.6.2.	The effect of STIM2 deletion on the innate immune system: Macrophages	92
5.6.2.1.	Stim2 deletion does not alter Ca ²⁺ homeostasis and SOCE in macrophages	92
5.6.2.2.	Upregulated FcγR expression in <i>Stim2</i> ^{-/-} macrophages	94
5.6.2.3.	<i>Stim2</i> ^{-/-} mice are protected in experimental thrombocytopenia and anaphylaxis	95
5.6.3.	Effect of STIM2 deletion on the adaptive immune system: T and B cells	97
5.6.3.1.	Decreased SOCE in STIM2-deficient T cells	97
5.6.3.2.	STIM2 deficiency does not alter CD3 and T cell receptor (TCR) expression in lymphocytes and splenocytes	99
5.6.3.3.	Normal cellularity and decreased CD8 ⁺ cells in primary and secondary lymphoid organs	100
5.6.3.4.	Normal T cell proliferation in naive and normal immune response in Keyhole limpet hemocyanin (KLH)-immunized <i>Stim2</i> ^{-/-} mice	103
5.6.3.5.	Experimental autoimmune encephalomyelitis (EAE) is significantly ameliorated in STIM2-deficient mice	105
5.7.	Analysis of STIM2 deficiency in neurons	106
5.7.1.	STIM2 regulates SOCE and ischemia-induced Ca ²⁺ accumulation in neurons	106
5.7.2.	STIM2-defective neurons are protected from ischemia	109
5.7.3.	<i>Stim2</i> ^{-/-} mice are protected from ischemic stroke	112
6.	DISCUSSION	115
6.1.	General description of the STIM2-deficient mouse	115
6.2.	Analysis of STIM2-deficient platelets	118
6.3.	Analysis of STIM2 deficiency in immune cells	120

6.3.1.	The effect of STIM2 deletion on the innate immune system: Mast cells	120
6.3.2.	The effect of STIM2 deletion on the innate immune system: Macrophages	121
6.3.3.	Effect of STIM2 deletion on the adaptive immune system: T and B cells	122
6.4.	Analysis of STIM2 deficiency in neurons	125
7.	REFERENCES	128
8.	ACKNOWLEDGEMENTS	142
9.	CURRICULUM VITAE	143
10.	LIST OF PUBLICATIONS	144
	AFFIDAVIT (Eidesstattliche Erklärung)	145

1. SUMMARY (Zusammenfassung)

1.1. English

An increase in cytosolic Ca^{2+} levels ($[\text{Ca}^{2+}]_i$) is a key event that occurs downstream of many signaling cascades in response to an external stimulus and regulates a wide range of cellular processes, including platelet activation. Eukaryotic cells increase their basal $[\text{Ca}^{2+}]_i$ allowing extracellular Ca^{2+} influx into the cell, which involves different mechanisms. *Store-operated Ca^{2+} entry* (SOCE) is considered the main mechanism of extracellular Ca^{2+} influx in electrically non-excitabile cells and platelets, and comprises an initial Ca^{2+} depletion from intracellular Ca^{2+} stores prior to activation of extracellular Ca^{2+} influx. Although the close relation between Ca^{2+} release from intracellular stores and extracellular Ca^{2+} influx was clear, the nature of the signal that linked both events remained elusive until 2005, when Stromal Interaction Molecule 1 (STIM1) was identified as an endoplasmic reticulum (ER) Ca^{2+} sensor essential for inositol (1,4,5)-trisphosphate (IP_3)-mediated SOCE *in vitro*. However, the function of its homologue STIM2 in Ca^{2+} homeostasis was in general unknown. Therefore, mice lacking STIM2 (*Stim2*^{-/-}) were generated in this work to study initially STIM2 function in platelets and in cells of the immune system. *Stim2*^{-/-} mice developed normally in size and weight to adulthood and were fertile. However, for unknown reasons, they started to die spontaneously at the age of 8 weeks. Unexpectedly, *Stim2*^{-/-} mice did not show relevant differences in platelets, revealing that STIM2 function is not essential in these cells. However, STIM2 seems to be involved in mammary gland development during pregnancy and is essential for mammary gland function during lactation. CD4^+ T cells lacking STIM2 showed decreased SOCE. Our data suggest that STIM2 has a very specific function in the immune system and is involved in Experimental Autoimmune Encephalomyelitis (EAE) at early stages of the disease progression. *Stim2*^{-/-} neurons were also defective in SOCE. Surprisingly, our results evidenced that STIM2 participates in mechanisms of neuronal damage after ischemic events in brain. This is the first time that the involvement of SOCE in ischemic neuronal damage has been reported. This finding may serve as a basis for the development of novel neuroprotective agents for the treatment of ischemic stroke, and possibly other neurodegenerative disorders in which disturbances in cellular Ca^{2+} homeostasis are considered a major pathophysiological component.

1.1. Deutsch

Der Anstieg des cytosolischen Ca^{2+} -Spiegels ($[\text{Ca}^{2+}]_i$) ist ein Schlüsselereignis, das vielen Signalkaskaden, durch extrazellulären Stimulus ausgelöst werden, nachgeschaltet ist, und eine große Reihe zellulärer Prozesse reguliert, z.B. die Aktivierung von Blutplättchen. Eukaryotische Zellen erhöhen ihren basalen ($[\text{Ca}^{2+}]_i$) durch Einstrom von extrazellulärem Ca^{2+} in die Zelle hinein, was durch verschiedene Mechanismen geschehen kann. Store-operated Ca^{2+} -entry (SOCE), wird als der Hauptmechanismus für den Einstrom von extrazellulärem Ca^{2+} in nicht elektrisch-erregbaren Zellen sowie Plättchen angesehen und beinhaltet einen initialen Ca^{2+} -Ausstrom aus intrazellulären Speichern der dem Ca^{2+} -Einstrom aus der Extrazellulärraum vorrausgeht. Obwohl die Beziehung zwischen Ca^{2+} -Ausstrom aus intrazellulären Speichern und extrazellulärem Ca^{2+} -Einstrom über die Plasmamembran viele Jahre bekannt war, so blieb doch das beide Ereignisse verknüpfende Element unbekannt. Im Jahre 2005 jedoch wurde Stromal Interaction Molecule 1 (STIM1) als Ca^{2+} -Sensor des endoplasmatischen Retikulums (ER) und als essentieller Bestandteil für inositol(1,4,5)-triphosphat (IP_3)-vermittelten SOCE *in vitro* identifiziert. Die Funktion seines Homologs, STIM2, in der Ca^{2+} Homeostase blieb jedoch unklar. Aus diesem Grund generierten wir STIM2-defiziente (*Stim2*^{-/-}) Mäuse um die Funktion dieses Proteins in Blutplättchen und Immunzellen untersuchen zu können. Bis zum Erwachsenenalter entwickelten sich *Stim2*^{-/-} Mäuse normal in Bezug auf Größe und Gewicht und waren fertil. Jedoch sterben die Tiere spontan aus unbekanntem Gründen, beginnend ab einem Alter von 8 Wochen. Unerwarteter Weise, zeigten *Stim2*^{-/-} Mäuse keine maßgeblichen Funktionsunterschiede in Plättchen, was eine essentielle Funktion von STIM2 in diesen Zellen ausschließt. Jedoch scheint STIM2 in die Entwicklung der Brustdrüsen während der Schwangerschaft involviert und essentiell für die Brustdrüsenfunktion während der Säugephase zu sein. Darüberhinaus zeigten STIM2 defiziente CD4^+ T-Zellen einen verminderten SOCE. Weiter deuten unsere Daten auf eine spezifische Funktion von STIM2 im Immunsystem hin, mit einem Einfluss auf die frühen Phasen und das Fortschreiten der Experimentellen Autoimmun-Enzephalomyelitis (EAE).

Stim2^{-/-} Neuronen wiesen ebenso wie CD4^+ T-Zellen einen gestörten SOCE auf. Desweiteren belegen unsere Ergebnisse, dass STIM2 überrascherweise an den Neuronen zerstörenden Mechanismen nach ischämischen Ereignissen des Gehirns mitwirkt. Dies ist die erste Studie, die von einer Beteiligung von SOCE

an ischämischen neuronalen Schäden berichtet. Diese Entdeckungen können vielleicht als Basis für die Entwicklung neuer neuroprotektiver Medikamente bei ischämischen Schlaganfall dienen - und möglicherweise auch bei anderen neurodegenerativen Erkrankungen, bei denen Störungen der zellulären Ca^{2+} Homöostase als hauptsächliche pathophysiologische Komponente angesehen werden.

1.2. Abbreviations

α AR	alpha-adrenoreceptor
β -TG	beta-thromboglobulin
$[Ca^{2+}]$	Ca^{2+} concentration
$[Ca^{2+}]_i$	cytosolic concentration of Ca^{2+}
$[Ca^{2+}]_o$	extracellular Ca^{2+} concentration
8-pCPT-cGMP	8-(4-Chlorophenylthio)-guanosine 3',5'-cyclic monophosphate
aa _s	amino acid residues
AC	adenylyl cyclase
ADP	adenosine diphosphate
APC	antigen presenting cells
ATP	adenosine triphosphate
BMMC	bone marrow derived Mast Cells
BSA	bovine serum albumin
Ca^{2+}	calcium
CaM	calmodulin
CaMK	Ca^{2+} - calmodulin-dependent kinase
CaMKI-IV	Ca^{2+} - calmodulin-dependent kinase I-IV
CCCP	carbonyl cyanide m-chlorophenylhydrazone
CCE	capacitive Ca^{2+} entry
CLEC-2	C-type lectin-like receptor-2
CNS	central nervous system
CPA	cyclopiazonic acid
c.p.m.	counts per minute
CRAC	Ca^{2+} release-activated Ca^{2+} channels
CRACM	Ca^{2+} release-activated Ca^{2+} modulator
CREB	cyclic- AMP-responsive-element-binding protein
CRP	collagen related peptide
CVX	convulxin
DAG	diacylglycerol
DIV	days <i>in vitro</i>

DNP-HSA	2,4-Dinitrophenyl hapten conjugated to human serum albumin
DREAM	Ca ²⁺ -binding downstream regulatory element modulator
D-Stim	drosophila melanogaster STIM
DTS	dense tubular system
EAE	experimental autoimmune encephalomyelitis
ECM	the extracellular matrix
EGFR	epidermal growth factor receptor
eNOS	endothelial nitric oxide synthase
ER	endoplasmic reticulum
ERM	ezrin/radixin/moesin domain
Fc γ Rs	IgG Fc gamma receptors
Fc ϵ Rs	IgE Fc etha receptors
GPCRs	G-protein coupled receptors
H&E	haematoxylin and eosin staining
i.p.	intraperitoneal injection
i.v.	intravenous injection
I _{CRAC}	Ca ²⁺ release-activated Ca ²⁺ current
Ig	antibody, immunoglobulin
iNOS	inducible nitric oxide synthase
IP ₃	inositol-1,4,5-triphosphate
IP ₃ Rs	inositol (1,4,5)-trisphosphate receptors
IRAG	Ins(1,4,5)P ₃ -receptor-associated cGMP kinase substrate
ITAM	immunoreceptor tyrosine-based activation motif
ITK	interleukin-2-inducible T-cell kinase
ITP	Immune thrombocytopenia purpura
KLH	keyhole limpet hemocyanin
LAT	linker of activated T cells
LPA	lysophosphatidic acid
LPS	E.Coli Lipolysaccharide
MCA	middle cerebral artery
MD-2	myeloid differentiation protein-2
MEF2	myocyte enhancer factor 2

MHC	histocompatibility complex proteins
MLC	myosin light chains
MRI	serial magnetic resonance imaging
MS	multiple sclerosis
NAADP	nicotinic acid adenine dinucleotide phosphate
NCXs, Na ⁺ /Ca ²⁺ exchangers	plasma membrane Ca ²⁺ transporters
NFATs	nuclear factor of activated T cells
NF κ B	nuclear factor kappa B
nNOS	neuronal nitric oxide synthase
NO	Nitric Oxide
NOS	Nitric oxide synthase
Orai	Orai Ca ²⁺ release-activated Ca ²⁺ modulator
PACAP	pituitary adenylate cyclase-activating polypeptide
PDGF	platelet derived growth factor
PDGFR	platelet-derived growth factor receptor
PF4	platelet factor 4
PGI ₂	Prostaglandin I ₂ (Prostacyclin)
PKA	protein kinase A
PKC	protein kinase C
PKG	protein kinase G
PLC	phospholipase C
PLC β	phospholipase C beta
PLC γ	phospholipase C gamma
PMC	peritoneal mast cells
PMCAs	plasma membrane Ca ²⁺ ATPases
PRL	prolactin
prp	platelet rich plasma
RhoGAP	Rho GTPase-activating protein
ROCs	receptor-operated Ca ²⁺ channels
RT	room temperature
RTKs	receptor tyrosine kinases
RyRs	ryanodine receptors
SAM	sterile α -motif
SCID	severe combined immune deficiency syndrome

s.d.	standard deviation
SEM	standard error of the mean
SERCAs	sarcoplasmic / endoplasmic reticulum Ca ²⁺ ATPases
sGC	guanylyl cyclase
SLP76	SRC-homology-2-domain-containing leukocyte protein of 76 kDa
SNP	sodium nitroprusside
SOC	Store-Operated Ca ²⁺
SOCE	Store-Operated Ca ²⁺ Entry
STIM1	Stromal Interaction Molecule 1
<i>Stim2</i> ^{+/+} BM ^{-/-}	chimera wild-type mice transplanted with <i>Stim2</i> ^{-/-} bone marrow
<i>Stim2</i> ^{-/-} BM ^{+/+}	chimera <i>Stim2</i> knockout mice transplanted with wild-type bone marrow
TCR	T cell receptor
TCR, BCR	T-cell and B-cell antigen receptors
TG	thapsigargin
TGII	tissue transglutaminase II
TLR4	Toll-like receptor 4
tMCAO	transient middle cerebral artery occlusion
TP α	thromboxane receptor alpha
TRP	the transient receptor potential channels
TRPC	the canonical TRP
TTC	2,3,5-triphenyltetrazolium chloride
TxA ₂	thromboxane A2
VOCs	voltage-operated Ca ²⁺ channels
vWF	von Willebrand factor

2. INTRODUCTION

Calcium (Ca^{2+}) is an ubiquitous second messenger that regulates basic cellular functions such as gene expression, contraction, secretion, cell migration cell death and more specialized functions like communication between neurons.

In electrically non-excitable cells, Ca^{2+} entry is mainly regulated by channels located in the plasma membrane, referred to as store-operated Ca^{2+} (SOC) channels because they are activated (operated) by a previous emptying of intracellular Ca^{2+} stores. The subsequent Ca^{2+} influx into the cells is called store-operated Ca^{2+} entry (SOCE) and the electrophysiological characteristics of this Ca^{2+} influx were studied in 1992 and termed Ca^{2+} release-activated Ca^{2+} current (I_{CRAC}) [1].

Despite intense research, the nature of the signal that triggers the activation of SOC channels after store depletion, as well as the molecular identity of the Ca^{2+} sensor within the stores, remained elusive until 2005, when the Stromal Interaction Molecule 1 (STIM1) was identified as a endoplasmic reticulum (ER) Ca^{2+} sensor essential for inositol (1,4,5)-trisphosphate receptors (IP_3Rs)-mediated SOCE *in vitro* [2-4]. Recently, it has also been demonstrated *in vivo*. The lack of STIM1-function in lymphocytes and in platelets results in severe impairment of IP_3Rs -mediated SOCE [5-7]. Later, it was demonstrated that STIM1 interacts functionally with the SOC channel Orai1 *in vitro*, indicating that STIM1 triggers SOCE mainly by STIM1-Orai1 interaction [8]. In 2005 STIM2 was also proposed to be involved in IP_3Rs -mediated signaling [2], but its function is still under discussion. *In vitro* experimental data indicates that STIM2 is also able to interact with Orai channels, but contrary to STIM1, downregulation or overexpression of STIM2 produced none or very weak effect on SOCE [2,9]. However, reports published in the last two years supported the emerging idea that STIM2 mainly regulates the cytoplasmic [Ca^{2+}] ($[\text{Ca}^{2+}]_i$) and ER [Ca^{2+}], possibly through interaction with Orai1 SOC channels [5,9].

A consensus model to describe STIM function in SOCE has been established (Fig. 1); the activation of G-protein coupled receptors (GPCRs) or ITAM-containing receptors (ITAM, immunoreceptor tyrosine-based activation motif) located in the plasma membrane leads to activation of inositol-1,4,5-trisphosphate (IP_3)-dependent pathways that results in Ca^{2+} release from the ER store. The depletion of the Ca^{2+} stored in the ER is detected by STIM isoforms, since Ca^{2+} is dissociated from STIMs, and induces conformational changes that switch the proteins to the activated state. STIM1 oligomerize and migrates to the plasma membrane forming small clusters (punctae) and triggers SOCE by

Orai1 channel interaction. STIM2 is more sensitive than STIM1 to small decreases in ER $[Ca^{2+}]$ and regulates the basal $[Ca^{2+}]_i$ and the ER $[Ca^{2+}]$, probably by Orai channel interactions [9]. In both cases, it is believed that SOCE mainly leads to refilling of the ER Ca^{2+} stores [10].

Despite the major progress made in understanding SOCE during these three years, still more work has to be done to fully uncover the role of STIM and SOCE at a cellular level. The present model and the main players will be described in more detail in the next sections of the introduction.

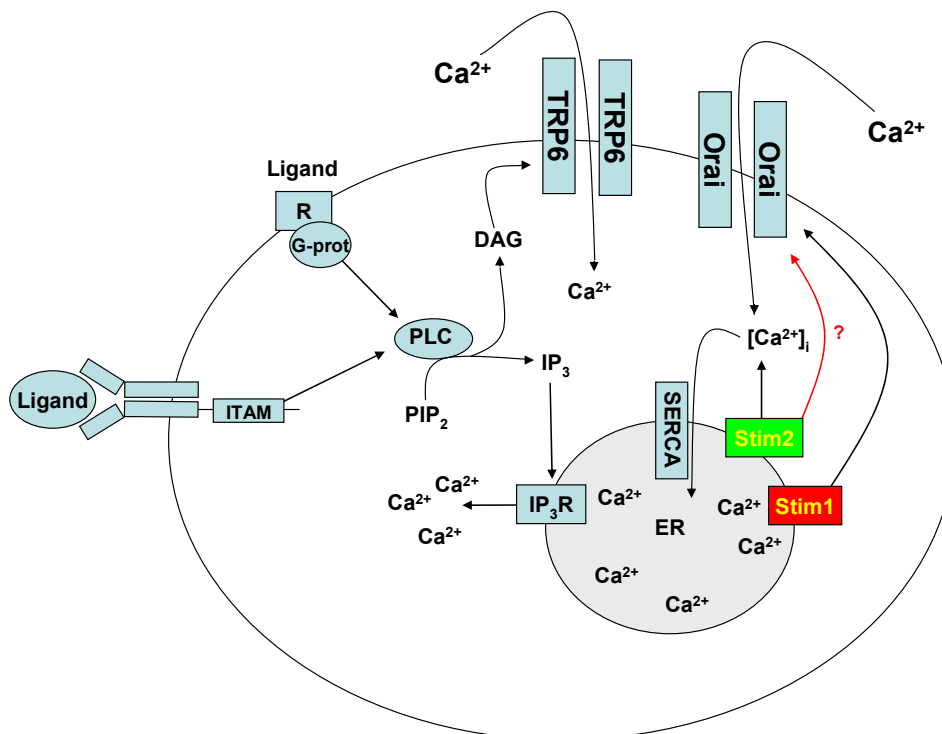


Figure 1. The SOCE model. Ligand-receptor interaction leads to PLC activation by G-protein-coupled receptors (G-Prot, R) or ITAM-containing receptors located in the plasma membrane, which in turn hydrolyzes phosphatidylinositolbisphosphate (PIP₂) into inositol 1,4,5-trisphosphate (IP₃) and diacylglycerol (DAG). DAG can directly activate Ca²⁺ channels located in the plasma membrane, for instance Transient Receptor Potential (TRP) channels. The increase of IP₃ in the cytoplasm results in Ca²⁺ release from the endoplasmic reticulum (ER) Ca²⁺ stores by activation of IP₃ receptors (IP₃R) located in the ER membrane. The subsequent depletion of ER Ca²⁺ stores is detected by STIM isoforms and they become activated. STIM1 migrates to the plasma membrane and triggers store-operated Ca²⁺ entry (SOCE) by Orai1 channel interaction. Instead, STIM2 is more sensitive than STIM1 to small decreases and mainly regulates the basal $[Ca^{2+}]_i$ and ER $[Ca^{2+}]$, probably by Orai channel interaction. Modified from Dr. Attila Braun original picture.

2.1. Ca²⁺ signaling in eukaryotic cells

Second messengers (cAMP, cGMP, IP₃ and Ca²⁺) are essential intracellular mediators of important basic functions in the cell. These small molecules are generated or released into the cytosol in response to an extracellular signal. An increase in [Ca²⁺]_i is a key event, used as an essential signal that regulates a wide range of basic cellular processes involving gene expression, enzyme control, exocytosis, adhesion, proliferation, and cell death [11]. This increase is generally produced at localized areas in the cell, generating intracellular microdomains of elevated [Ca²⁺]_i that show distinct spatial and temporal patterns [12]. In unstimulated cells, the basal [Ca²⁺]_i is tightly regulated to keep it constant at a concentration approximately 10,000-fold below the extracellular Ca²⁺ concentration ([Ca²⁺]_o, 1-3 mM), process that is vital for sustaining the life of the organism [11]. A combined action of molecules that acts as buffers, pumps and exchangers controls at any moment in time the [Ca²⁺]_i, introducing additional Ca²⁺ into the cytoplasm or removing this Ca²⁺ signal from the cytoplasm. These molecules form a heterogeneous group located in the plasma membrane and in membranes of the diverse organelles such as mitochondria, ER and Golgi apparatus, which act as intracellular Ca²⁺ stores. The active molecules that maintain [Ca²⁺]_i in human cells are four different plasma membrane pump isoforms (PMCA, plasma membrane Ca²⁺ ATPases) [13,14], three plasma membrane Ca²⁺ transporters (NCXs, Na⁺/Ca²⁺ exchangers) [15] as well as three different ER Ca²⁺ pump isoforms (SERCA, sarcoplasmic / endoplasmic reticulum Ca²⁺ ATPases) [16].

SERCA pumps are key proteins for empirical study of intracellular Ca²⁺ release signaling. They continuously pump Ca²⁺ from the cytoplasm into the ER, maintaining the steady-state of [Ca²⁺] within the lumen of the stores and compensating the continuous Ca²⁺ leak through the plasma membrane. It is possible to deplete the ER Ca²⁺ store by passive release to the cytoplasm using a selective inhibitor of SERCA called thapsigargin (TG). This drug has been extensively used as a pharmacological tool as it selectively activates mechanisms dependent on the release of the intracellularly stored Ca²⁺ and minimizes the roles of other upstream players in the pathway (receptors, G-proteins, phospholipase C, etc).

2.1.1. IP₃ dependent signaling

In response to a stimulus, eukaryotic cells can increase their basal $[Ca^{2+}]_i$ in two related ways: by release of Ca^{2+} from intracellular stores or allowing extracellular Ca^{2+} influx into the cell. In electrically non-excitabile cells, these events are consecutive; Ca^{2+} signaling is initiated upon the activation of phospholipase C (PLC) signaling pathways by GPCRs or ITAM-containing receptors located in the plasma membrane. Activated PLC hydrolyzes phosphatidylinositolbisphosphate (PIP₂) into IP₃ and diacylglycerol (DAG). It has been reported that DAG and some of its metabolites can induce non-store operated Ca^{2+} entry (non-SOCE) [17]. IP₃ triggers the release of Ca^{2+} from the IP₃-sensitive intracellular Ca^{2+} stores, causing a transient increase in $[Ca^{2+}]_i$. This is rapidly followed by a sustained extracellular Ca^{2+} influx and a longer increase in $[Ca^{2+}]_i$. This extracellular Ca^{2+} influx is referred to as “capacitive Ca^{2+} entry” (CCE), also referred to as SOCE (Fig. 2).

To date, thirteen mammalian PLC isozymes classified in six different subtypes have been identified in various tissues and cell types PLC(β1-4), PLC(γ1,2), PLC(δ1,3,4), PLCε, PLCζ, PLC(η1,2), showing different molecular masses, isoelectric points and Ca^{2+} dependency (for review see [18]). Additionally, alternative splice variants have been reported in several PLC isozymes, for instance in rat PLCβ1, human PLCβ2, rat PLCβ4, rat PLCδ4, and human PLCε. PLCs (but PLCζ, expressed only in testis) are widely expressed at different levels in all tissues, showing preferences for different organs. For instance, PLCγ1 mRNA is expressed mainly in brain, while PLCγ2 is expressed in the hematopoietic lineage.

PLCs are regulated by different stimuli and signaling pathways in the cytoplasm. PLCβ isoforms are activated by Gα and Gβ/γ -protein subunits coupled to receptors belonging to the rhodopsin superfamily of transmembrane proteins. PLCγ1 is activated in response to polypeptide growth factors that bind to receptor tyrosine kinases (RTKs) such as the epidermal growth factor receptor (EGFR) and platelet-derived growth factor receptor (PDGFR). PLCγs can also be activated downstream of a variety of receptors that lack intrinsic tyrosine kinase activity, including GPCRs, such as the angiotensin II and bradykinin receptors, cytokine receptors. Also immunoreceptors such as the T cell receptor (TCR) for PLCγ1, immunoglobulin and adhesion receptors on immune cells such as B cells, platelets and mast cells in the case of PLCγ2 (for review see [18]). PLCδs are among the most sensitive isozymes to Ca^{2+} , suggesting a role

of $[Ca^{2+}]_i$ in PLC δ regulation. Interestingly, the Rho GTPase-activating protein (RhoGAP) was also reported to bind and activate PLC δ 1 directly, inducing cytoskeleton reorganization. Various ligands can lead to activation of PLC ϵ , including several agonists of GPCRs such as thrombin, adrenaline, PGE $_1$, lysophosphatidic acid (LPA) and S1P. Finally, recent results suggested that PLC η isozymes are activated through GPCR stimulation with LPA or the pituitary adenylate cyclase-activating polypeptide (PACAP) in Neuro2A cells (for review see [18]).

2.1.2. Intracellular Ca^{2+} stores and stored Ca^{2+} release

Ca^{2+} release from intracellular stores plays a pivotal role in the modulation of intracellular Ca^{2+} signals [11]. Several cellular organelles have been identified as agonist-releasable Ca^{2+} pools. Among them, the ER (the sarcoplasmic reticulum in muscle cells) is considered as the major source of inducible Ca^{2+} release in cellular signaling. The estimated free Ca^{2+} content in the ER store in eukaryotes is ~0.2–2 mM, very close to extracellular conditions (1-3 mM) [19,20]. The other organelles that serve as sources of Ca^{2+} includes the nuclear envelope (which regulates gene transcription according to the pattern of Ca^{2+}), lysosome-related organelles (nicotinic acid adenine dinucleotide phosphate - NAADP-sensitive Ca^{2+} stores), the Golgi apparatus, the mitochondria and secretory granules (see for review [21]). They are essential for many cellular functions, for instance to contribute to the regulation of basal $[Ca^{2+}]_i$, trigger apoptosis and SOCE. The release of Ca^{2+} from the ER to the cytoplasm is mediated by two types of Ca^{2+} channels located in the ER membrane, the IP $_3$ R and ryanodine receptors (RyRs). Researchers mainly focused on the IP $_3$ R signaling predominantly because IP $_3$ R is the major Ca^{2+} channel in the ER which depletes the Ca^{2+} store after its activation by IP $_3$ in electrically non-excitable and excitable cells. Numerous regulatory proteins, including cytochrome c, huntingtin, IP $_3$ R-binding protein released with inositol 1,4,5-trisphosphate (IRBIT), ERp44, Homer, 4.1N, and neuronal Ca^{2+} sensor 1 (NCS-1), have been reported to interact with the IP $_3$ R isoforms, modifying their properties [22].

Till date, three isoforms of the IP $_3$ R have been found in mammals, known as type I, IP $_3$ R type II, and IP $_3$ R type III. Additional splice forms of type I and type II receptors have been found [23]. Despite the 65 % homology in their protein sequence, they have different properties, for instance, differences in the

magnitude of their response and ligand-binding affinity for IP₃ (K_d values of ~1, ~2, and ~40 nM, respectively). Therefore selective expression of a particular receptor type would influence the sensitivity of cellular Ca²⁺ stores to IP₃ [24]. Type I receptors are widely expressed in virtually all tissues and cell types, but predominantly in cerebellum, lung and heart. Type II receptors are also found in brain and lung and additionally present in placenta and thymocytes. Finally, type III receptors are mainly expressed in the gastrointestinal tract [23]. The IP₃R channel is actually a tetramer and, considering that different isoforms can be present in the same cell, there is evidence that they are able to form heterotetramers [22]. At cellular level, IP₃Rs have been found in ER, sarcoplasmic reticulum, nuclear envelope, Golgi apparatus and secretory vesicles [21,22].

Continuing with the Ca²⁺ mobilisation in non-excitable cells, the depletion of ER Ca²⁺ store leads to activation of particular Ca²⁺ channels located in the plasma membrane, the so-called SOC (CRAC) channels, allowing extracellular Ca²⁺ influx into the cell and SOCE [11,25].

2.1.3. Store-Operated- Ca²⁺ (SOC) channels

Cells can increase [Ca²⁺]_i up to 10-fold by opening Ca²⁺ channels in the plasma membrane that trigger an influx of extracellular Ca²⁺. Those Ca²⁺ channels can be divided into three main groups depending on the mechanism that activates them: (1) channels activated by changes on membrane voltage (VOCs, voltage-operated Ca²⁺ channels); (2) channels activated by receptor-ligand binding (ROC, receptor-operated Ca²⁺ channels); and (3) channels activated by previous depletion of intracellular Ca²⁺ stores (SOCs, store-operated Ca²⁺ channels) [26]. SOC channels are the main regulators of extracellular Ca²⁺ entry in electrically non-excitable cells, mechanism referred to as SOCE. These channels are a heterogeneous group of non-selective Ca²⁺-permeable channels with different biophysical properties. Till date, the most relevant SOC channels are members of the Orai and TRP family [27,28].

The Orai family, also named as CRACM (for Ca²⁺ release-activated Ca²⁺ modulator), comprises three homologues in humans: Orai1, Orai2 and Orai3, and they are considered subunits that homo- or heteromultimerize forming a tetrameric SOC channel [29-31]. These tetrameric SOC channels show different properties depending on which Orai isoforms are integrated in their structure [31-33]. Orai1 is a relatively small (301 amino acid) protein with four predicted transmembrane domains and cytosolic N- and C-terminal tails [34], and it has

been shown to be the most important isoform since an *Orai1* mutant gene was identified as the responsible component of a hereditary severe combined immune deficiency (SCID) syndrome in humans [34]. The expression of the wild-type *Orai1* in such a mutant T cells restored SOCE [34]. In addition to the three *Orai* homologues, two spliced variants of *Orai2*, *Orai2* short (*Orai2S*) and *Orai2* long (*Orai2L*) have been described in mice. *Orai2S* plays a negative dominant role in the formation of Ca^{2+} channels when co-expressed with *Orai1* [35]. Very recently, *Orai1* has been shown to be essential for SOCE also in mice [36-38].

The next relevant SOC channels are the mammalian homologues of the transient receptor potential (TRP) family, classified into three closely related subfamilies (TRPC, TRPV and TRPM), and two additional distantly related subfamilies (TRPP and TRPML). There is considerable evidence supporting a role for some members of the canonical TRP (TRPC) subfamily in SOCE. This subfamily involves seven related members (TRPC1-7) [27]. Using different approaches, such as overexpression of specific TRPC proteins, *in vitro* knockdown or *in vivo* knockout of endogenous TRPC and pharmacological studies, it was possible to determine that several TRPC proteins can be activated by depletion of intracellular Ca^{2+} stores, being potential SOC channel candidates [27].

In addition to TRPC channels, other members of the TRP family have been suggested to be potential mediators of SOCE, for instance TRPV6 (CaT1) [39,40].

Interestingly, experiments using the *in vivo* knockout approach in mouse strongly suggested that the importance of the different SOC channels in SOCE could be highly dependent on the tissue or cell type. For instance, TRPC1 deletion in mice has very few or no significant effect on platelets, while *Orai1* deletion dramatically reduces SOCE, indicating *Orai1* as the main SOC channel in platelets [36,41]. However, an 80 % loss of SOCE has been found in submaxillary acinar cells of TRPC1 knockout mice [42].

Finally, recent studies also suggested that *Orai* and TRPC isoforms may interact directly or indirectly forming heteromeric complexes in order to regulate SOCE [43]. Thus, the role of *Orai* and TRPC in SOCE appears to be complex and the underlying mechanisms are not well understood.

2.2. Stromal Interaction Molecule 2 (STIM2)

In 2001, *STIM2* was identified as a new human homologue of the *STIM1* gene, representing the second member of a two-gene family in vertebrates [44]. The *Stim2* gene contains 12 exons and 11 introns located on the human chromosome 4p15.1, and on the large arm of the mouse chromosome 5, close to the centromere.

The members of STIM family most probably have evolved from a single gene in lower multicellular eukaryotes into two related genes in vertebrates, since human *STIM1* and *STIM2* as well as *Drosophila melanogaster Stim (D-Stim)* have a conserved genomic organization. The D-STIM protein of 570 aa_s exhibits equal similarity to both *STIM1* (33 % identical; 50 % of amino acid sequence conserved) and *STIM2* (31 % identical; 46 % of amino acid sequence conserved). No *STIM*-like genes have been identified in prokaryotes or unicellular eukaryotes. No additional STIM-like proteins have been identified until now in vertebrates [44].

STIM2 protein is a type I transmembrane protein located in the ER. Human *STIM2* consists of 833 amino acid residues (aa_s) (105-115 kDa) (Fig. 2), 148 additional aa_s when compared to human *STIM1*. Their N-terminal regions share 66 % similarity over 577 aa_s (85 % of the amino acid sequence of *STIM1*). Only the extreme of the C-terminal region shows a significant sequence divergence. The domain architecture of both isoforms is highly conserved in vertebrates (Fig. 2).

Mouse *STIM2* shares a 92 % identity with human *STIM2* in the amino acid sequence according to the pairwise alignment generated by BLAST (<http://blast.ncbi.nlm.nih.gov/>). Their domain structure is also highly conserved (Fig. 2).

Human *STIM2* is post-translationally modified *in vivo*, such as maturation by cleavage of N-terminal ER signaling peptide (14 aa_s), glycosylation and variable degrees of phosphorylation, but the phosphorylated sites are still unknown (Fig. 2) [44].

STIM2 mRNA is expressed by most human tissues. The *STIM2* protein is expressed by many human cell lines together with *STIM1*, indicating that *STIM* isoforms are co-expressed in the same cell, at least in the established cell lines [44].

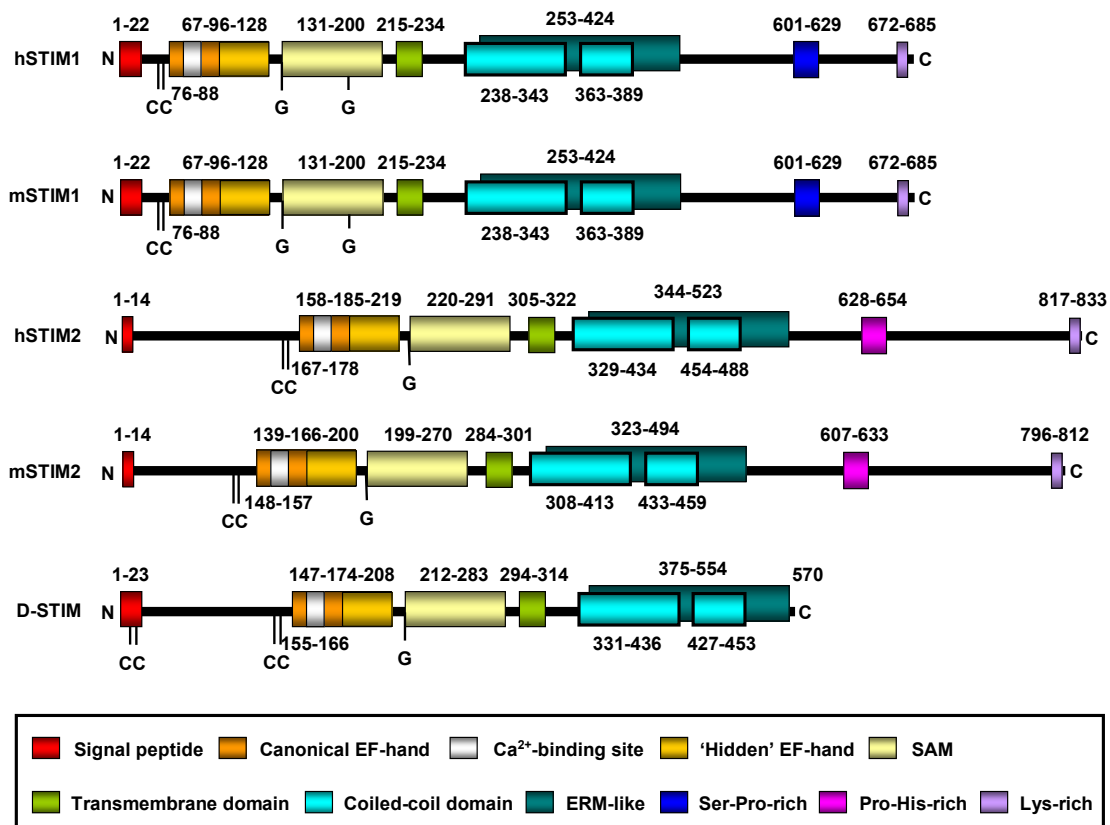


Figure 2. STIM protein family. Representation of domain organization of the STIM family in human (hSTIM), mouse (mSTIM) and drosophila (D-STIM). N and C represent the amino- and the carboxyl-terminus, respectively. Colour boxes represent the different domains. Numbers above and below the domains indicate their boundaries and the amino acid position. (CC) pair of highly conserved cysteines. (G) glycosylation sites. Boundaries of EF-hand and SAM motifs in hSTIM were biophysically characterized by [45-47], while transmembrane, coiled-coil and Ser/Pro/His/lys regions were predicted by computer models and protein sequence alignment. Boundaries of mSTIM and D-STIM were predicted by computer models and protein sequence alignment.

2.2.1. Domain architecture

The N-terminal region of STIM2 is located in the ER lumen and contains a canonical EF-hand Ca²⁺-binding motif, a “hidden” EF-hand Ca²⁺-binding motif discovered recently and a sterile α -motif (SAM) domain, a well-known protein-protein interaction motif (Fig. 2) [48-50].

The N-terminal portion is separated from the C-terminal region by a single-pass transmembrane motif that is highly conserved in all STIM proteins. The C-terminal region contains a high degree of α -helical structures. A large proportion close to the transmembrane domain comprises a region similar to an ezrin/radixin/moesin (ERM) domain that contains two coiled-coil domains (for

review see [51]). The coiled-coil domains mediate interactions between STIM proteins, allowing them to bind each other and form homo and heterodimers (Fig. 2) [52-54].

Finally, further towards the C-terminus, STIM2 contains a proline/histidine-rich motif and a lysine-rich tail of 17 aa_s (Fig. 2) [44].

2.2.1.1. EF-hand-SAM region

Since the EF-hand and SAM (EF-SAM) domains are vital to STIM function and SOCE regulation, they are now discussed in detail. The EF-hand domain is a Ca²⁺ sensor used by STIM protein to detect changes in Ca²⁺ concentration inside the ER. STIM isoforms become activated when Ca²⁺ bound to the EF-hand motif is released as a result of a decrease in Ca²⁺ levels inside the ER store after IP₃Rs-mediated depletion. It has been reported that STIM EF-hand mutants that are not able to bind Ca²⁺ are constitutively active and continually activate SOCE independently of ER [Ca²⁺], *in vitro* [2,32,55] and *in vivo* [56].

The SAM domain is important for STIM oligomerization, since mutants in this domain lack the ability to form inducible punctae [57].

Ca²⁺-binding experiments *in vitro* using human STIM1 EF-SAM (residue 58–201) or STIM2 EF-SAM (residue 149–292) fragments show that both isoforms bind Ca²⁺ with similar affinity (STIM2 K_d~0.5 mM; STIM1 K_d~0.2–0.6 mM) [45,58], which is within the range of values reported for ER [Ca²⁺] [19,20]. However, STIM2 differs from STIM1 in that it is already partially active at basal ER [Ca²⁺] and becomes fully activated earlier during ER store depletion. Despite the same Ca²⁺ affinity shown by STIM EF-SAM fragments, the full STIM2 protein showed a lower [Ca²⁺] sensitivity than STIM1 in transfected cells *in vitro* [9]. This discrepancy indicates that other protein regions in addition contribute to the different [Ca²⁺] sensitivity or activation threshold shown by both isoforms.

The “hidden” EF-hand domain does not bind Ca²⁺, but it is critical for intramolecular association, folding and stability of the EF-hand and SAM domains. Very recently it has been reported that structurally critical mutations in the canonical EF-hand, “hidden” EF-hand, or SAM domain disrupt Ca²⁺ sensitivity due to the destabilization of the entire EF-SAM region [46].

2.2.1.2. C-terminal region

Besides the N-terminus, the C-terminal region is also an essential part of STIM proteins. It shows a significant sequence divergence between both isoforms and in STIM1, the C-terminal region is essential for the interaction with SOC channels [59]. Human STIM2 contains a proline- and histidine-rich motif (PHAPHPSHPRHPHPHQHTPHSLPSPDP) at a similar position to a serine- and proline-rich region (SPSAPPGGSPHLDSSRSHSPSSPDPDTPSP) in STIM1. The significant divergence in these regions could indicate a divergence in function of STIM isoforms. Finally, similar lysine-rich tails of 14 and 17 residues in STIM1 and STIM2 respectively are located at the very end of the C-terminal region.

Linear peptides from C-terminal polybasic region of human STIM1 (residues 667-685) and STIM2 (residues 730-746) bind to calmodulin with high or low affinity in presence or absence of Ca^{2+} , respectively [60]. Most of studies on interactions of the C-terminal region have been performed with the STIM1 isoform. The addition of TG (the SERCA pump inhibitor that stimulates SOCE by passive depletion of intracellular Ca^{2+} stores) to human salivary gland cells as well as dispersed mouse submandibular gland cells increase coimmunoprecipitation of TRPC1 and Orai1 with STIM1 [61].

By *in vitro* co-expression of different human STIM1 mutants that lack the different C-terminal regions in HEK293 cells, three recent works reported that the ERM domain in the C-terminus (aa_s 251-535, Fig. 2), containing the coiled-coil domains, mediates the binding of STIM1 to TRPC(1, 2,4 and 5) and the STIM1 migration to the plasma membrane.

Furthermore, the cationic lysine-rich region is essential for gating of TRPC1 [54,59,62]. Li *et al.* further delineated these regions (aa_s 425-672) as possible STIM1-Orai1 interaction sites [54]. Interestingly, *in vitro* coimmunoprecipitation experiments after transient coexpression of STIM2 and Orai1 proteins in HEK293 cells revealed that also STIM2 can physically interact with Orai1, probably through the STIM2 C-terminal region [63].

2.2.2. STIM2 function

The STIM2 function has been controversial and still is under discussion. First studies found that iRNA knockdown of STIM1, but not STIM2, strongly reduced SOCE in mammalian cells [2-4,9,64]. Liou *et al.* reported a slight reduction in SOCE also by knockdown of STIM2 in HeLa cells [2]. Soboloff *et al.* suggested

that STIM2 inhibits SOCE when expressed alone [53], but coexpressed with Orai1 causes substantial constitutive SOCE [65]. In contrast, Brandman *et al.* suggested that STIM2 could act as a regulator that stabilizes basal $[Ca^{2+}]_i$ and ER Ca^{2+} levels [9]. Parvez *et al.*, using *in vitro* transient coexpression of human STIM2 and different SOC channels in HEK293 cells, reported that STIM2 is able to interact with Orai (1,2 and 3) channels and mediates SOCE via two store-dependent and store independent modes [63]. Therefore, further studies are necessary in order to understand STIM2 function in the cell.

2.3. Platelets

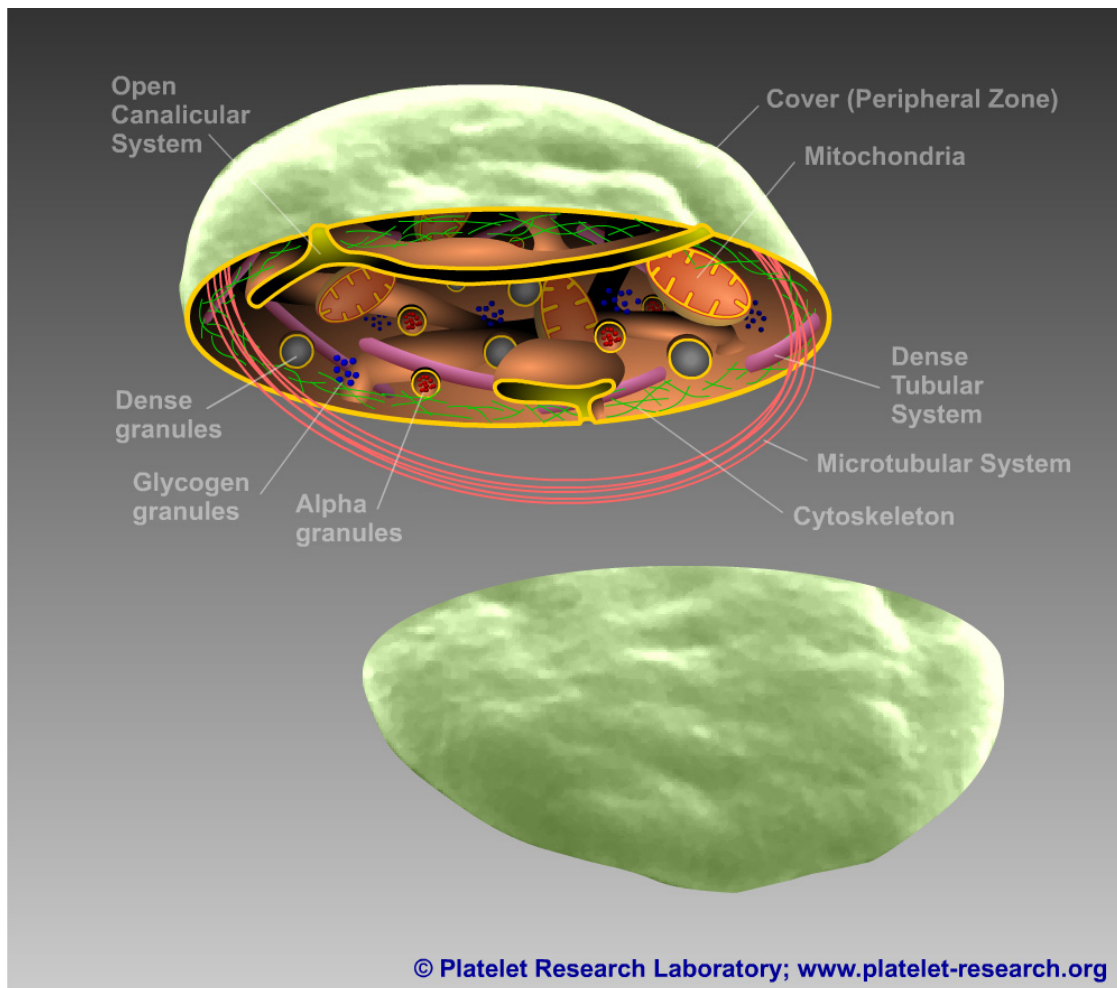


Figure 3. Platelet structure (kindly donated by Dr. Ginés Escolar, Platelet Research Laboratory, Hospital Clínic, Barcelona: <http://www.platelet-research.org/1/intro.htm>).

Platelets are 2 μm diameter discoid cell fragments derived from the cortical cytoplasm of the megakaryocytes located in the bone marrow and are only present in mammals. Their physiological number in blood varies from 1.5×10^5

to 3×10^5 platelets per μl in humans, and 1×10^6 platelets per μl in mice. Their life span is only 10 days, before they are cleared from the blood stream by macrophages in liver and spleen. They play an important role in hemostasis, thrombosis, and several other biological processes. Platelets are anucleated but still conserve a cytoskeleton and intracellular organelles such as mitochondria, glycogen granules, storage granules (α -granules and dense granules), lysosomes, and peroxisomes (Fig. 3). The α -granules contain proteins such as platelet factor 4 (PF4), β -thromboglobulin (β -TG), platelet derived growth factor (PDGF), fibrinogen, thrombospondin, plasminogen activator inhibitor I, von Willebrand factor (VWF), P-selectin and glycoprotein (GP) IIb/IIIa ($\alpha\text{IIb}\beta\text{3}$) [66]. Dense granules contain Ca^{2+} , adenosine triphosphate (ATP), adenosine diphosphate (ADP), pyrophosphate, serotonin and histamine [66,67]. Upon platelet activation, the contents of platelet granules are secreted, further promoting both platelet adhesion and activation. The plasma membrane extends into the cytoplasm forming a complex canalicular system into the cell [68].

Under normal conditions, resting platelets circulate close to the endothelial wall of the blood vessel. As a response to vascular injury and subsequent exposure to subendothelial extracellular matrix (ECM) platelets rapidly become activated, adhere to ECM and to each other to form a platelet plug, which allows the reestablishment of normal blood flow and avoids blood's leakage in the disrupted blood vessels (Fig. 4) [69]. Upon platelet activation, platelets change shape to a spherical structure and extend long pseudopods, a process driven by cytoskeleton rearrangement, and the contents of platelet granules are secreted, further promoting both platelet adhesion and activation (Fig. 4).

Although murine platelets differ from human platelets in numbers, size, and structure, functionally they are very similar and murine transgenic models have been shown to be very useful to study platelet physiology [70,71].

2.3.1. Platelet activation pathways

Activation of platelets is a complex process that includes stimulation of plasma membrane receptors, reorganization of the cytoskeleton involved in shape change and relocation of intracellular secretory granules, secretion of substances and secondary autocrine and paracrine activators that further activates receptors in the plasma membrane. Upon injury of the blood vessel, the first step of platelet activation is triggered by adhesion to subendothelial matrix proteins such as collagens, laminins, fibronectin or vWF (Fig. 4).

Additionally, other soluble agonist circulating in the blood such as thromboxane A_2 (TxA_2) and ADP released from activated platelets, and thrombin generated by the coagulation cascade can trigger platelet activation [69].

The mechanisms of platelet adhesion are determined by the prevailing rheological conditions. Blood flows with a greater velocity in the centre of the vessel than near the wall, thereby generating shear forces between adjacent layers of the fluid that become maximal at the wall. The drag, which opposes platelet adhesion and aggregation, increases with the prevailing shear rates. Under conditions of high shear, such as is found in small arteries and arterioles, this tethering event is mediated by the platelet receptor glycoprotein (GP)Ib α β -IX-V receptor complex via VWF bound to collagen. However, this interaction is not relevant under conditions of low shear found in veins and large arteries. The GPIb α -VWF interaction is insufficient to mediate stable adhesion, presenting a fast association and dissociation, allowing platelets to slow down and move in close contact with the vessel wall on the site of vascular injury, a process also known as “rolling” [72,73]. During this phase, platelets establish contacts with its two main collagen receptors: GPVI and integrin $\alpha 2\beta 1$ [73]. GPVI binds collagen with low affinity, therefore is unable to mediate adhesion by itself, but triggers an inside-out activation of integrin $\alpha IIb\beta 3$ and $\alpha 2\beta 1$ that change from a low- to high-affinity binding state [73,74] and induce the release of the second wave mediators TxA_2 , ADP and epinephrine. These agonists together with locally produced thrombin (a protease which cleaves and activates PAR1 and PAR4 receptors) act synergistically stimulating receptors coupled to heterotrimeric G-proteins (G_q , G_{12}/G_{13} , G_i) [75], which activates different Ca^{2+} -dependent signaling cascades required for full platelet activation (Fig. 4).

Activated $\alpha 2\beta 1$ now binds collagen strongly, and together with other high-affinity $\beta 1$ -integrins which bind to fibronectin ($\alpha 5\beta 1$) and laminin ($\alpha 6\beta 1$) as well as the major platelet integrin $\alpha IIb\beta 3$ which binds with fibronectin and vWF bound to collagen, finally results in stable platelet adhesion. The secretion of the second wave mediators is a self-amplifying process that allows the recruitment of additional platelets for the formation of the growing thrombus, since high concentrations of these soluble agonists may be sufficient to mediate platelet activation independently of GPVI [76]. Platelet-platelet interactions are mainly mediated by the active form of integrin $\alpha IIb\beta 3$ through the plasma protein fibrinogen (Fig. 4). Finally, it has been shown that GPIb α is also important in the recruitment of additional platelets to the growing thrombus [77].

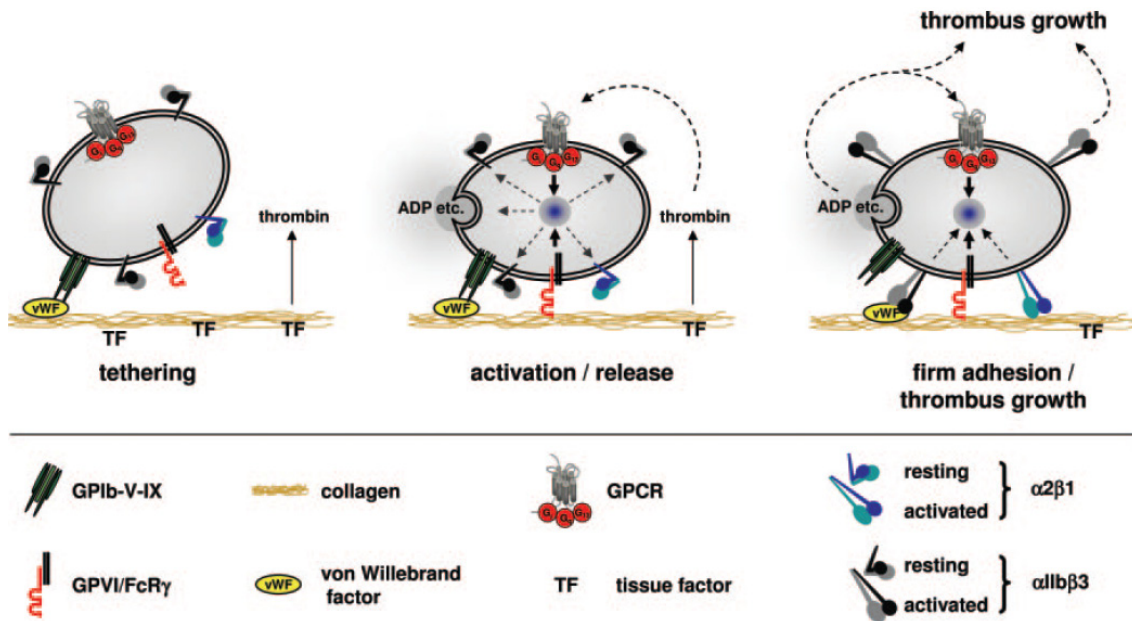


Figure 4. Model for platelet adhesion to the subendothelial matrix at sites of vascular injury. The GPIb–vWF interaction mediates the initial contact (tethering) to the exposed ECM in the vessel wall, essential at high shear rates ($> 500 \text{ sec}^{-1}$). In a second step, GPVI–collagen binding initiate cellular activation followed by shifting of integrins from low- to high-affinity state and the release of second-wave agonists, such as ADP, ATP, and TxA_2 . In parallel, the exposed tissue factor (TF) in the ECM locally triggers the formation of thrombin, which cleaves and activates PAR1 and PAR4 receptors, acting synergistically together with GPVI, and mediates cellular activation and firm adhesion. Finally, the firm adhesion of platelets to collagen through activated $\alpha_2\beta_1$ and $\alpha_{IIb}\beta_3$ results in sustained GPVI signaling and enhanced release of second-wave agonists. Released ADP, ATP, and TxA_2 amplify integrin activation on adherent platelets, allowing the recruitment of additional platelets for the formation of the growing thrombus. Platelet-platelet interactions are mainly mediated by the active form of integrin $\alpha_{IIb}\beta_3$ through the plasma protein fibrinogen. Picture source: [69].

2.3.2. Platelet activation and Ca^{2+} homeostasis

A central event in the platelet activation is an increase in the intracellular Ca^{2+} concentration (Fig. 5). Although different agonists trigger different signaling pathways, most activate PLC isoforms, leading to production of DAG and IP_3 , following a classical activation cascade (described in section 2.1.1) that finally triggers SOCE. IP_3 induces release of Ca^{2+} from the ER, while DAG is involved in Ca^{2+} entry from the extracellular compartment by activation of non-store-operated Ca^{2+} channels, such as some members of the TRP family [11,78].

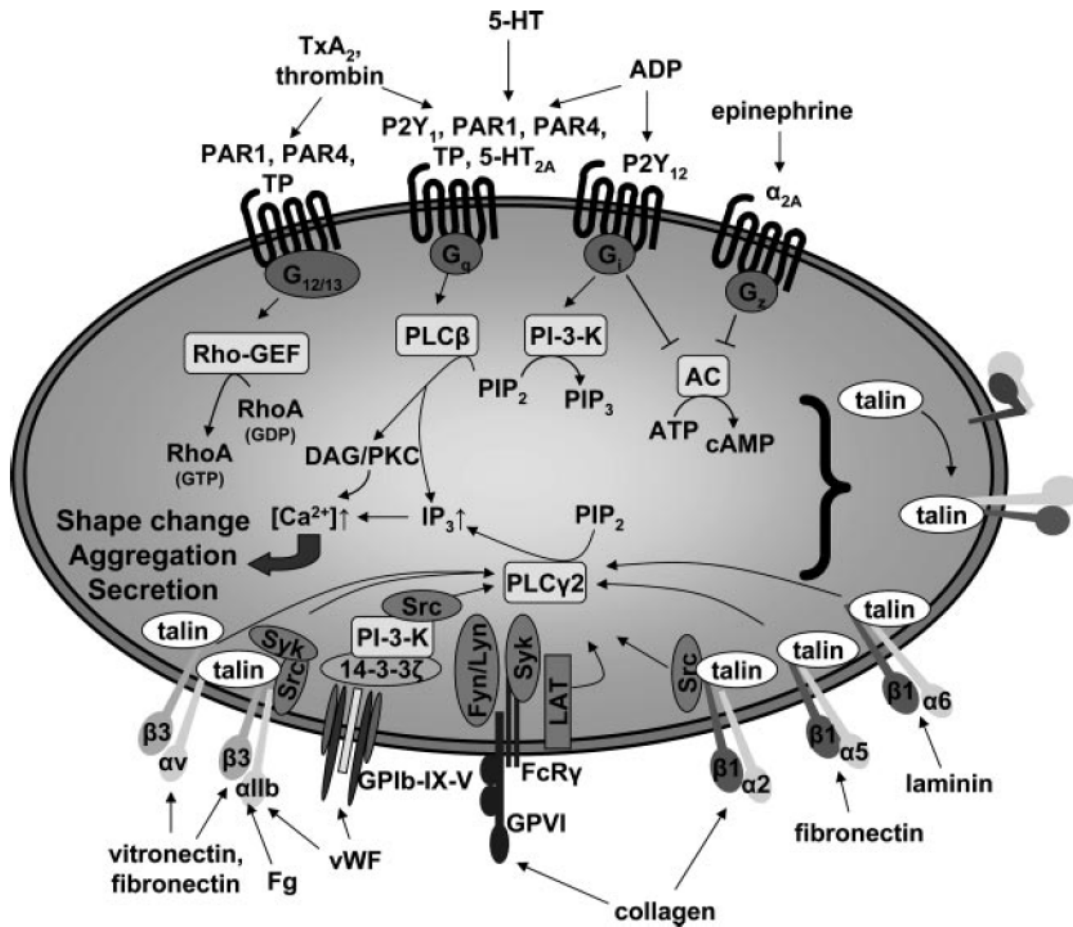


Figure 5. Signaling mechanisms linking platelet receptors to integrin activation. Collagen-GPVI interaction activates the ITAM-signaling pathway, which in turn activates PLC γ isoforms, whereas stimulation of G protein-coupled receptors by thrombin, thromboxane (TxA₂) or ADP triggers pathways involving G_q, G_{i/z}, G_{12/13}, which in turn activate PLC β isoforms, phosphoinositide-3-kinase (PI-3-K), Rho-specific guanine nucleotide exchange factor (Rho-GEF) and inhibits adenylyl cyclase (AC). The diacyl glycerol (DAG) and the inositol-1,4,5-trisphosphate (IP₃) generated by PLC isoforms increases the [Ca²⁺]_i, which leads to aggregation and the secretion of second-wave mediators, while Rho-GEF activates RhoA-dependent pathways that in turn regulates actin cytoskeleton and leads to platelet shape change. Adhesion molecules such as integrins, GPIIb-IX-V complex or GPVI also activates PLC γ isoforms, leading to a further increase of [Ca²⁺]_i. Inhibition of AC activity by ADP and epinephrine receptors avoids activation of cAMP-dependent inhibition pathways. Picture source: David Varga-Szabo *et al.* *Arterioscler. Thromb. Vasc. Biol.* 2008;28;403-412.

In platelets, two subfamilies of the PLC enzymes are expressed, the PLC β (comprising four isoforms, β 1-4) and the PLC γ (comprising two isoforms, γ 1-2). Human platelets express the β 1-3 and the γ 2, whereas mouse platelets express all isoforms. In both, β 3 and γ 2 are the predominant isoforms, together with β 2 in humans and β 1 in mouse platelets [79,80].

The PLC β isoforms are regulated by GPCRs through the α -subunit of the G-protein G $_q$, in response to soluble agonists such as thrombin (PAR1 and PAR4 receptors in humans and PAR3 and PAR4 receptors in mice), ADP (P2Y $_1$), and TXA $_2$ (TP $_{\alpha}$ and TP $_{\beta}$). Additionally, PLC γ 2 can be also regulated by phosphatidylinositol 3-Kinase (PI-3-K), which is activated by the ADP receptor P2Y $_{12}$ (coupled to the G-protein G $_i$) (Fig. 5) [81].

PLC γ 2 is located downstream the signaling cascade similar to that used by immunoreceptors and involves tyrosine phosphorylation cascades downstream of the receptor-associated immunoreceptor tyrosine activation motif (ITAM). This pathway is triggered by activation of the major platelet collagen receptor GPVI, the platelet adhesion complex vWF-GPIb-V-IX and CLEC-2, the receptor for the snake venom toxin rhodocytin (Fig. 5). The PLC γ 2 isoform is also regulated by the Fc γ receptor IIA (Fc γ RIIA) in human platelets [73,82-85].

Activation of GPVI leads to tyrosine phosphorylation of the ITAM located in the FcR γ -chain by the Src kinases Fyn and Lyn. This leads to phosphorylation and subsequent activation of the SH2 domain-containing tyrosine kinase (Syk), which phosphorylates the adaptor molecule “linker for activation of T cells” (LAT), which in turn recruits additional adaptor molecules such as SRC-homology-2-domain-containing leukocyte protein of 76 kDa (SLP76) and effector enzymes including PLC γ 2, finally leading to Ca $^{2+}$ -mobilization [73].

There are evidences that the signaling pathway downstream CLEC-2 and the vWF-GPIb-V-IX complex might be similar to GPVI signaling, but how the molecules exactly co-operate in both pathways is not clear. The main players also include the non-receptor tyrosine kinases Src, Fyn, Lyn and Syk, adapter proteins such as LAT and SLP-76 and the effector enzyme PLC γ 2 (Fig. 5) [82,83].

The PLC γ 2 isoform is also regulated by integrins such as α IIb β 3 and α 2 β 1, during a series of intracellular events referred to as “outside-in signaling”. This process is activated by ligand-integrin interactions and leads to stable platelet adhesion (for review, see [86]). For instance, upon fibrinogen binding to integrin α IIb β 3, the integrin cytoplasmic tail becomes associated with actin skeleton through interactions with cytoskeletal proteins like talin, vinculin and actinin. Then, a number of signaling molecules are recruited: serine/threonine and tyrosine kinases (PKC, Src, Syk, FAK, PI-3-K), serine threonine and tyrosine phosphatases (PP2A, PTP1B, SHP1) and SHIP among others, which finally leads to PLC γ activation (for review, see [86]).

Concerning to the intracellular structure, platelets show a more specialized intracellular store system than other eukaryotic cells. Two separate Ca $^{2+}$ stores

have been reported in human platelets: the dense tubular system (DTS, the equivalent to the ER in other mammalian cells) and lysosome-like acidic organelles (Fig. 3) (for a review, see [21]). There is consensus that the major intracellular Ca^{2+} pool in platelets is the DTS. The complete identity of the acidic stores has not been clarified yet, several acidic organelles show properties of releasable Ca^{2+} pools, including lysosomes, dense granules, and the Golgi apparatus.

Two of the three IP_3R isoforms have been found in platelets, $\text{IP}_3\text{R1}$ and $\text{IP}_3\text{R2}$. Pharmacological evidence suggested the existence of two distinct Ca^{2+} stores based on their differences in the affinity to IP_3 [87] or their sensitivity to the SERCA inhibitor thapsigargin and to 2,5-di-(t-butyl)-1,4-hydroquinone (TBHQ) [87-89].

The release of Ca^{2+} from the described intracellular stores induces SOCE , basal $[\text{Ca}^{2+}]_i$ rises and activates Ca^{2+} -dependent effector pathways in platelets. For example, the Ca^{2+} -dependent Calmodulin (CaM) activates the myosin light chain kinase (MLCK), which in turn phosphorylates myosin light chains (MLC) inducing actin cytoskeleton remodelling and triggering platelet shape change [86]. Phosphorylation of MLC can be also regulated by the Ca^{2+} -independent Rho/ROCK pathway. This pathway is stimulated by the G_{12} and G_{13} proteins coupled to PAR receptors, which are activated by thrombin and TxA_2 [90,91].

DAG also activates protein kinase C (PKC) involved in the “inside-out” integrin activation and the secretion of granules with contains the second wave mediators.

Studies also identified a Ca^{2+} -sensitive signaling pathway that acts synergistically with PKC in the “inside-out” activation of integrin $\alpha\text{IIb}\beta_3$. The CalDAG-GEFI/Rap1 signaling pathway is regulated by elevations in $[\text{Ca}^{2+}]_i$ and DAG, and has been reported to play an essential role in platelet aggregation and thrombus formation [92,93].

2.4. Lymphocytes T, mast cells, macrophages and Ca^{2+} signaling

In cells of the immune system, including T cells, B cells, mast cells, macrophages and other cell types, Ca^{2+} signals control differentiation, proliferation, apoptosis, and a variety of transcriptional programs, including production of cytokines and chemokines. Most of these events need sustained

Ca^{2+} influx to keep the $[\text{Ca}^{2+}]_i$ higher than basal levels [25,94]. In immune cells, the predominant pathway of Ca^{2+} entry is thought to involve SOCE, a mechanism that was described before in chapter 2.1. CRAC channels (SOC channels in immune cells) such as Orai are expressed in lymphocytes [25]. The existence of patients with severe combined immunodeficiency (SCID) associated with defects in Orai channel function and SOCE highlights the importance of CRAC channels and such a Ca^{2+} influx mechanism in immune response in human [34,95-97].

Other Ca^{2+} channels have been found in lymphocytes, such as P2X receptors, L-type voltage-gated Ca^{2+} channel subunits, TRPV channels, TRPC channels, and some TRPM channels, but their physiological importance in lymphocytes is a hot topic still in discussion [25,98,99].

CRAC channels open in response to activation of immunoreceptors, such as T cell receptor (TCR) in T cells and the Fc receptors (FcR) in mast cell and macrophages, resulting in tyrosine phosphorylation and activation of PLC γ 1 [25,98,100].

2.4.1. T cell activation pathways and Ca^{2+} signaling

Several subsets of T cells have been characterized. The most important are the T helper (T_H or CD4^+) and the T cytotoxic (T_C or CD8^+) cells, each with a distinct function in the adaptive immune system (specific defense to pathogens). CD4^+ cells are involved in activating and directing other immune cells and are very important in the immune system, while CD8^+ cells are capable of inducing the death of infected somatic cells, tumor cells, damaged or dysfunctional cells.

The main activating pathway in T cells involves the T cell receptor ($\alpha\beta\text{TCR}$) complex, which consist in six different transmembrane proteins (Fig. 6). These proteins include the Ag-binding subunits ($\text{TCR}_{\alpha\beta}$) that are non-covalently associated with the signal-transducing chains CD3_{γ} , CD3_{δ} , CD3_{ϵ} , and TCR_{ζ} and/or TCR_{η} [25]. All these signaling chains contain an ITAM sequence. Upon antigen recognition, these molecules associate together forming the TCR-CD3 complex. One of the initial events following TCR-CD3 complex formation is the phosphorylation of tyrosine residues in the ITAM motifs, a process regulated by the Src-family protein tyrosine kinases (PTKs) Lck or Fyn (Fig. 6). This event results in the recruitment and activation of a second family of PTKs, such as LCK and ZAP70, which initiate phosphorylation events of adaptor proteins, such as SLP76 and LAT. This leads to the recruitment and activation of the

interleukin-2-inducible T-cell kinase (ITK), PLC γ 1 and subsequent depletion of the intracellular Ca $^{2+}$ stores and SOCE (for a review, see [101]).

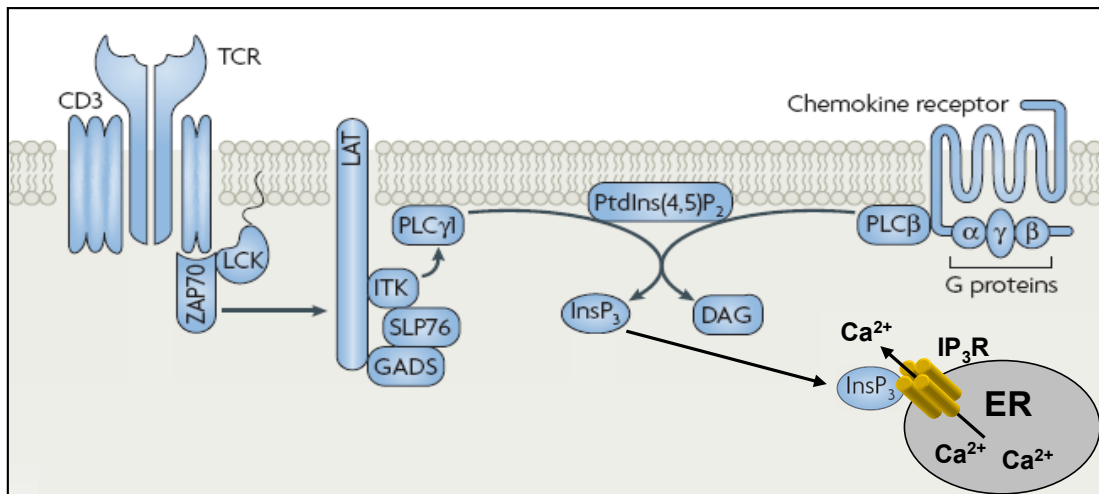


Figure 6. Simplification of the activating signaling cascade in T-cells. Antigen recognition through the TCR results in the activation of protein tyrosine kinases, such as LCK and ZAP70 (ζ -chain-associated protein kinase of 70 kDa), which initiate phosphorylation events of adaptor proteins, such as SLP76 (SRC homology-2-domain-containing leukocyte protein of 76 kDa) and LAT (linker for activation of T cells). This leads to the recruitment and activation of the TEC kinase ITK (interleukin-2-inducible T-cell kinase), the adaptor molecule GADS (GRB2-related adaptor protein) and phospholipase C γ 1 (PLC γ 1). Similarly, binding of G-protein-coupled chemokine receptors results in the activation of PLC β . PLC γ 1 and PLC β catalyse the hydrolysis of the membrane phospholipid phosphatidylinositol-4,5-bisphosphate (PtdIns(4,5)P $_2$) to IP $_3$ (InsP $_3$) and DAG. IP $_3$ binds to and opens IP $_3$ R in the membrane of the ER, resulting in the release of Ca $^{2+}$ from intracellular Ca $^{2+}$ stores. Modification of the original picture: [25].

2.4.2. Mast cell activation pathways and Ca $^{2+}$ signaling

Two subclasses of Fc receptor (Fc ϵ R) for immunoglobulin E (IgE) exist: low affinity receptors (Fc ϵ RII) and high affinity receptors (Fc ϵ RI). In mast cells, the main activating pathways involve the Fc ϵ RI, expressed at the cell surface. Mast cells contribute to host-defense mechanisms that are associated with innate immunity (non-specific defense) and play a central role in allergic inflammatory responses (Fig. 7).

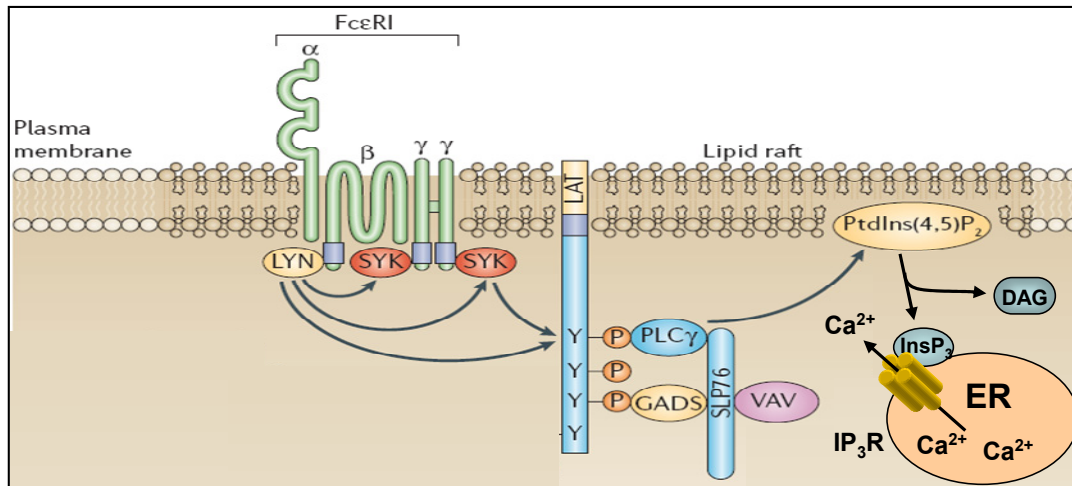


Figure 7. Simplification of the activating signaling cascade in mast cells. In mast cells, following FcεRI aggregation, the adaptor molecule LAT becomes phosphorylated in a LYN- and SYK (spleen tyrosine kinase)-dependent manner. This results in direct or indirect binding of cytosolic adaptor molecules to LAT, for instance GADS (GRB2-related adaptor protein) and SLP76, as well as exchange factors and adaptor molecules such as VAV and the signaling enzyme PLC γ 1. The release of Ca $^{2+}$ from intracellular Ca $^{2+}$ stores follows the activation of PLC γ , which leads to an increase of [Ca $^{2+}$] $_i$. Modification of the original picture: [102].

They are also responsible for the exaggerated reactions to antigen observed in anaphylaxis, atopy, and rhinitis [103]. Although multiple receptors are capable of mediate or modify mast cell activation, the manifestations of mast-cell-driven allergic reactions are considered to be mainly a consequence of the release of potent inflammatory mediators after mast cell activation by the IgE-antigen complex bound to FcεRI. This receptor is a tetramer that comprises an α -chain, a β -chain and two γ -chain (forming a homodimer linked by a disulphide bridge) (for a review, see [102]). The α -chain is responsible for binding IgE, the β -chain and the γ -chain contains one and two ITAM motif respectively, and they are responsible for initiating signaling. FcεRI requires the recruitment and activation of Src family tyrosine kinases and Syk to induce the early receptor-proximal signaling events (Fig. 7). Syk is recruited via ITAM motifs located in the γ -chain-cytoplasmic domains. The resulting phosphorylation of Syk and subsequent activation, leads to the phosphorylation of the transmembrane adapter molecules LAT. Upon phosphorylation, these proteins serve as scaffolds for PLC γ 1 and multimolecular signaling complexes comprising various cytosolic adapter molecules such as Gads, Grb2, SLP76, and SHC as well as GTP exchangers including Sos and Vav1. As a result, PLC γ 1 switches to the active state, giving rise to stored Ca $^{2+}$ depletion and SOCE. Finally, these signals lead to mast cell degranulation and eicosanoid generation and also contribute to

activation of transcription factors required for cytokine and chemokine production (for a review, see [102]).

2.4.3. Macrophage activation pathways and Ca^{2+} signaling

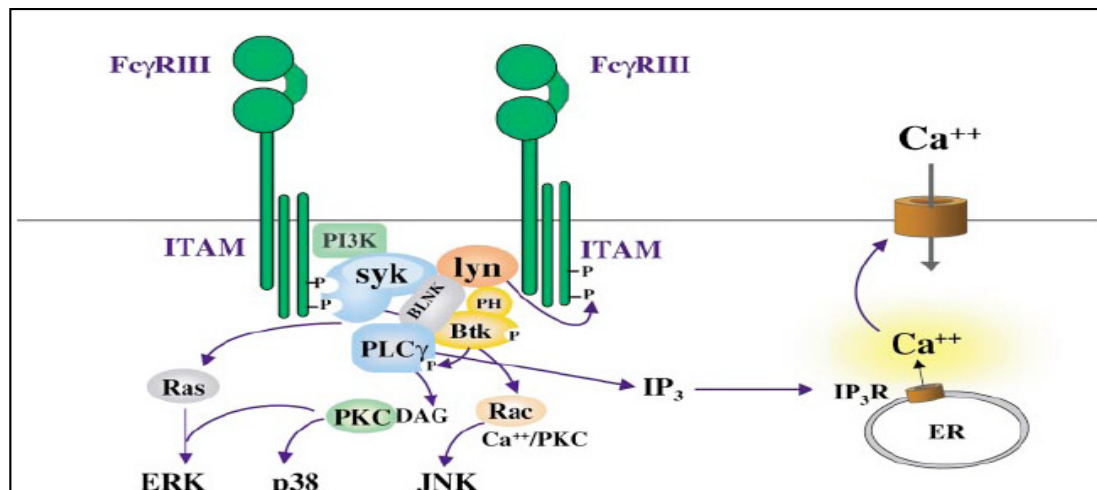


Figure 8. Simplification of the activating signaling cascade in macrophages. Syk kinase is activated after Fc γ R (for instance Fc γ RIII) aggregation and ITAM phosphorylation. Subsequent signaling pathways associated with the activation by Fc γ Rs are similar to that observed for other ITAM-containing receptors such as TCR in T cells. Picture source: [104].

Macrophages are phagocytes derived from activated monocytes that play an important role in innate and adaptive immunity. Their role is to engulf and digest cellular debris and pathogens or act as antigen presenting cells (APC) to stimulate lymphocytes and other immune cells to respond to pathogens. The main activating pathways in macrophages involve the IgG Fc receptors (Fc γ R), expressed at the cell surface. Fc γ Rs belong to the immunoglobulin superfamily and are the most important Fc receptors for inducing phagocytosis of opsonized (IgG-coated) pathogens. They are also expressed in other cells such as mast cells, neutrophils, eosinophils or dendritic cells [104]. In the mouse, there are 3 classes of activating Fc γ R: the high affinity receptor Fc γ RI, the low-affinity receptor Fc γ RIII, and the recently described Fc γ RIV [127]. All of these Fc γ Rs form heterooligomeric complexes with the FcR γ -chain (FcR γ), which contains an ITAM motif that is required for cell activation (Fig. 8). The IgG-antigen complex is detected by the Fc γ Rs and crosslinks with the FcR γ . This complex formation results in tyrosine phosphorylation of the ITAM motif with subsequent recruitment of SH2-containing molecules, Syk kinase and adaptor proteins that regulate the activation of PLC γ 1 and other effector

proteins (Fig. 8). Subsequent signaling pathways associated with the activation by $Fc\gamma R$ s are similar to that observed for other ITAM-containing receptors such as TCR in T cells. Finally, activation of $PLC\gamma$ leads to increase of cytoplasmic IP_3 and IP_3R -mediated release from intracellular Ca^{2+} stores (for a review, see [104]).

2.4.4. Ca^{2+} -dependent effector signaling in cells of the immune system

As a result of the elevated $[Ca^{2+}]_i$, several Ca^{2+} -dependent signaling proteins are activated, such as the Ca^{2+} -calmodulin-dependent kinase (CaMK) and its target cyclic-AMP-responsive-element-binding protein (CREB), the phosphatase calcineurin and its target nuclear factor of activated T cells (NFATs), the myocyte enhancer factor 2 (MEF2) which is activated via the calcineurin and CaMK pathways, as well as the nuclear factor kappa B ($NF\kappa B$) [25,105]. In addition, Ca^{2+} signaling directly regulates the Ras-MAPK signaling pathway, which plays an important role during double-negative and double-positive selection stages during thymocyte maturation [106-108].

Simultaneously, after PIP_2 hydrolysis by $PLC\gamma$, liberated DAG can directly activate non-store-operated Ca^{2+} influx through some TRPC channels and stimulate the GTPase Ras-mitogen-activated protein kinase signaling cascade, which in turn activates the AP-1 transcriptional complex (that includes c-Jun and c-Fos proteins). In lymphocytes, the transcription factors AP-1, NFAT and $NF\kappa B$ modulate gene expression [17,25,105,109]. Thus Ca^{2+} signaling is integrated with other signaling pathways, resulting in cytokine gene expression, cell proliferation and a activation of a large number of activation-associated genes [94,110].

2.5. Neurons and Ca^{2+} signaling

In neurons, Ca^{2+} signals derived from intracellular stores or extracellular space are essential for fundamental functions, including synaptic transmission and plasticity. Under pathological conditions, such as cerebral ischemia, a 'calcium overload' can induce neuronal cell death [11,111-114].

Two principal types of Ca^{2+} channels are firmly established to mediate Ca^{2+} entry into neurons: voltage-operated Ca^{2+} channels (VOCCs) and ionotropic receptor-operated (ligand-gated) channels (ROCs), including N-methyl-D-

aspartate receptors (NMDARs) and some α -amino-3-hydroxy-5-methylisoxazole-4-propionate acid receptors (AMPA receptors), which are activated by the excitatory neurotransmitter glutamate, the major excitatory neurotransmitter in the central nervous system [115,116]. Glutamate excitotoxicity is a common mechanism contributing to neurodegeneration in ischemia [112,114,116].

The increased $[Ca^{2+}]_i$ in neurons is sensed and transmitted by Ca^{2+} -binding proteins. Most of them contain EF-hand motifs. The EF-hand proteins in neurons comprise the ubiquitous calmodulin, S100 proteins, neuronal Ca^{2+} sensors (NCS), and calmyrins which are similar to NCS [117,118].

The downstream signaling pathways are complex and mostly related to phosphorylation cascades. The main players involved in this process are calmodulin (CaM) dependent kinases I-IV (CaMKI-IV), PKC, protein kinase A (PKA), IP-3-k, Ca^{2+} -dependent phosphatase calcineurin B, cAMP phosphodiesterase, adenylyl cyclase (AC), Ca^{2+} /Calmodulin-dependent neuronal nitric oxide synthase (nNOS) and calpains, which are Ca^{2+} -activated proteases [112].

Transcription factors that are dependent on Ca^{2+} signaling in neurons include the NFAT, CREB and the Ca^{2+} -binding downstream regulatory element modulator (DREAM), also known as calsenilin [112].

Ca^{2+} release from the ER also occurs in neurons via the RyRs, which are more characteristic of neurons and muscle cells and IP₃Rs, which are widely expressed. The RyR-mediated Ca^{2+} release has been shown to be very important for neuronal plasticity, secretion, gene transcription and other neuronal functions [119,120]. In contrast, less is known about the functional significance of IP₃R-mediated Ca^{2+} release and the presence of SOC, SOCE and store replenishment in neurons [27,121,122]. For instance, PLC β 1 null mice showed epileptic seizures which led to the sudden death of the mice [123]. IP₃-induced Ca^{2+} release was almost completely abolished in neurons from IP₃R type I null mice. Most of newborn died perinatally and survivors exhibited severe neurological symptoms, ataxia and epilepsy [124].

2.6. Aim of the work

Agonist-induced elevation of $[Ca^{2+}]_i$ is a central step in electrically non-excitable cells and platelet activation, but the underlying mechanisms are not fully understood. A major pathway for Ca^{2+} entry in non-excitable cells involves receptor-mediated release of intracellular Ca^{2+} stores followed by SOCE. STIM1 has been shown to play an essential role in activation SOC channels in T-cells. However, the STIM2 function in mammalian physiology was in general unknown when I started my work. Since the EF-hand domain is highly conserved between STIM isoforms it was suspected that STIM2 could be an important player in the regulation of Ca^{2+} homeostasis in platelets. The high divergence in the C-terminal region between both isoforms suggested different functions.

The goals of the presented work can be divided into three parts:

- Generation and characterization of mice with a germline knockout of the *Stim2* gene.
- The main goal is to study the function of STIM2 in platelets, using STIM2-deficient platelets and the knockout technology as *in vivo* model.
- Assess STIM2 function in immune cells and neurons, where an important role was suspected.

3. MATERIALS

3.1. Reagents

1.1.1. Chemicals

2,3,5-triphenyltetrazolium chloride (TTC) (Sigma, Germany)	Enhanced chemoluminescence detection substrate (ECL) (MoBiTec, Germany)
ADP (Sigma, Germany)	Epinephrine (Sigma, Germany)
Adrenaline (Sigma, Germany)	FeCl ₃ (Sigma, Germany)
Apyrase (grade III) (Sigma, Germany)	Fentanyl (Janssen-Cilag GmbH, Germany)
Atipamezol (Pfizer, Germany)	Fibrillar type I collagen (Horm) (Nycomed, Germany)
BamHI (Invitrogen, Germany)	Flumazenil (Delta Select GmbH, Germany)
Bovine serum albumin (BSA) (Sigma, Germany)	Fetal calf serum (FCS) GIBCO® (Invitrogen, Germany)
Carbonyl cyanide m-chlorophenylhydrazone (CCCP) (Sigma, Germany)	Fura-2 acetoxymethyl ester (AM) (Molecular Probes, Oregon)
Carmine (Sigma, Germany)	Geneticin (G418) (Sigma, Germany)
Complete Freund's adjuvant (CFA) Gibco® (Invitrogen, Germany)	H ³ -Thymidine (Amersham GE Healthcare, UK)
Convulxin (Alexis, San Diego)	High molecular weight heparin (Sigma, Germany)
Cyclopiazonic acid (CPA) (Sigma, Germany)	Human fibrinogen (Sigma, Germany)
Collagen-related peptide (CRP) [125]	Ionomycin (Molecular Probes, Oregon)
DAPI (Merck, Germany)	Kanamycin (Roth, Germany)
DMEM+GlutaMax®-I (Invitrogen, Germany)	KLH (Sigma, Germany)
DMSO (Invitrogen, Germany)	LIF ESGRO (Millipore, Massachusetts)
DNP-HAS (Fermentas, Lithuania)	Luxol fast blue (LFB) (Sigma, Germany)
Dylight-488 (Pierce, Illinois)	Medetomidine (Pfizer, Germany)
EcoRI (Invitrogen, Germany)	Midazolam (Roche Pharma AG, Germany)

MOG₃₅₋₅₅-peptide (Biotrend, Germany)

N,N,N',N'-tetrakis-ethylenediamine (TPEN)
(Sigma, Germany)

Naloxon (Delta Select GmbH, Germany)

Neomycin (Sigma, Germany)

Non-essential aminoacids (NEAA)
(Invitrogen, Germany)

Nonidet P-40 (NP-40) (Roche Diagnostics,
Germany)

NotI (Invitrogen, Germany)

Penicillin/streptomycin (PAN, Germany)

Pertussis toxin (Alexis, San Diego)

Pluronic F-127 (Invitrogen, Germany)

Prostacyclin (PGI₂)(Calbiochem, Germany)

Rhodocytin [126]

Serotonin (Sigma, Germany)

Staurosporine (Sigma, Germany)

Thapsigargin (Molecular Probes, Oregon)

Thrombin (Roche Pharma AG, Germany)

Tetramethylbenzidine (TMB) (BD
Pharmingen, Canada)

TiterMax adjuvant (Alexis, San Diego)

U46619 (Alexis Biochemicals, San Diego)

1.1.2. Buffers

All buffers were prepared and diluted in Milli-Q water.

LB medium, pH 7.5: Bacto-Tryptone 1 %, yeast extract 0.5 %, NaCl 1 %, all from Roth (Germany)

DNA isolation buffer: Tris-HCl (pH 8.0) 50 mM, EDTA 100 mM, NaCl 100 mM, SDS 1 %, all from Roth (Germany), Proteinase K 100 µg/mL (Invitrogen, Germany).

Phosphate-buffered saline (PBS), pH 7.14: NaCl 137 mM, KCl 2.7 mM, KH₂PO₄ 1.5 mM, Na₂HPO₄·2H₂O 8 mM, all from Roth (Germany).

Tris-buffered saline (TBS), pH 7.3: NaCl 137 mM (0.9 %), Tris-HCl 20 mM, all from Roth (Germany).

LB-Agar plates: LB medium, agar 1.5 %, ampicillin 100 µg/mL or kanomycin 50 µg/mL.

Tyrode's buffer, pH 7.3: NaCl 137 mM, KCl 2.7 mM, NaHCO₃ 12 mM, NaH₂PO₄ 0.43 mM, Glucose 0.1 %, HEPES 5 mM, BSA 0.35 %, CaCl₂ 1 mM, MgCl₂ 1 mM all from Roth (Germany).

TE buffer: Tris-HCl 10 mM, EDTA 1 mM (pH 8.0) all from Roth (Germany).

TAE buffer, pH 8.5: Tris-acetate 40 mM, EDTA 1 mM all from Roth (Germany).

PCR reaction medium 25 µL: 2.5 µL PCR buffer (10x), 2.5 µL MgCl₂ (10x), 0.5 µL dNTPs (10 mM), 0.5 U Taq polymerase (all from invitrogen, Germany), 0.5 µL forward primer (100 ng/µL), 0.5 µL reward primer B (100 ng/µL), 25 ng DNA, H₂O to 25 µL

FACS buffer: PBS (Invitrogen, Germany), 0.1 % BSA, 2 mM CaCl₂ (Roth, Germany).

Tyrosine Phosphorylation lysis buffer, pH 7.5: 300 mM NaCl, 20 mM TRIS, 2 mM EGTA, 2 mM EDTA, 2 % NP-40, 1 tablet/10 mL Complete Mini (Protease inhibitor cocktail, Roche, Germany), 2 mM Na₃VO₄.

ES cell culture

ES cell freezing medium: DMEM+GlutaMax[®]-I 70 %, foetal bovine serum (FCS, ES Cell tested) 20 %, DMSO 10 % all from invitrogen (Germany).

ES cell medium: DMEM+GlutaMax[®]-I 70 %, foetal bovine serum (FCS, ES Cell tested) 20 %, non-essential aminoacids (NEAA), 2-mercaptoethanol 2 mM, Leukemia inhibitory factor (LIF) 1000 U/mL all from invitrogen (Germany).

EF medium: DMEM+GlutaMax[®]-I 70 %, foetal bovine serum (FCS) 10 %, non-essential aminoacids (NEAA) all from invitrogen (Germany).

Trypsin-EDTA solution: Trypsin-EDTA ready-to-use 0.25 % (invitrogen, Germany).

ES cell selection medium: ES cell medium, geneticin (G418) 500 µg/mL, all purchased from invitrogen (Germany).

ES cell DNA lysis buffer: Tris-HCL 100 mM (pH 8.5), EDTA 5 mM, SDS 0.2 %, NaCl 200 mM (all from Roth, Germany), Proteinase K 100 µg/mL (Invitrogen, Germany).

Southern blot analysis

10XSSC, pH 7.6: Sodium citrate 150 mM, NaCl 1.5 M all from Roth (Germany).

Church Buffer: Sodium phosphate buffer 0.25 M, EDTA 1 mM, Bovine serum albumin (BSA) 1 %, SDS 7 %, Salmon sperm DNA 0.1 mg/mL all from Sigma (Germany).

Denaturation buffer: NaCl 1.5 M, NaOH 0.5 M all from Roth (Germany).

Gel depurination solution: HCl 0.25 M (Roth, Germany).

Neutralization Buffer: Tris-HCl 0.5 M (pH 7.2), NaCl 1.5 M, EDTA, 1 mM; autoclave all from Roth (Germany).

Sodium phosphate buffer 0.5 M, pH7.2: Na₂HPO₄·2H₂O (1 M) 34.2 %, NaH₂PO₄·H₂O (1 M) 15.8 % all from Roth (Germany).

Church washing buffer (5L): 200 mL 0.5 M sodium phosphate buffer, pH7.2+250 mL 20 % SDS all from Roth (Germany).

Western Blot

Blocking buffer: Fat-free milk powder 5 % (Applichem, Germany), PBS.

Blotting buffer A: Tris, pH 10.4 0.3 M, Methanol 20 % all from Roth (Germany).

Blotting buffer B: Tris, pH 10.4 25 mM, Methanol 20 % all from Roth (Germany).

Blotting buffer C: ϵ -amino-n-caproic acid 4 mM (Sigma, Germany), Methanol 20 % (Roth, Germany).

Laemmli buffer: Tris 40 mM, Glycin 0.95 M, SDS 0.5 % all from Roth (Germany).

RIPA buffer: Triton-X100 1%, Dioxycholate (DOC) 0.5 %, SDS 0.1 %, NaCl 150 mM, Tris-HCl pH. 8 50 mM (all from Roth, Germany), Dithiothreitol (DTT) 10 mM (Sigma, Germany), protease inhibitors cocktail 1 tablet/10 mL (Roche, Germany).

SDS sample buffer, 2X: β -mercaptoethanol (reducing conditions) 10 %, Tris buffer (1.25 M), pH 6.8 10 %, Glycerin 20 %, SDS 4 % all from Roth (Germany), Bromophenol blue 0.02 % (Sigma, Germany)

Washing buffer: PBS, Tween 20 0.1 %.

Histology

Carmine solution: Carmine 0.2 %, aluminium potassium sulphate 0.5 % all from Sigma (Germany), filtered.

Carnoy's Fixative solution: Ethanol 60 %, methanol 30 %, glacial acetic acid 10 % all from Roth (Germany).

Eosin solution: Eosin 0.05 % (Sigma, Germany), glacial acetic acid 0.06 % (Roth, Germany).

Hematoxylin solution: Hematoxylin ready-to-use (Sigma, Germany), filtered.

NISSL solution: Cresyl violet acetate 0.1 % (Sigma, Germany), glacial acetic acid 0.3 %, filtered (Roth, Germany).

PFA fixative solution: Paraformaldehyde (PFA) 4 % in PBS.

1.1.3. Plasmids

Topo TA (Invitrogen, Germany)

PBlueScript KS minus (Stratagene, California)

PBlueScript KS minus containing IRES – NEO- PGK promoter – LacZ – poly A construct

1.1.4. Bacteria

XL10-Gold[®] Ultracompetent Cells (Stratagene, California)

1.1.5. Oligonucleotides

BAC probe amplification:

Stim2/BACprobe_F: 5'-GAAGAGAAGCACAGTCTTTG-3'

Stim2/BACprobe_R: 5'-CTGGAAACTGTGGCACGATT-3'

External probe amplification:

Stim2/Extprobe_F1: 5'-GTGCTTCAGAGCTTTTCTGT-3'

Stim2/Extprobe_R1: 5'-CAAGACTAACACCAAATGAA-3'

***Stim2* gene 5'-arm amplification:**

5'flanking/*Stim2*KO/i3_F1: 5'-GATTGCTGCCAACTCTGAGT-3'

5'flanking/*Stim2*KO/E4_R: 5'-CTCAACTGTCCAATTGTGAA-3'

***Stim2* gene 5'-arm sequencing:**

5'flanking/*Stim2*KO/i3_F1: 5'-GATTGCTGCCAACTCTGAGT-3'

*Stim2*KO/i3seq1_F: 5'-GTAGGCTCAGCATGGGAATA-3'

*Stim2*KO/i3seq2_F: 5'-CAGTAAGGAACTTATACATC-3'

*Stim2*KO/i3seq3_F: 5'-GCAGAGAGAATCTTATCCTG-3'

*Stim2*KO/i3seq4_F: 5'-GTTTCAGATCCAGTCTTTCC-3'

3'-arm probe amplification:

STIM2/BACprobe_F: 5'-GAAGAGAAGCACAGTCTTTG-3'

STIM2/BACprobe_R: 5'-CTGGAAACTGTGGCACGATT-3'

Stim2 mouse PCR genotyping

Stim2 wild-type 5': 5'-CCCATATGTAGATGTGTTTCAG-3'

Stim2 wild-type 3': 5'-GAGTGGTGTTC-CCTTCACAT-3'

Stim2 knock-out 5': 5'-TTATCGATGAGCGTGGTGGTTATGC-3'

Stim2 knock-out 3': 5'-GCGCGTACATCGGGCAAATAATATC-3'

3.1.1. Antibodies

Primary antibodies					
Name/Clone	Antigen	Type	Host	Final conc.	Company
Dylight-488 conjugated anti-GPIX Ig derivative	GPIX	IgG ₁	Rt	5 µg/mL	[132]
PE-Cy5-anti-GPIb	GPIb	IgG	Rt	5 µg/mL	Emfret Analytics
9EG7	β1 integrin	IgG _{2a,K}	Rt	1:150	BD Pharmingen
21H4	α2 integrin	IgG _{2b}		5 µg/mL	Emfret Analytics
YL1/2	α-tubulin	IgG _{2a}	Rt	1:1000	Chemicon
RA3-6B2	B220 (CD45R)	IgG _{2a,K}	Rt	1:250	BD Pharmingen
Asp175 (5A1E)	Cleaved-Caspase-3	IgG	Rb	1:150	Cell Signaling
KT3	CD3	IgG _{2a}	Rt	1:100	AbD Serotec
145-2C11	CD3ε	IgG _{1,K}	Hm	10 µg/mL	eBioscience
RM4-5	CD4	IgG _{2a,K}	Rt	1:250	BD Pharmingen
IM7	CD44	IgG _{2b,K}	Rt	1:750	BD Pharmingen
MEL44	CD62L	IgG _{2a,K}	M	1:200	BD Pharmingen
LY-2(53-6.7)	CD8α	IgG _{2a,K}	Rt	1:200	BD Pharmingen
ULF1	CD9	IgG _{2a}	Rt	5 µg/mL	[132]
SPE-7	DNP-HSA	IgE	M	30 µg i.v. 10 µg/mL	Sigma
BM8	F4/80	IgG _{2a,K}	Rt	1:250	eBioscience
290322	FcγRI	IgG _{2a}	Rt	1:200	R&D Systems
275003	FcγRIII	IgG _{2a}	Rt	1:250	R&D Systems
2.4G2	FcγRII, IIIa	IgG _{2b,K}	Rt	10 µg/mL	BD Pharmingen
9E9	FcγRIV	IgG	Rt	5 µg/mL	[127]
Xia.C3	GPIb	IgG _{2a}	Rt	5 µg/mL	Emfret Analytics
EDL1	GPIIb/IIIa	IgG _{2a}	Rt	5 µg/mL	[132]
JON1 / 6C10	GPIIb/IIIa	IgG _{2b}	Rt	4-100 µg i.v. 5 µg/ml	Emfret Analytics
JON3 / 5D7	GPIIb/IIIa	IgG ₁	Rt	4-100 µg i.v.	Emfret Analytics
JON/A	GPIIb/IIIa	IgG _{2b}	Rt	5 µg/mL	[143]
6C10	GPIIIa (CD61)	IgG _{2b}	Rt	5 µg/mL	Emfret Analytics

p0p6	GPIX	IgG _{2b}	Rt	5 µg/mL	[132]
DOM1	GPV	IgG ₁	Rt	5 µg/mL	[132]
JAQ1	GPVI	IgG _{2a}	Rt	5 µg/mL	Emfret Analytics
B56	Ki-67	IgG _{1, κ}	M	1:20	BD Pharmingen
AP20	MAP2a/b	IgG ₁	M	1:200	Abcam
A60	NeuN	IgG ₁	M	1:1000	Chemicon
4G10	phospho-Tyrosin	IgG _{2b,κ}	M	1:1000	Millipore
BRU1	P-selectin	IgG ₁	Rt	5 µg/mL	Emfret Analytics
STIM1	STIM1	IgG	Rb	1:500	Cell Signaling
STIM2	STIM2	IgG	Rb	1:400	Cell Signaling
STIM2(CT)	STIM2	IgG	Rb	1:400	ProSci
H57-597	TCRβ	IgG	Hm	1:200	eBioscience
Hm = hamster M = mouse Rb = rabbit Rt = rat i.v. = intravenous					

Secondary antibodies

Goat anti-rabbit, rabbit anti-mouse and rabbit anti-rat IgG (-HRP) were purchased from DAKO (Germany) and Jackson ImmunoResearch (Pennsylvania). Goat anti-rabbit (-Cy3) was purchased from Dianova (Germany). Goat anti-mouse (-Alexa 488) was purchased from BD Bioscience (Canada). Goat anti-Hamster was purchased from Jackson ImmunoResearch (Pennsylvania).

4. METHODS

4.1. Western blot

Western blotting was performed using standard protocols in total protein lysates from different mouse organs extracted with RIPA buffer and mixed with 2x SDS sample buffer. The mixture was heated at 95 °C for 5 minutes (min) and loaded in 7.5 % SDS-PAGE gel. Samples were separated for 1 hour (h) in a SDS-PAGE chamber (Bio-Rad, California) containing Laemmli buffer at 25 mA/gel and transferred onto a polyvinylidene difluoride membrane (Immobilon-P transfer membrane, Millipore, Massachusetts). Briefly, Semi-dry blotting was performed as follows: One tower of Whatman paper was built in between the two electrode surfaces of a dry blotting system (Biometra, Germany). The lower layer of Whatman paper was embedded with blotting buffer A, a second layer embedded with blotting buffer B was placed on top. The transfer membrane was activated with methanol, washed with blotting buffer B and placed on the tower of Whatman papers. On top, the gel with the sample was placed and finally a further layer of Whatman paper embedded in blotting buffer B was placed. The blotting was performed at 60 mA/gel for 1 h at RT. To prevent non-specific antibody binding, membrane was incubated in blocking buffer overnight at 4 °C. The following primary antibodies were used for western blotting: rabbit anti-STIM2-CT (1:400, ProSci Incorporated, Poway), rabbit anti-STIM1 (1:500, Cell Signaling, Massachusetts), rat anti- α -tubulin (1:1000, Chemicon international, Massachusetts). The membrane was incubated 3x with washing buffer for 10 min at RT. All HRP-conjugates antibodies were purchased from Jackson ImmunoResearch (Suffolk, UK) or Dianova (Hamburg, Germany). After several washing steps bound antibodies were detected with enhanced chemiluminescent Western Lightning™.

4.2. Knockout mice generation

Experiments were conducted in accordance to the regulations of the local authorities (Regierung von Unterfranken) and were approved by the institutional review boards of all participating institutions. *Stim2*^{-/-} knockout mice were generated by deletion of most part of exon four to seven of the *Stim2* gene using standard molecular techniques. Mice generation was performed as previously described [128].

4.2.1. Isolation of BAC clones containing the *Stim2* gene

Genomic DNA clones were isolated from a 129Sv BAC library (Chori, USA) by southern blot (described below) using a specific probe targeting the exon 4 of the *Stim2* gene that had been isolated by PCR using the primers: *Stim2/BACprobe_F* and *Stim2/BACprobe_R*.

4.2.2. Isolation of plasmid DNA from BAC clones

Plasmid DNA was isolated from the BAC clones using the BACHAM™ kit (Epicentre®, Wisconsin) according to the manufacturer's specifications. For the isolation of a specific DNA fragment, PCR or DNA restriction enzyme digestion were used.

4.2.3. Isolation of DNA from agarose gels

PCR products or digested DNA were separated by electrophoresis using a 1 % agarose gel. One cm³ of agarose gel containing the desired fragment was isolated and DNA fragments were extracted using the PCR NucleoSpin® Extract II kit (Macherey-Nagel, Germany). Subsequently, DNA fragments were subcloned in the appropriate vector and transformed in XL10-Gold® ultracompetent cells (Stratagene, California) using general methods of molecular biology.

4.2.4. Colony hybridization

Approximately 100 bacteria colonies were picked and transferred to an agarose petri dish containing a Hybond™-N⁺ membrane (Amersham GE Healthcare, UK). Bacteria clones grown overnight on the membrane and next day membrane was treated as described below for Southern blot method. Positive clone containing the *Stim2* gene was detected using the same probe used for BAC clone identification.

4.2.5. Isolation of plasmid DNA from competent bacteria

Plasmid DNA preparations of bacteria cultures - "Mini/Midi/Maxi Preps" – were performed according to the manufacturer's specifications (Qiagen, Germany). DNA was resuspended in TA buffer and concentrations were assessed photometrically at 260 nm by a BioPhotometer (Eppendorf, Germany).

4.2.6. Long term PCR amplification

The 5'- and 3'- homologue arms were amplified using the Triple Master PCR System (Eppendorf, Germany), according the manufacturer's specifications. This kit allows amplifying very long DNA products (up to 40 Kb) with a high fidelity.

4.2.7. Culture of embryonic stem (ES) cells

Generation of feeder cells resistant to geneticin was performed as previously described [128]. Feeder cells were obtained from E18 embryos heterozygous for a collagen IX null allele which contains a neomycin-resistant cassette [129]. ES cell culture was performed as previously described [128]. Culture flasks were previously prepared with a monolayer culture of irradiated feeder cells, which provide the essential factors that keep the pluripotency of the ES cells. Frozen R1 ES cells (Andras Nagy Lab, Canada) were thawed and grown in co-culture on the feeder layer in the presence of ES cell medium. Cells were detached with trypsin-EDTA solution and passaged every two days to fresh culture flasks containing new feeder cultures.

4.2.8. DNA electroporation in ES cells

Approximately 100 µg of *Stim2* targeting vector was linearized by 2 h digestion with NotI restriction enzyme. Digested targeting vector was purified by gel-electrophoresis separation and isolation using the PCR NucleoSpin® Extract II kit (Macherey-Nagel, Germany). 60 µg of sterile linearized DNA was mixed together with 4×10^7 ES cells in 700 µL PBS and placed into an electroporation GenePulser® cuvette (Bio-Rad, California). DNA was electroporated into the cells by a pulse of 0.8 kV and 3 µF (the time constant should be 0.04 msec) at

RT, using the electroporation system GenePulser Xcell™ (Bio-Rad, California). The cell death percentage was between 30-50 %.

4.2.9. Positive selection of electroporated ES cells

Electroporated cells were seeded in 10 cm culture dish and next day cells were positively selected with ES cell selection medium. This medium contains the antibiotic geneticin, which kills the wild-type cells that did not incorporate the neomycin resistant gene of the targeting vector. Cells were selected for 8 days and during this time they formed colonies from a single clone. 360 colonies were picked, transferred in 24 well plates and selected for additional 8 days.

4.2.10. Freezing ES clones

Cell clones were washed two times with PBS, trypsinized and half of the cells were frozen at -80 °C with ES cell freezing medium. The remaining half was cultured for 4 days and cells were used for DNA extraction and genotyping.

4.2.11. ES cell genotyping

ES DNA was extracted as described below for mouse DNA isolation. Targeted stem cell clones were screened by Southern blot as described below using a gene specific external probe. *Stim2*^{+/-} positive ES clones were thawed and re-cultured for blastocyst injection in collaboration with Dr. Michael Bösl (Max Planck Institute of Neurobiology, Martinsried) to generate chimeric mice.

4.3. Bone marrow mice generation

For the generation of bone marrow chimeras, 5-6 weeks old *Stim2*^{+/+} and *Stim2*^{-/-} female mice were irradiated with a single dose of 10 Gy, and bone marrow cells from 6 weeks old *Stim2*^{+/+} or *Stim2*^{-/-} mice from the same litter were injected intravenously into the irradiated mice (4x10⁶ cells/mouse). Water supplemented with 2 g/L neomycin was provided to the mice. Bone marrow chimerism was confirmed by western blot, studying the STIM2 expression in platelets isolated as described below.

4.4. Mouse DNA isolation

5 mm² of ear tissue was digested in 500 µL DNA digestion buffer at 56 °C overnight under shaking conditions. Next day samples were mixed (1:1 vol) with Phenol/Chloroform, then vortexed for 5 min and centrifuged at 14000 rpm for 10 min and the aqueous phase containing the DNA was pipetted and precipitated with isopropanol (1:1 vol). After centrifugation at 14000 rpm for 10 min, the DNA pellet was washed twice with ice cold 70 % ethanol. The DNA pellet was left to dry and finally resuspended in 50 µL H₂O.

4.5. Mouse genotyping

4.5.1. PCR genotyping

Two separated reactions with different primer pairs were performed to amplify the wild-type (*Stim2* wild-type 5' and *Stim2* wild-type 3') or the knockout allele (*Stim2* knockout 5' and *Stim2* knockout).

PCR programs:

Wild-type allele: 1) 96 °C 3 min; 2) 94 °C 30 sec; 3) 51.5 °C 30 sec; 4) 72 °C 1 min; 5) repeat step 2.-4. 30 cycles; 6) 72 °C 10 min; 7) 4 °C hold.

Knockout allele: 1) 96 °C 3 min; 2) 94 °C 30 sec; 3) 55 °C 30 sec; 4) 72 °C 1 min; 5) repeat step 2.-4. 30 cycles; 6) 72 °C 10 min; 7) 4 °C hold.

4.5.2. Southern blot

15 µg of ES cell or mouse DNA were digested overnight at 37 °C with 20 U/sample of BamHI restriction enzyme (Invitrogen, Germany). Next day fragments were separated in 0.7 % agarose gel electrophoresis for several hours and separation of the bands were documented together with a ruler on a UV imaging system (Herolab GmbH Laborgeraete, Germany). Gels were placed in gel depurination solution for 10 min, then in denaturation solution 2 x 20 min and finally in neutralization solution 2 x 20 min. DNA transfer was performed by capillarity in 20 x SSC buffer on HybondTM-N⁺ membranes (Amersham GE

Healthcare, UK). Membranes were air-dried and the DNA was covalently bound using a UV-linker (1200 J/m², UV Stratalinker®1800, Stratagene, California).

Radioactive labeling of the probe: 50-100 ng of DNA probe was denatured at 95 °C for 5 min and labeled with radioactive ³²P- α -dCTP (50 μ Ci; Amersham GE Healthcare, UK) using the rediprime II labeling kit (Amersham GE Healthcare, UK) according to the manufacturer's instructions. To reduce unspecific background, unincorporated nucleotides were removed by gel filtration with Probe Quant G-50 MicroColumns (Amersham GE Healthcare, UK). The probe was ready for hybridization reaction after boiling at 95 °C for 5 min.

Hybridization: Membranes containing the DNA samples were blocked for 2 h in church buffer at 65 °C in a water bath shaker and after 2 h the labeled probe was added and hybridized for 16 h under the same conditions. Next day membranes were washed twice for 20 min in church washing buffer. Signals were detected by exposure of 3-7 days to X-ray film (Amersham GE Healthcare, UK) at -80 °C.

4.6. Histology

Organs were fixed in 4 % paraformaldehyde (PFA) for 2 h at 4 °C, embedded in paraffin (Histolab Products AB, Germany), cut into 7 μ m thick sections and mounted in glass slices. After removal of paraffin, tissues were stained with hematoxylin and eosin (Sigma, Germany) or with Nissl staining method following standard protocols. Whole inguinal mammary glands were isolated, stretched on glass slides and fixed in Carnoy's fixative for 2 to 4 h at RT. They were washed in 70 % EtOH for 15 min afterwards and changed gradually to distilled water. Glands were stained in carmine solution at RT overnight and next day they were washed in 70 % EtOH for 15 min, cleared in xylene and mounted with Eukitt® (Sigma, Germany).

4.7. Blood analysis

150 μ L blood was collected from the retroorbital plexus, clotted, and centrifuged to separate the serum. Analyses of different blood parameters were performed in collaboration with Dr. Thomas Renné from Institute of Clinical Biochemistry of Würzburg.

4.8. Platelet analysis

4.8.1. Platelet isolation

Mice were anesthetized with ether and bled from the retroorbital plexus. Blood was collected into an Eppendorf tube containing 300 µl heparin in TBS (20 U/mL), pH 7.3. Blood was centrifuged (Eppendorf, Germany) at 1800 rpm for 5 min. The supernatant was centrifuged again at 800 rpm for 6 min at to obtain platelet rich plasma (prp). To wash platelets, prp was centrifuged at 2500 rpm for 5 min in the presence of prostacyclin (PGI₂) (0.1 µg/mL) and the pellet was resuspended in Ca²⁺-free Tyrode's buffer containing PGI₂ (0.1 µg/mL) and apyrase (0.02 U/mL). Repeating the washing two times, the platelet pellet was resuspended in Tyrode's buffer containing apyrase (0.02 U/mL) (500 µL) and left to incubate for at least 30 min at 37 °C before analysis.

4.8.2. Platelet counting

Blood (50 µL) was obtained from the retroorbital plexus of anesthetized mice using heparinised microcapillaries and collected into an eppendorf tube containing 300 µL heparin in TBS (20 U/mL), pH 7.3. Platelet counts and size were determined using a Sysmex KX-21N automated hematology analyzer (Sysmex Corp, Japan). Platelet counts were additionally confirmed by Flow cytometry.

4.8.3. Flow cytometry

Approximately 1x10⁶ platelets were activated with the indicated agonists or reagents (10 min, RT) in Tyrode's buffer and stained for 10 min with saturating amounts of fluorophore-conjugated antibodies. The reaction was stopped by addition of 500 µL PBS, and samples were immediately analyzed on a FACScalibur (Becton Dickinson, New Jersey).

4.8.4. Platelet life span experiments

Circulating platelets were labeled in vivo by i.v. injection in the retroorbital plexus of 5 µg Dylight-488-anti-GPIX Ig derivative in 200 µL PBS. 30 min after antibody injection (and every 24 h for 5 days) 50 µL blood was taken from the retroorbital plexus of the treated mice and diluted 1:20 in heparin containing PBS. The diluted whole blood was in turn incubated with 10 µL of the platelet marker PE-Cy5-anti-GPIb for 10 min at RT. The Dylight-488 positive platelet population was determined as the percentage of the whole PE-Cy5 positive population by flow cytometry.

4.8.5. Intracellular Ca²⁺ measurements

Platelets isolated from blood and washed as described above, were suspended in Tyrode's buffer without Ca²⁺ and loaded with fura-2 AM (5 µM) in the presence of Pluronic F-127 (0.2 µg/mL) (both from Molecular Probes) for 30 min at 37 °C. After labeling, platelets were washed once and resuspended in Tyrode's buffer in the absence or presence of 1 mM Ca²⁺. 500 µL of the platelet suspension was placed in quartz cuvettes previously blocked with 1 % bovine serum albumin (BSA) (Sigma, Germany). Stirred platelets were activated with different agonists and fluorescence was measured with a PerkinElmer LS 55 fluorimeter (PerkinElmer, Massachusetts).

Excitation was alternated between 340 and 380 nm, and emission was measured at 509 nm. Each measurement was calibrated using 1 % Triton X-100 and 0.5 M EGTA. The system software automatically calculates the [Ca²⁺]_i from the fluorescent ratios. Briefly, fluorescence ratios were converted to relative [Ca²⁺]_i according to the following equation:

$$[Ca^{2+}]_i = 224 \times (R - R_{min}) / (R_{max} - R) \times F_{max} / F_{min}$$

where 224 nM is the K_D value of fura-2 AM Ca²⁺ binding; R represents the actual fluorescence ratio; R_{max} is the maximum fluorescence ratio determined from cells suspended in Tyrode's buffer supplemented with 0.1 % Triton-X100 and 1 mM CaCl₂; R_{min} is the mean fluorescence ratio determined from cells preincubated with 5 µM fura-2 AM and resuspended in Tyrode's buffer supplemented with 0.1 % Triton-X100, 1 mM CaCl₂, 5 mM EGTA; F_{max} and F_{min} represent the fluorescence values (arbitrary units) of fura-2 AM for R_{max} and R_{min}, respectively.

4.8.6. Aggregometry experiments

Platelets were isolated from blood and washed as described above. Washed platelets were resuspended in Tyrode's buffer and adjusted to a concentration of 3×10^8 cells/mL. Heparinized prp was used in ADP stimulated platelets. Agonists or reagents were added 20 sec after light transmission was started and recorded over 10 min on an Apect 4-channel optical aggregation system (APACT, Germany). Before starting the measurements, Tyrode's buffer (for washed platelets) or plasma (for prp) was set as 100 % aggregation and washed platelet suspension (for washed platelets) or prp (for prp) was set as 0 % aggregation. The activity of most agonists was assessed in Tyrode's buffer supplemented with 100 μ g/mL human fibrinogen, except in case of thrombin and ADP measurements.

4.8.7. Tyrosine phosphorylation assay

Platelets from three mice were isolated from 700 μ L blood as described above, pulled and resuspended in 350 μ L Tyrode's buffer without Ca^{2+} and supplemented with 10 μ M indomethacin, 5 mM EDTA and additional 2 U/mL apyrase to avoid platelet aggregation after activation. Platelets were activated with 2.5 μ g/mL convulxin and 50 μ L aliquots were taken after 30, 60, 120 and 240 sec. An additional aliquot was taken before activation and considered as time point 0 sec. Platelets were kept at 37 °C at constant stirring during the entire procedure. 50 μ L aliquots were immediately mixed 1:1 with the tyrosine phosphorylation lysis buffer at 4 °C, centrifuged at 14000 rpm for 10 min at 4 °C and supernatant was mixed with 25 μ L NuPAGE 4x LDS sample buffer (Invitrogen, Germany). The mixture was heated at 70 °C for 10 min and samples were run on NuPAGE Novex 4-12 % (gradient) Bis-Tris gel (Invitrogen, Germany) according to the instructions of the provider. Next steps were performed according to standard protocols for western blotting described above. The primary antibody anti-phosphotyrosine 4G10 (1:1000, Millipore, Massachusetts) was used to detect tyrosine phosphorylated proteins. An anti-mouse secondary Ig HRP-conjugated was used to detect the 4G10 antibody (1:1000, Dianova, Germany).

4.8.8. Flow chamber assay

Blood (700 μL) was collected into 300 μL TBS buffer, pH 7.3, containing 20 U/mL heparin and diluted 2:1 with Tyrode's buffer. Coverslips (24 x 60 mm) were coated with 0.25 mg/mL of fibrillar type-I collagen (Horm) (Nycomed, Germany) and blocked for 1 h with 1 % BSA (Sigma, Germany). Perfusion studies were performed as follows. Transparent flow chambers with a slit depth of 50 μm , equipped with the coated coverslips, were connected to a syringe filled with the diluted whole blood. Perfusion was performed using a pulse-free pump under high shear stress equivalent to a wall shear rate of 1000 s^{-1} or 1700 s^{-1} (4 min). Thereafter, chambers were rinsed by 4 min perfusion with Tyrode's buffer at the same shear stress and phase-contrast [130]. The entire process was recorded by time-lapse (1 sec for 4 min) using a 40x objective on an inverted microscope Zeiss HBO 100 (Zeiss, Germany). Image analysis was performed using MetaVue® software. Thrombus formation was expressed as the mean percentage of total area covered by thrombi.

4.8.9. Spreading assay

Platelets were isolated from blood and washed as described above. Washed platelets were resuspended in Tyrode's buffer and adjusted to a concentration of 2×10^8 cells/mL. 60 μL of the platelet suspension was stimulated with 0.05 U/mL thrombin and immediately placed on coverslips (24 x 60 mm) that had been coated overnight with 100 $\mu\text{g}/\text{mL}$ human fibrinogen (Sigma, Germany) and blocked for 1 h with 1 % BSA (Sigma, Germany). Coverslips were mounted in 1 % BSA-coated glass slides and placed on an inverted microscope Zeiss HBO 100 (Zeiss, Germany). Time-lapse images were recorded (every 5 sec for 20 min) with a 40x objective and analyzed using MetaVue® software. Starting points and percentages of adhered and completely spread platelets were considered as indicators of platelet adhesion and spreading dynamics.

4.8.10. *In vivo* experiments

4.8.10.1. Tail bleeding time experiments

Mice were anesthetized by intraperitoneal injection of a mixture of fentanyl (Janssen-Cilag GmbH, Germany), midazolam (Roche Pharma AG, Germany)

and medetomidine (Pfizer, Germany), and a 2 mm segment of the tail tip was cut off with a scalpel. Tail bleeding was recorded by absorbing blood drops with Whatman[®] filter paper every 20 sec, avoiding the direct contact with the wound surface. Bleeding was determined to have ceased as soon as no blood was observed on the paper. For ethical concerns, experiments were stopped within 20 min by wound cauterization with a cauterizing scalpel Kausto-Lux II (MECAN b.v., Netherlands) and the anaesthesia was antagonized with atipamezol (Pfizer, Germany), flumazenil and naloxon (both from Delta Select GmbH, Germany).

4.8.10.2. Intravital microscopy of thrombus formation in FeCl₃ injured mesenteric arterioles

Four week old mice were anesthetized as described previously and the mesentery was exteriorized through a midline abdominal incision. Arterioles (35-60µm diameter) were visualized with a Zeiss Axiovert 200 inverted microscope (x10) equipped with a 100-W HBO fluorescent lamp source and a CoolSNAP-EZ camera (Visitron, Germany). Digital images were recorded every second and analyzed off-line using Metavue[®] software. Injury was induced by topical application of a 3 mm² Whatman[®] filter paper saturated with FeCl₃ (20 %) for 10 sec. Adhesion and aggregation of fluorescently labeled platelets (Dylight-488 conjugated anti-GPIX Ig derivative) in arterioles was monitored for 30 min or until complete occlusion occurred (blood flow stopped for > 1 min).

4.9. Isolation and analysis of cells of the immune system

4.9.1. Isolation of cells of the immune system

Bone Marrow Mast cells (BMMCs) were derived as described before [131]. Briefly, bone marrow cells (1x10⁶/mL) from 6 to 8 weeks old male mice (129/Sv) were cultured (37 °C, 5 % CO₂) in a single cell suspension in RPMI 1640 medium containing 20 %, 1 % X63Ag8-653-conditioned medium as a source of IL-3, 2 mM L-glutamine, 1x10⁻⁵ M 2-mercaptoethanol, 50 units/mL penicillin, and 50 mg/mL streptomycin. At weekly intervals, the non-adherent cells were reseeded at 1x10⁶ cells/mL in fresh medium. By 4 to 6 weeks in culture, more than 99 % of the cells were c-kit- and FcεR1-positive as assessed by

phycoerythrin-labeled anti-c-kit antibodies (BD Pharmingen, Canada) and FITC-labeled IgE (anti-erythropoietin 26), respectively.

Resident peritoneal macrophages were flushed out of the peritoneal cavity of the mice with 10 mL PBS without Ca^{2+} supplemented with 1 % BSA, washed twice with the same solution and suspended in Tyrode's buffer.

Cells from the primary and secondary lymphoid organs (bone marrow, thymus, spleen and lymph nodes) were isolated from 8 week old mice as follows. Organs were isolated, placed inside a 70 μm cell strainer (BD FalconTM, Canada) with ice-cold FACS buffer and gently smashed with a piston, from a 10 mL syringe.

Spleen cell suspensions were further subjected to hypo-osmotic shock for red blood cell depletion.

Both tips of the femurs were cut and the bone marrow was flushed in ice-cold FACS buffer and filtered with 70 μm cell strainer (BD FalconTM, Canada).

Cells were collected, centrifuged at 1600 rpm for 5 min and washed twice. CD4^+ T cells were purified by negative magnetic separation from spleen and lymph nodes using the MACS[®] CD4^+ T cell isolation kit (Miltenyi Biotec, Germany) and suspended in Tyrode's buffer.

4.9.2. Cellularity assessment in primary and secondary lymphoid organs

Cells were isolated as described above. Cells counts were determined using a Sysmex KX-21N automated hematology analyzer (Sysmex Corp, Japan).

4.9.3. Intracellular Ca^{2+} measurements in cells of the immune system

Cells were isolated as described above and suspended in Tyrode's buffer without Ca^{2+} . Intracellular Ca^{2+} measurements were performed as described above for platelets. Stirred cells were activated with different agonists and fluorescence was measured with a PerkinElmer LS 55 fluorimeter (PerkinElmer, Massachusetts).

4.9.4. *In vivo* anaphylaxis experiments

Fc ϵ R-mediated hypothermia was induced by i.v. injection of 30 μ g anti-DNP IgE (company) per mouse 24 h before and the next day the body temperature was measured every 10 min after injection of the DNP-HSA antigen (250 μ g per mouse) with a rectal probe.

Fc γ R-mediated hypothermia was induced by injecting high dosage (100 μ g/mouse) anti-GPIIb/IIIa antibodies (JON1 and JON3). The rat anti-mouse GPIIb/IIIa antibodies have been described previously [132]. The isotypes of JON1 and JON3 are IgG_{2b} and IgG₁, respectively. Body temperature was measured every 10 min with a rectal probe.

4.9.5. Induction of Immune thrombocytopenia purpura (ITP) in mice

Initial platelet counts were assessed as described above for each mouse. These values were considered 100 % and subsequent counts (until day 4) were normalized to these values. Mice were i.v. injected with the indicated amounts (4, 7 or 11 μ g per mouse) of anti-GPIIb/IIIa antibodies (JON1 and JON3) to induce thrombocytopenia. After injection, platelet counts were assessed every 24 h.

4.9.6. Flow cytometry in cells of the immune system

Cells were isolated as described above and resuspended in FACS buffer at 4 °C. Fc γ Rs in T cells (but not macrophages) were blocked with 25 μ L FACS buffer supplemented with 10 μ g/mL 2.4G2 (BD Pharmingen, Canada) antibody for 15 min at 4 °C. Cells were subsequently labeled with a fluorescent-conjugated primary antibody against surface molecules in dark for 30 min at 4 °C. For intracellular staining, labeled cells were fixed overnight at 4 °C, and permeabilized with the fixation/permeabilization kit (eBioscience, San Diego). Then, cells were blocked with rat serum (1:50) for 30 min at RT and labeled with a fluorescent-conjugated primary rat antibody against intracellular antigens for 30-45 min at RT. The reaction was stopped by adding PBS and cells were washed twice before flow cytometry assessment.

4.9.7. Antibody isotype titer determination in mouse serum

Concentrations of antibodies of the IgM, IgG_{2a}, IgG₁, and IgE isotype were determined by the ELISA Quantitation Kits (Bethyl Laboratories, Texas), according to the manufacturer's recommendations. ODs were measured and translated into protein concentrations using the MultiSkan EX ELISA reader (THERMO electron corp., Massachusetts).

4.9.8. Keyhole limpet hemocyanin (KLH) immunizations

Mice were immunized subcutaneously with an emulsion of 45 μ L of PBS containing 25 μ g of KLH (Sigma, Germany) and 15 μ L of TiterMax (Alexis, San Diego). Twenty days after the initial immunization, mice were boosted with 25 μ g of KLH in 250 μ L of PBS i.p. Blood was taken on days 16 and 34 and anti-KLH Ig were detected in serum by ELISA using KLH-coated plates (150 μ g/mL in PBS at a final volume of 100 μ L/well). Wells were blocked with BSA (5 % in PBS) before serum was added. Bound anti-KLH Ig were detected with anti-mouse IgG-biotin (Dianova, Germany) followed by streptavidin-peroxidase (Dianova, Germany) and tetramethylbenzidine (TMB) was used as substrate. ODs were measured at 450 nm.

On day 43 or 63, CD4⁺ T cells were purified by negative magnetic separation from total splenocyte suspensions and 5x10⁴ or 1x10⁵ CD4⁺ cells were cocultured with 5x10⁴ or 1x10⁵ irradiated splenocytes (B6) in 96-well U-bottom plates to assess T cell proliferation rates. Different concentrations of KLH (0.1, 1 and 10 μ g/mL) were added to the co-cultures to re-stimulate T cells that specifically react to KLH. Stimulated Anti-CD3 Ig (0.1 mg/mL) T cells were used as a positive control. Proliferation was measured by determining [³H]-thymidine incorporation (12.5 mCi; Amersham GE Healthcare, UK) during the final 16 h of a 3-day culturing period. Radioactive incorporation was determined by beta counting (c.p.m., counts per minute).

4.9.9. Induction and evaluation of experimental autoimmune encephalomyelitis (EAE)

EAE was induced by immunization of mice with 200 μ g myelin oligodendrocyte glycoprotein (MOG₃₅₋₅₅) peptide (Biotrend, Germany). Complete Freund's adjuvant (CFA) Gibco[®] (Invitrogen, Germany) was supplemented with MOG to

obtain a 1 mg/mL emulsion and 2x 100 µL were injected subcutaneously at two different sites of the flank of deeply anesthetized mice. Pertussis toxin was injected at the day of immunization and two days later (400 ng, Alexis, San Diego). All animals were kept under standard conditions and had constant access to water and food.

The clinical course of EAE was monitored using the following score system: grade 0, no abnormality; grade 1, limp tail tip; grade 2, limp tail; grade 3, moderate hind limb weakness; grade 4, complete hind limb weakness; grade 5, mild paraparesis; grade 6, paraparesis; grade 7, heavy paraparesis or paraplegie; grade 8, tetraparesis; grade 9, quadriplegia or premoribund state; grade 10, death.

4.9.10. Immunohistochemistry

Mice spinal cord cryo sections were slowly thawed and dried at RT, fixed with 4 % paraformaldehyde (Merck, Germany), washed with PBS buffer and incubated with 5 % BSA in PBS for 30 min. Then, primary antibody (rat anti-CD3, 1:100, AbD Serotec, UK) were added and incubated for 12 h at 4 °C. Secondary antibody (Cy 3 labeled goat anti-rat 1:300, Dianova, Germany) was incubated for 60 min at room temperature. Staining with 0.5 µg/mL DAPI (Merck, Germany) was performed for 7 min. Pictures were collected by Axiophot immunofluorescence microscopy (Zeiss, Germany). Haemalaun-staining (1 ‰ haematoxylin (Sigma-Aldrich, Germany) in aqua dest. containing 0.2 ‰ NaIO₃ (Fluka, Sigma, Germany), 5 % KAISO₃ (Merck, Germany), 5 % chloral hydrate (Merck, Germany) and 1 ‰ citric acid (Serva, Germany) was performed for 10 min. For detection of demyelination slides were incubated with Luxol fast blue (LFB) solution for 12 h at 60 °C (0.1 %, Sigma, Germany), washed in 95 % alcohol, and then placed in lithium carbonate (0.05 %, Sigma, Germany).

4.10. Isolation and analysis of neuronal tissue

4.10.1. Isolation and culture of neurons

Neuronal cultures were obtained from *Stim2*^{-/-} or control embryos at day 18 of development (E18) according to previously described preparation protocols [133]. In brief, pregnant mice were sacrificed by cervical dislocation and

embryos were removed and transferred into warmed Hank's buffered salt solution (HBSS) Gibco® (Invitrogen, Germany). After preparation of hippocampi, the tissue was collected in a tube containing 5 mL of 0.25 % trypsin in HBSS. After five min of incubation at 37 °C, the tissue was washed twice with HBSS. Thereafter, the tissue was dissociated in 1 mL of neuronal medium by triturating with fire polished Pasteur pipettes of decreasing tip diameter. Neurons were diluted in neuronal medium (10 % 10x modified earl's medium (MEM); 0.2205 % sodium bicarbonate; 1 mM sodium pyruvate; 2 mM L-glutamine; 2 % B27 supplement (all Gibco®, Invitrogen, Germany); 3.8 mM glucose; 1 % penicillin/streptomycin (Biochrom AG, Germany), and plated in a density of 60.000 cells/cm² on poly-D-lysine coated cover slips in 4-well plates (Nunc, Denmark). Prior to experiments all cell cultures were incubated at 37.0 °C and 5 % CO₂ and held in culture for up to 5-7 days. To induce ischemic conditions pH was changed to 6.4, glucose concentrations were lowered and the O₂ was restricted as described for the slice preparations. In additional sets of experiments 300 nM of staurosporine (Sigma, Germany) or 2 µM of N,N,N',N'-tetrakis (2-pyridylmehtyl) ethylenediamine (TPEN) (Sigma, Germany) were added to the cell cultures.

For Ca²⁺ measurements, primary neuronal cultures were obtained from E18 embryos or P0 newborns as described above except for the following: Tissue was collected from whole cortices and cells were cultured in Neurobasal-A medium Gibco® (Invitrogen, Germany) containing 2 % B27 supplement, 1 % GlutaMAX-I and 1 % penicillin/streptomycin (all Gibco, Germany). Cells were plated in a density of 50,000 cells/cm² on poly-L-lysine coated coverslips in 24-well plates (Sarstedt, USA) and were held in culture for up to 14 days.

4.10.2. Brain slice preparation and culture

Brain slices including the hippocampus were prepared from 6-10 weeks old *Stim2^{-/-}* mice and wild type littermates as described earlier [134]. In brief, coronal sections were cut on a vibratome (Vibratome®, Series 1000 Classic, St. Louis) in an ice-chilled solution containing (mM): Sucrose, 200; PIPES, 20; KCl, 2.5; NaH₂PO₄, 1.25; MgSO₄, 10; CaCl₂, 0.5; dextrose, 10; pH 7.35 adjusted with NaOH. After preparation slices were transferred to a holding chamber continuously superfused with a solution containing NaCl 120 mM, KCl 2.5 mM, NaH₂PO₄ 1.25 mM, HEPES 30 mM, MgSO₄ 2 mM, CaCl₂ 2 mM and dextrose 10 mM. PH values were adjusted using HCl. To induce *in vitro* ischemic conditions ph values were reduced from 7.25 to 6.4 and lowered glucose

concentration to 5 mM under hypoxic conditions. Restriction of O₂ was achieved by perfusion with an external solution that had been bubbled with nitrogen for at least 60 min prior to and throughout the recordings [135].

4.10.3. Immunocyto- and immunohistochemistry in neurons

After incubation of the hippocampal cell culture or brain slices, they were fixed with 4 % PFA (Merck, Germany), washed 3 times with 10 mM PBS and incubated for 60 min at 4 °C in 10 mM PBS containing 5 % goat serum (GS; PAA Laboratories, Austria) and 0.3 % Triton X100 (Sigma, Germany). Primary antibodies mouse anti-NeuN (1:1000, Chemicon International, Massachusetts), mouse anti-MAP2a/b (1:200, abcam, United Kingdom), rabbit anti-cleaved Caspase-3 (1:150, Cell Signaling, Massachusetts) were diluted in 10 mM PBS and incubated for 12 h at 4 °C. After washing steps with 10 mM PBS, secondary antibodies (Alexa 488 labeled goat anti-mouse 1:100, BD Bioscience Canada; Cy-3 labeled goat anti-rabbit 1:300, Dianova, Germany) were incubated in the same manner. Staining with 0.5 µg/mL DAPI (Merck, Germany) was performed for 7 min. Finally, cultures were washed and subsequently covered with DABCO (Merck, Darmstadt). Pictures were collected by immunofluorescence microscopy (Axiophot; Zeiss, Jena).

4.10.4. Ca²⁺ imaging

Measurements of [Ca²⁺]_i in single cortical neurons were carried out using the fluorescent indicator fura-2 AM in combination with a monochromator-based imaging system (T.I.L.L. Photonics, Germany) attached to an inverted microscope (BX51WI, Olympus, Germany). Emitted fluorescence was collected by a CCD camera. Cells were loaded with 5 µM fura-2-AM (Molecular Probes, The Netherlands) supplemented with 0.01 % Pluronic F127 for 35 min at 20-22 °C in a standard bath solution containing (mM): 140 NaCl, 5 KCl, 1 MgCl₂, 2 CaCl₂, 10 glucose and 10 HEPES, adjusted to pH 7.4 with NaOH. For measurements of [Ca²⁺]_i, cells were held in standard bath solution and fluorescence was excited at 340 and 380 nm. Fluorescence intensities from single cells were acquired in intervals of 2 sec or 20 sec. After correction for the individual background fluorescence, the fluorescence ratio $R = F_{340}/F_{380}$ was calculated. Quantities for [Ca²⁺]_i were then calculated by the equation:

$$[\text{Ca}^{2+}]_i = K_D \beta (R - R_{\min}) / (R_{\max} - R)$$

with $K_D = 224$ nM [136], $\beta = 2.64$, $R_{\min} = 0.272$ and $R_{\max} = 1.987$ obtained from single dye-loaded cells in the presence of 5 μM ionomycin added to standard bath solution or to a solution containing 10 mM EGTA instead of 2 mM CaCl_2 . Individual cells in a given culture dish showed variable kinetics but similar peak amplitudes of the Ca^{2+} transients. Thus, for the average example traces illustrated in Fig. 37, the peak amplitude, but not the kinetics are comparable between dishes and/or cell types. For oxygen-glucose deprivation (OGD) experiments, cells were immediately transferred to a sealed, N_2 -purged (~ 2 l/min) chamber continuously superfused with a N_2 -bubbled solution containing (mM): 140 NaCl, 5 KCl, 1 MgCl_2 , 2 CaCl_2 and 10 HEPES, adjusted to pH 7.4. All experiments were carried out at 20-22 °C. All chemicals were obtained from Sigma (Germany).

4.10.5. tMCAO model

Experiments were conducted on 10-12 weeks old *Stim2^{-/-}* or bone marrow chimeras according to published recommendations for research in mechanism-driven basic stroke studies [137]. Transient middle cerebral artery occlusion (tMCAO) was induced under inhalation anesthesia using the intraluminal filament (6021PK10; Doccol Company, California) technique. After 60 min, the filament was withdrawn to allow reperfusion. For measurements of ischemic brain volume, animals were sacrificed 24 h after induction of tMCAO and brain sections were stained with 2 % 2,3,5-triphenyltetrazolium chloride (TTC; Sigma, Germany). Brain infarct volumes were calculated and corrected for edema as described [138]. Neurological function and motor function were assessed by two independent and blinded investigators 24 h after tMACO as described [138].

4.10.6. Stroke assessment by MRI

Magnetic resonance imaging (MRI) was performed repeatedly at 24 h and 5 days after stroke on a 1.5 Tesla MR-unit (Vision Siemens, Germany) as described [138]. For all measurements, a custom made dual channel surface coil designed for examination of the mice head was used (A063HACG; Rapid Biomedical, Germany). The image protocol comprised a coronal T2-w sequence

(slice thickness 2 mm), and a coronal 3D T2-w gradient echo CISS (Constructed Interference in Steady State; slice thickness 1 mm) sequence. MR images were visually assessed blinded to the experimental group with respect to infarct morphology and the occurrence of intracranial hemorrhage (IHC).

4.11. Statistical analysis

Statistical analysis was performed using the SigmaPlot® software (Systat Software Inc, California). Statistical methods used are given in the figure legends. For the stroke model, results are presented as means \pm SD. Infarct volumes and functional data were tested for Gaussian distribution with the D'Agostino and Pearson omnibus normality test and then analyzed using the two-tailed Student's t test. $p < 0.05$ was considered statistically significant.

5. RESULTS

5.1. STIM2 is expressed in most organs in mouse and is the main isoform in brain

To determine the relevance of STIM2 in different organs, the abundance of both STIM1 and STIM2 isoforms was studied in total protein lysates using western blot (Fig. 9). A STIM2-specific band of 105 kDa and a STIM1-specific band of 90 kDa was detectable in most tissues, except kidney. STIM2 showed an expression pattern partially overlapping with STIM1, except for brain, thymus and platelets. Importantly, STIM2 was clearly detectable in brain, whereas STIM1 was hardly detectable (Fig. 9A). In fact, densitometric analysis of STIM2/STIM1 ratio clearly showed that STIM2 is the dominant isoform in brain and increased in liver, whereas in all other organs tested STIM1 was clearly the dominant (Fig. 9B). This data indicates a higher expression of STIM1 in most organs but brain, where STIM2 seems to be the predominant isoform.

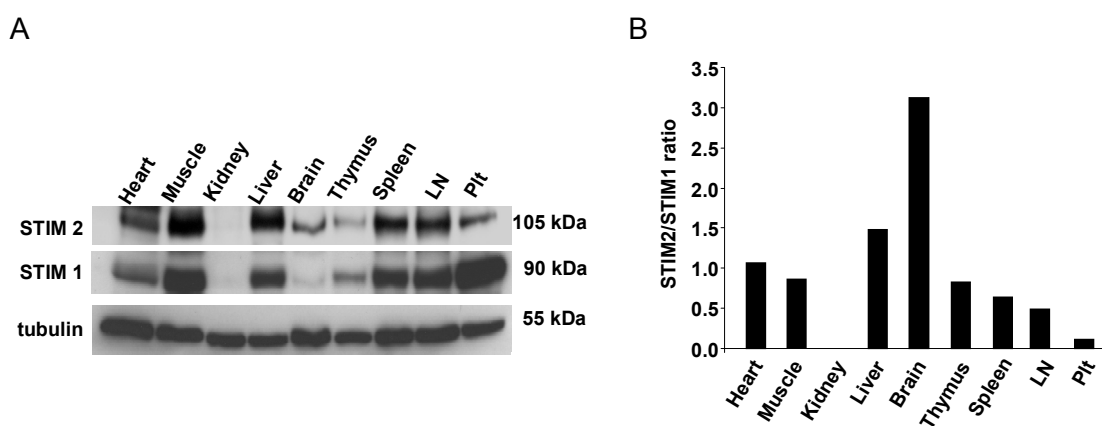


Figure 9. STIM2 is the main STIM isoform in brain. (A) Western blot analysis of STIM1 and STIM2 expression in different organs of 8 weeks old wild-type mice. Tubulin expression was used as loading control. (B) Representative densitometric analysis of STIM2 compared to STIM1 and normalized with tubulin expression in different organs of 8 weeks old wild-type mice, given as STIM2/STIM1 expression ratio (n = 3). LN = lymph nodes, Plt = platelets.

5.2. *Stim2* gene isolation and generation of a *Stim2* knockout mouse

The STIM2 knockout (*Stim2*^{-/-}) mouse was generated together with my laboratory colleague Dr. Attila Braun. Two genomic DNA clones encoding the murine *Stim2* gene (RPC122-446E8; RPC122-394I22) were isolated from a 129Sv BAC library (BACPAC resources center-BPRC-, Children's Hospital Oakland Research Institute-CHORI-, USA), using a probe specific for the exon 4 of murine *Stim2*, isolated by PCR (primers: *Stim2*/BACprobe_F and *Stim2*/BACprobe_R). The targeting vector was designed to delete the *Stim2* gene region that comprises most of the exon 4 and exon 7 (Fig. 11A). The deleted area was substituted by a selection cassette containing the Neomycin resistant gene (Neo) and the β-galactosidase gene (LacZ). The deletion is predicted to result in a frame shift and creation of a premature termination site in the next exon. The targeting vector was built as follows (Fig. 10). The 5'-flanking arm was isolated by long term PCR amplification (Triple Master PCR System, Eppendorf, Germany; primers: 5'flanking/*Stim2*KO/i3_F1 and 5'flanking/*Stim2*KO/E4_R) from the *Stim2* BAC clone and was subcloned in Topo XL[®] vector. It comprises a 3.6 kb region that contains the intron 3 and part of the exon 4 (Fig. 10A). The 3'-flanking arm was isolated by digestion of the *Stim2* BAC clone with the restriction enzyme EcoRV. Digested DNA fragments were subcloned into PBlueScript KS minus vector and the different clones were screened by colony hybridization using a probe specific for the 3'-flanking arm (primers: *Stim2*/BACprobe_F and *Stim2*/BACprobe_R). The 3'-flanking arm comprises a 5.6 kb region that contains the intron 7 to exon 10 (Fig. 10A). These flanking regions facilitate the homologous recombination between the *Stim2* knockout targeting vector and the *Stim2* allele (Fig. 11A). The PCR products were sequenced to confirm the absence of any point mutation or alteration in their DNA sequence. After that, the 5'- and 3'-flanking arms were subcloned into the pWH9 vector, which comprises the pBluescript vector (Fig. 10B) containing a selection cassette (IRES-NEO-PGK promoter-lacZ-polyA). The 5'- and the 3'-arm were subcloned upstream and downstream the selection cassette, respectively. The construct was sequenced again with T3 and T7 primers in order to confirm the correct orientation of the flanking arms. The *Stim2* knockout targeting vector was mapped and verified by different restriction enzymes (Fig. 10C).

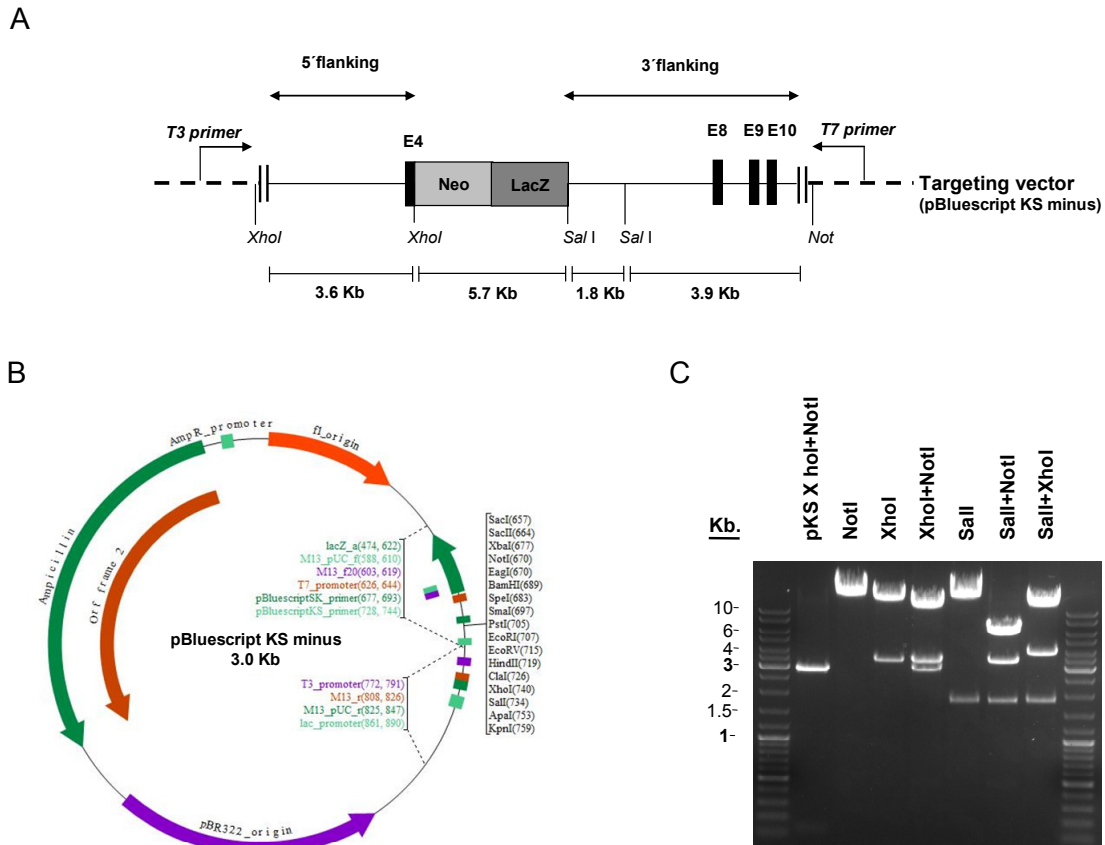


Figure 10. The *Stim2* targeting construct. (A) Restriction map of the *Stim2* knockout targeting vector showing the most important restriction sites and the expected sizes of the digested DNA fragments. **(B)** Schematic representation of the BlueScript KS minus vector. The targeting construct was finally inserted in XhoI-NotI restriction sites. **(C)** Agarose gel electrophoresis showing the enzymatic digested *Stim2* targeting vector and their different products. pKS = BlueScript KS minus vector, Kb = Kilobase.

The targeting vector was linearized with NotI and electroporated into R1 embryonic stem (ES) cells derived from 129Sv mouse strain and selected with the antibiotic geneticin (G418). The ES clones containing the IRES-NEO-LacZ cassette were resistant to geneticin and were able to survive. Targeted ES clones were screened by southern blot using a specific external probe for the *Stim2* gene (Fig. 11B, clone 239). This external probe was generated by PCR amplification (*Stim2*/Extprobe_F1 and *Stim2*/Extprobe_R1) of the *Stim2* BAC clone. The amplified region comprises a 500 bp fragment outside the targeting construct downstream of the 3'-flanking arm (Fig. 11A). *Stim2*^{+/-} ES cells were injected into C57Bl/6 blastocyst in collaboration with Dr. Michael Bösl (Max Planck Institute of Neurobiology, Martinsried), to generate chimeric mice. Chimeric mice were backcrossed with C57Bl/6 (Harlan Laboratories) and subsequent progenies were intercrossed to obtain *Stim2*^{-/-} mice (Fig. 11C). Mouse genotypes were determined by PCR analysis (*Stim2* wild-type 5' and

Stim2 wild-type 3'; *Stim2* knock-out 5' and *Stim2* knock-out 3') or by southern blot (Fig. 11D).

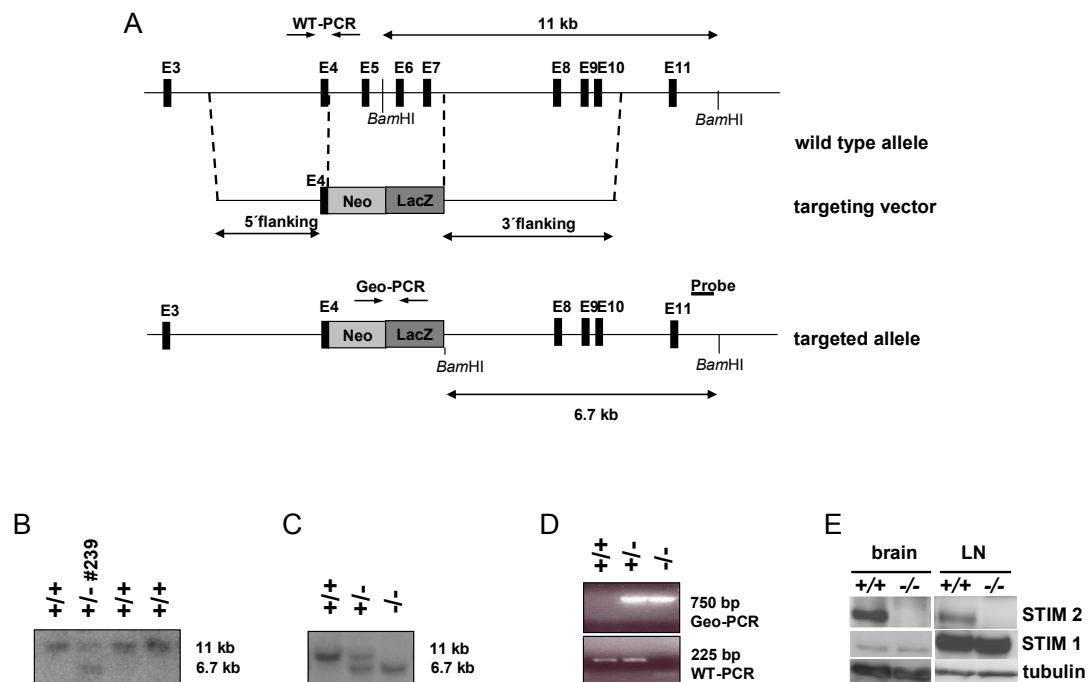


Figure 11. Targeting strategy for the generation of *Stim2*^{-/-} mice. (A) The targeting vector was generated by deletion of most part of the exon four to seven and introduction of Neo-LacZ selection cassette. The neo-LacZ cassette is flanked upstream and downstream by 3 Kb (containing most of the intronic area between exon 3 and 4) and 5 Kb (containing exon 8 to 10) homologous arms, respectively. Neo-LacZ: neomycin resistance and β -galactosidase cDNA cassette. **(B)** Southern blot analysis of BamHI-digested DNA from targeted ES clones labeled with the external probe. Example of a *Stim2* heterozygous (+/-) ES clone (number #239) used for blastocyst injection. **(C)** Southern blot analysis of BamHI-digested genomic DNA of wild-type (+/+), heterozygous (+/-) or *Stim2* knockout (-/-) mice labeled with the external probe. **(D)** PCR analysis of knockout (Geo-PCR) or wild-type (WT-PCR) allele in wild-type (+/+), heterozygous (+/-) or *Stim2* knockout (-/-) mice. **(E)** Western blot analysis of STIM2 and STIM1 expression in brain and lymph node (LN) of 8 weeks old wild-type and *Stim2*^{-/-} mice.

5.3. *Stim2*^{-/-} mice are viable and fertile, but adults die spontaneously

Mice heterozygous for the STIM2-null allele were apparently healthy and had a normal life expectancy (not shown). Intercrossings of these animals yielded *Stim2*^{-/-} mice at the expected Mendelian ratio (*Stim2*^{-/-}: 27.7 %, heterozygous: 51.0 %, wild-type: 21.3 %, n = 249), which developed normally in size and weight to adulthood and were fertile (Fig. 12A, B, D).

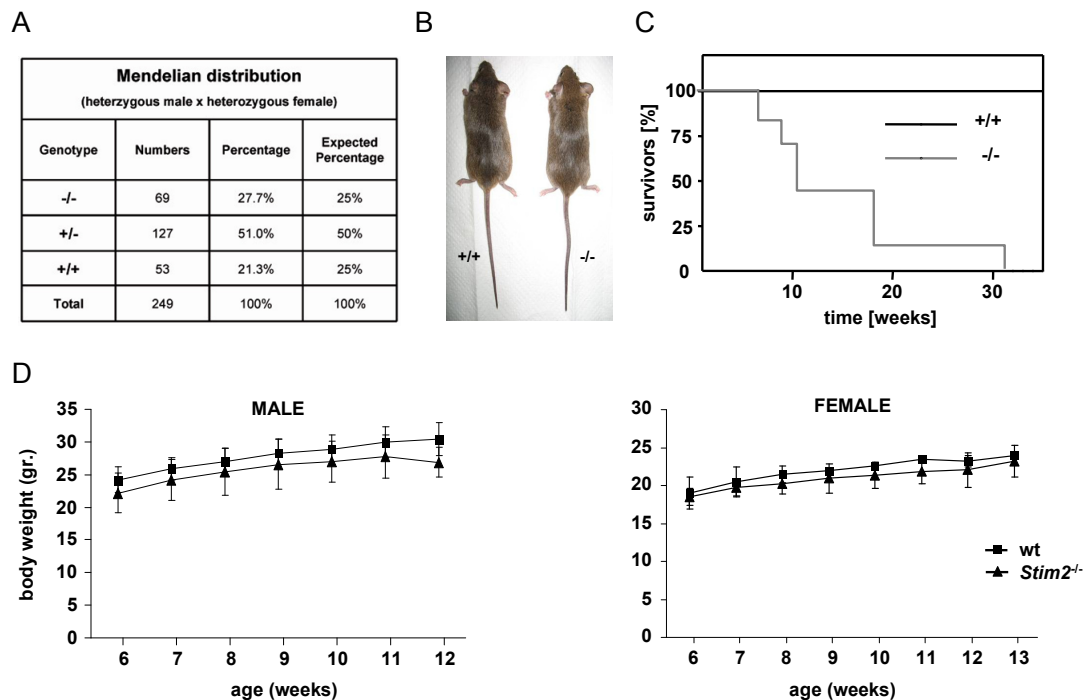
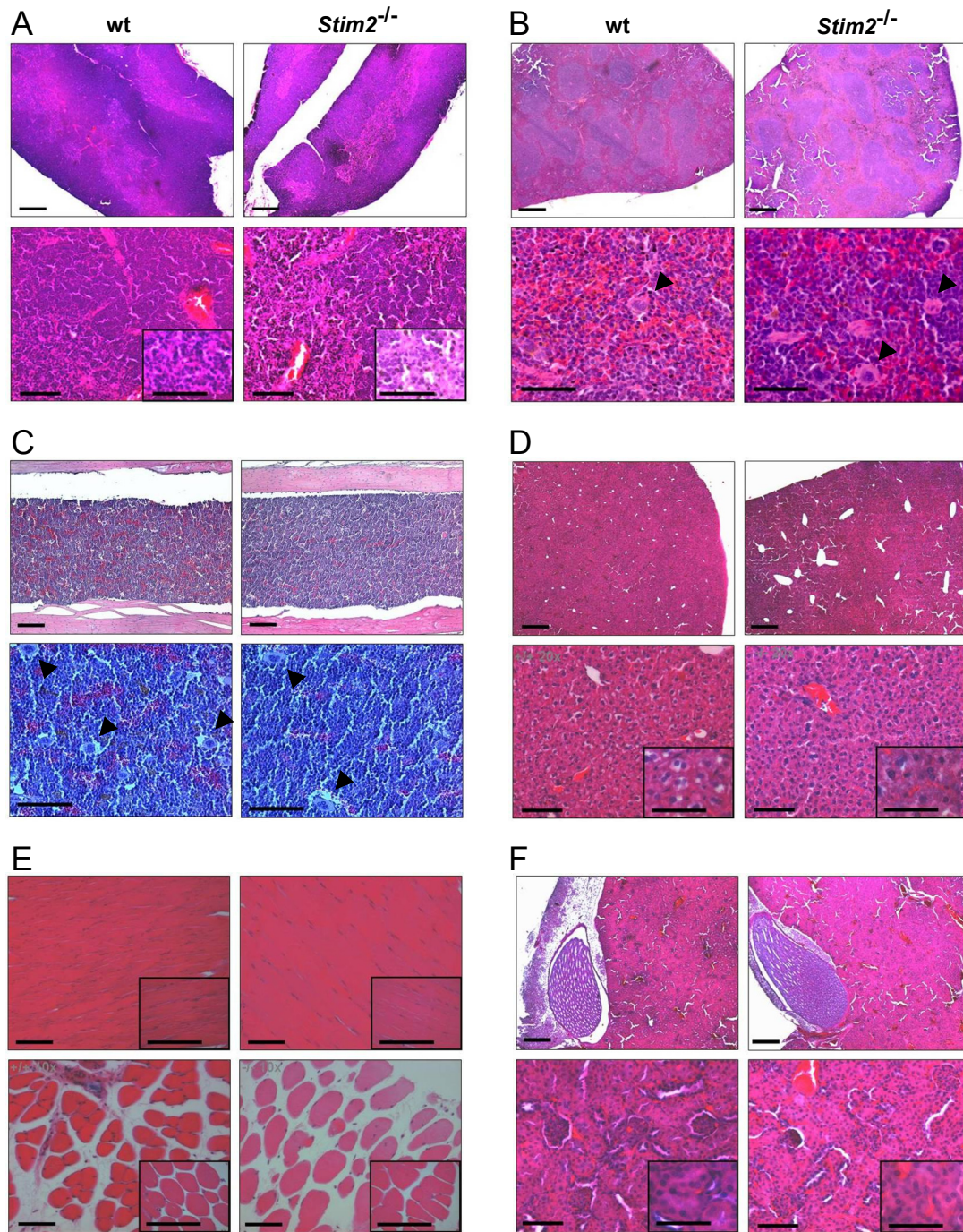


Figure 12. Characterization of *Stim2*^{-/-} mice. (A) Mendelian distribution of *Stim2*^{-/-} (-/-), heterozygous (+/-) and wild-type (+/+) mice as determined in 3-4 weeks old litters. (B) Representative picture of 8 weeks old *Stim2*^{-/-} (-/-) and a littermate wild-type (+/+) male mouse. (C) Lifespan experiment for 10 *Stim2*^{-/-} (-/-, gray line) and 10 littermate wild-type (+/+, black line) male mice over 35 weeks. (D) Body weight evaluation of 6 to 12 weeks old *Stim2*^{-/-} (triangles) and wild-type (squares) control mice (n ≥ 13), represented as mean body weight ± s.d. Differences were considered significant if p < 0.05 (Mann-Whitney U-test).

Western blot analysis confirmed the absence of STIM2 in Knockout brain and lymph nodes (LN) whereas STIM1 expression levels were unaltered (Fig. 11D). Histological examination of major organs showed no obvious abnormalities (Fig. 13).

Starting at the age of 8 weeks after birth pronounced sudden death in *Stim2*^{-/-} mice was observed, and for unknown reasons, only 10 % of the animals reached the age of 30 weeks (Fig. 12C). In humans and small animals, sudden death is a rare and not well understood phenomenon observed in cardiovascular alterations such as heart hypertrophy and arrhythmia, genetic malformations of the heart and epileptic episodes and seizures in the brain [139,140]. Analysis of heart physiology by electrocardiography (ECG) in collaboration with PD. Dr. Sebastian Maier, Inner Medizin, Cardiology, University of Würzburg revealed a normal heart function (Data not shown). Therefore cardiac reasons were discarded.



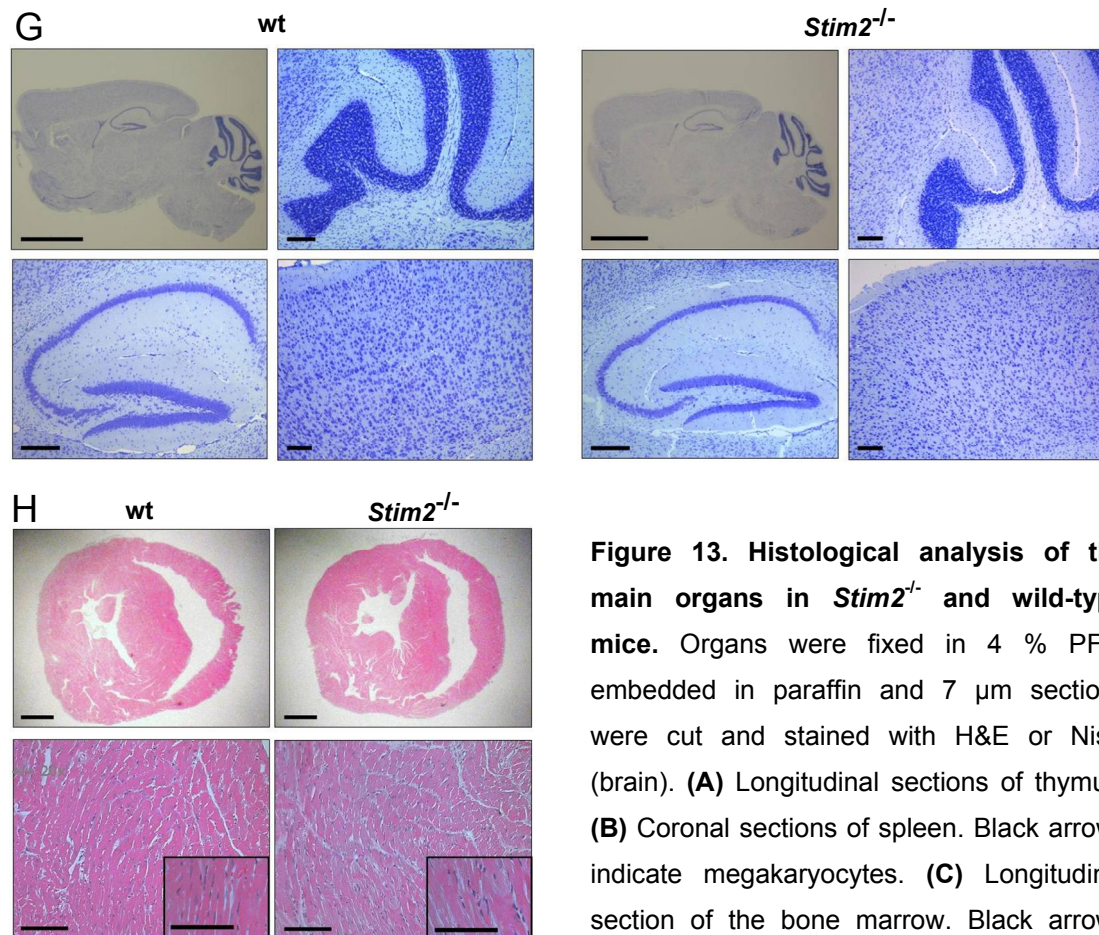


Figure 13. Histological analysis of the main organs in *Stim2*^{-/-} and wild-type mice. Organs were fixed in 4 % PFA, embedded in paraffin and 7 μ m sections were cut and stained with H&E or Nissl (brain). **(A)** Longitudinal sections of thymus. **(B)** Coronal sections of spleen. Black arrows indicate megakaryocytes. **(C)** Longitudinal section of the bone marrow. Black arrows

indicate megakaryocytes. **(D)** Longitudinal sections of liver. **(E)** Longitudinal (upper) and coronal (lower panels) sections of skeletal muscle. **(F)** Longitudinal sections of Kidney. **(G)** Longitudinal sections of whole brain (upper right), cerebellum (upper right), hippocampus (CA1, CA2, CA3 fields and dentate gyrus, lower left) and frontal pole and somatomotor areas of the neocortex. **(H)** Coronal sections of the heart. Scale bars are as follows; upper panels: 400 μ m in all cases but (H) 100 μ m; (G) left: 2.5 mm, right: 250 μ m; (H) 1 mm. lower panels: 50 μ m in all cases but (E) 100 μ m and (G) 250 μ m. Inset: 50 μ m in all cases.

Analyses of different blood parameters (in collaboration with Dr. Thomas Renné (from Institute of Clinical Biochemistry of Würzburg)) were performed to detect possible alterations in the physiology of the different organs (Fig. 14). No obvious differences were detected in 8 weeks old *Stim2*^{-/-} as compared to control mice. Additionally, no sudden death was observed over a period of 50 weeks in 8 weeks old wild-type chimeric mice reconstituted with *Stim2*^{-/-} bone marrow, suggesting that blood cells are also not involved in this process (data not shown). Thus, sudden death in *Stim2*^{-/-} mice is neither associated with alterations in the tested blood parameters, nor with macroscopic alterations in the structure of the main organs, and it is most likely not related to heart

dysfunction. Therefore, a possible hypothesis could be that sudden death can be related to brain dysfunction, although the mechanism remains unclear.

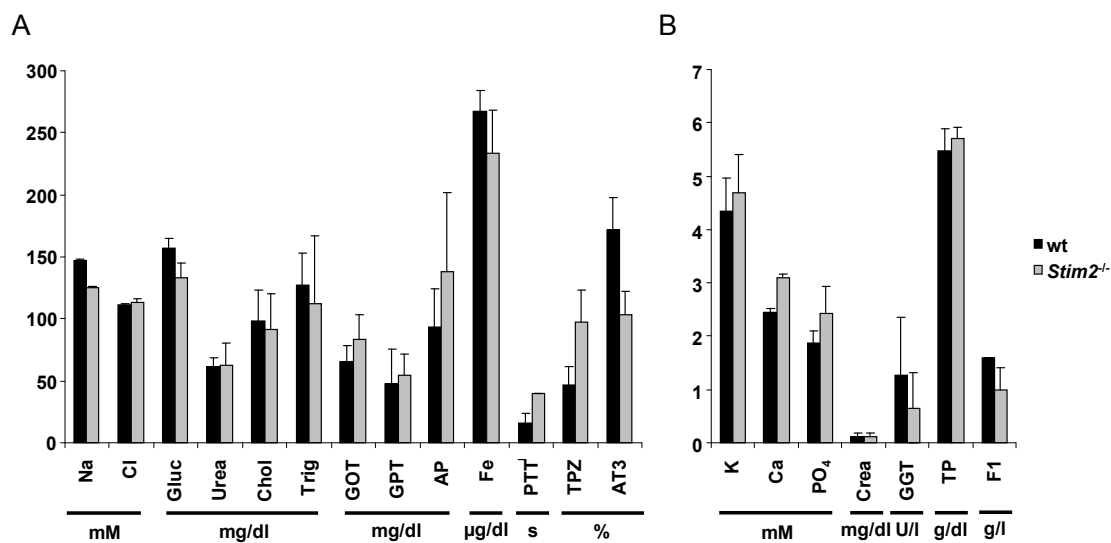


Figure 14. Blood analysis of 8 weeks old mice. (A, B) Levels of different parameters in 8 weeks old wild-type (black bar) and *Stim2*^{-/-} (gray bar) mice blood expressed as a mean \pm s.d., (n = 5). As follows; Ions (Na = Sodium; Cl = chlorine; Fe = iron; K = potassium; Ca = calcium; PO₄ = inorganic phosphates), Transaminases (GOT and GPT), Gluc = glucose, AK = alkaline phosphatase, Chol = Cholesterol, Trig = Triglycerides, TPZ = Prothrombin time, PTT = Partial thromboplastin time, AT3 = Antithrombin III, Crea = Creatinin, GGT = Gamma-Glutamyltransferase, TP = Total Protein, F1 = Fibrinogen. Differences were considered significant if $p < 0.05$ (Mann-Whitney U-test).

5.4. *Stim2*^{-/-} females are not able to feed their offspring

As mentioned before in section (5.3), mating of virgin heterozygous mice yielded apparently healthy *Stim2*^{-/-} mice at the expected Mendelian ratio. In contrast, offspring from virgin *Stim2*^{-/-} breeding died after 7 days (Fig. 15A). The fact that *Stim2*^{-/-} newborns developed normally and were viable in heterozygous breeding indicated that *Stim2*^{-/-} mothers were not able to feed their offspring. In order to confirm this hypothesis, virgin wild-type or *Stim2*^{-/-} females were mated with *Stim2*^{-/-} or wild-type males respectively, and the weight of their heterozygous offspring was measured over time (Fig. 15B).

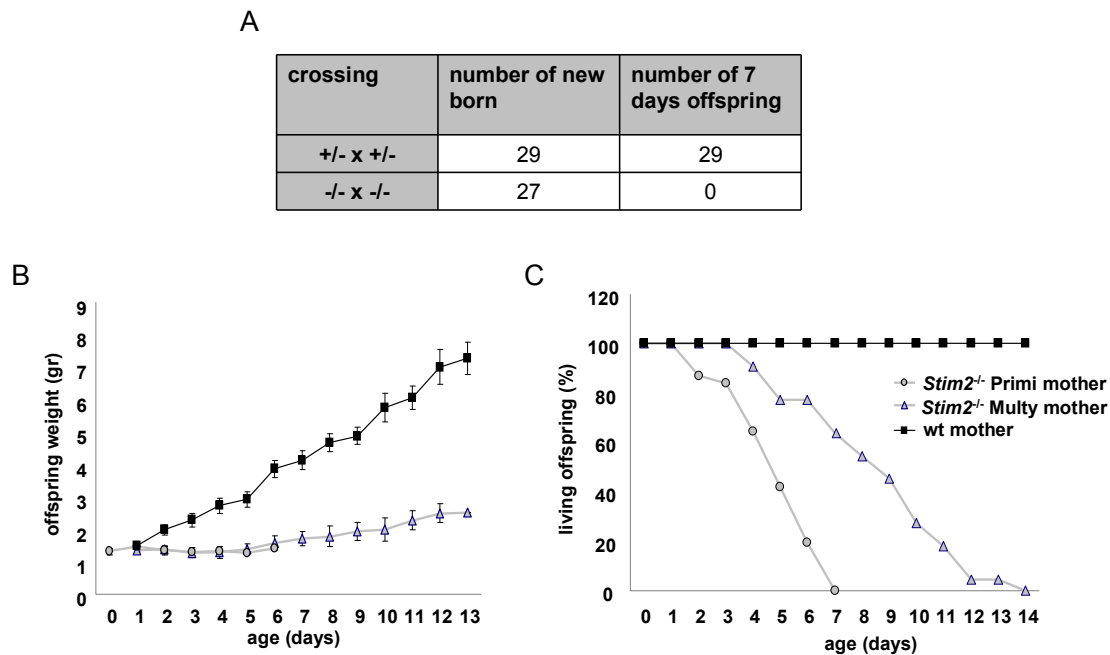


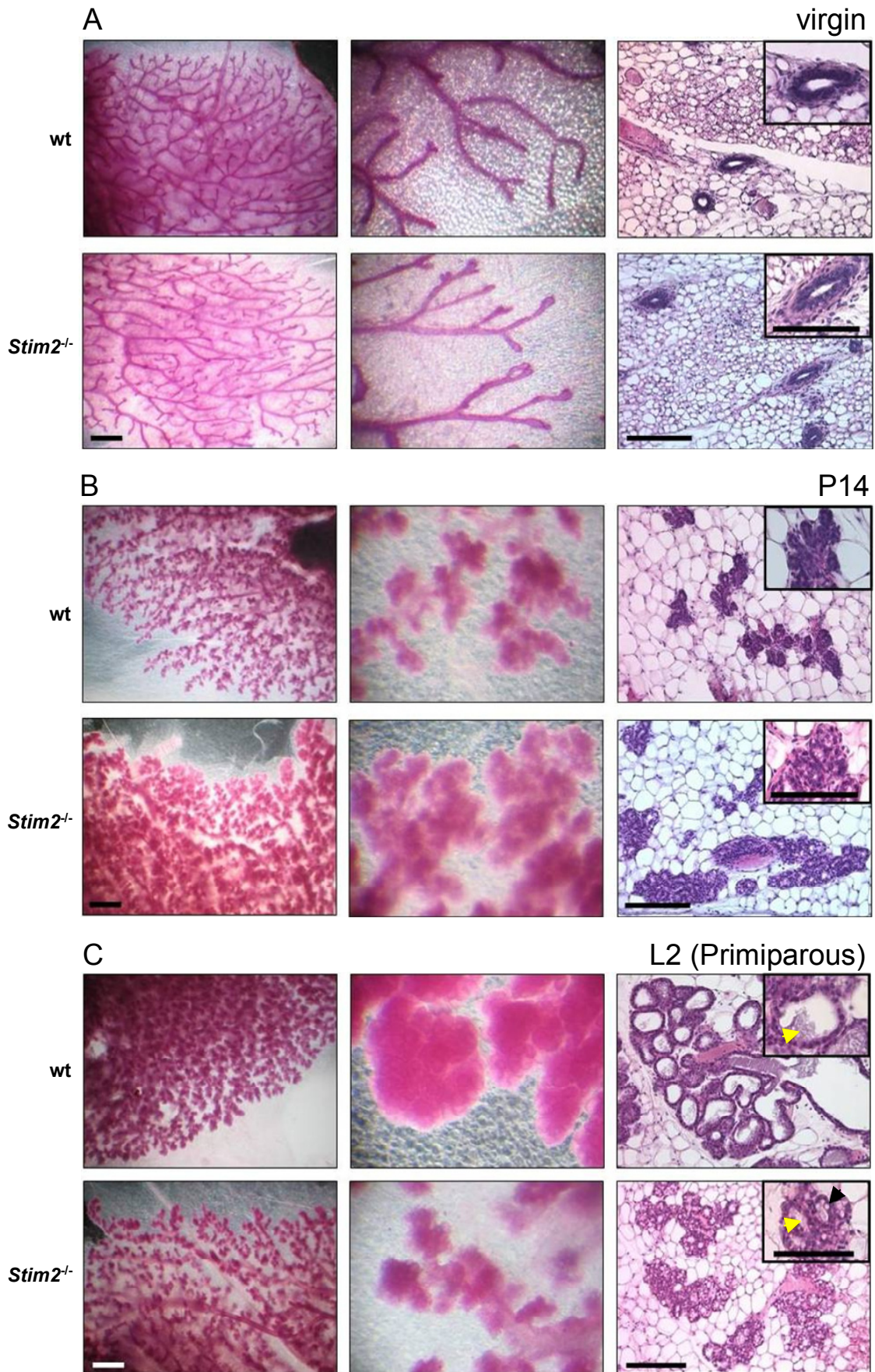
Figure 15. *Stim2*^{-/-} females fail to feed their litters. (A) Table comparing the number of offspring 7 days after birth between heterozygous (+/- x +/-) or homozygous (-/- x -/-) crossings. **(B)** Gain of weight over time of heterozygous newborn fed by wild-type (black square), *Stim2*^{-/-} primiparous (gray circle) or *Stim2*^{-/-} multiparous (gray triangle) females, represented as mean weight (gr.) \pm s.d. ($n \geq 23$). **(C)** Percentage of living offspring fed by wild-type (black square), *Stim2*^{-/-} primiparous (gray circle) or *Stim2*^{-/-} multiparous (gray triangle) females over time ($n \geq 23$).

As a result, heterozygous offspring fed by a primiparous (mated for the first time) *Stim2*^{-/-} female were not able to gain weight and they finally died after 7 days. Additionally, heterozygous offspring fed by multiparous (mated more than one time) *Stim2*^{-/-} females were able to survive longer and gain more weight, but they finally died at day 13 after birth (Fig. 15B, C). This indicates that *Stim2*^{-/-} females are not able to feed their offspring, probably due to a mammary gland dysfunction, and that such an alteration can be partially rescued in further pregnancies.

The mammary gland is a unique organ that undergoes further development during adult stage, which is dependent on hormone signals. This gland shows repeated cycles of development, lactation, and involution for each pregnancy. In newborn, the mammary gland consists of only few rudimentary ducts in the vicinity of the nipple. Pronounced ductal outgrowth and branching starts at puberty and in pregnancy an expanded lobulo-alveolar compartment develops. Functional differentiation of the secretory epithelium coincides with parturition and large amounts of milk are produced and secreted during lactation (for additional information, please refer to [141,142]).

To investigate possible alterations of the mammary gland development during pregnancy, macroscopic analyses of mammary glands in primiparous and multiparous females were performed at different time points (virgin, at day 14 of pregnancy (P14) and lactating day 2 (L2)) (Fig. 16). Whole mammary gland stained with carmine and the H&E paraffin sections revealed normal ductal outgrowth, density and branching at virgin state in *Stim2*^{-/-} and wild-type control females (Fig. 16A). Interestingly, *Stim2*^{-/-} females showed a better developed alveolar system in the mammary gland at P14 as compared to wild-type control females (Fig. 16B), indicating an accelerated development or/and cell proliferation. Primiparous *Stim2*^{-/-} females showed condensed alveoli in the mammary gland with a very small luminal area at L2, in contrast with the well expanded alveoli found in wild-type control females (Fig. 16C). This indicates that alveoli had not differentiated further to a secretory epithelium during delivery, a step considered as the final phase of mammary gland development during pregnancy, and failed to expand the luminal area. *Stim2*^{-/-} mice showed condensed alveoli that contained milk (pink material) in the reduced luminal area (Fig. 16C, yellow arrow) indicating secretion of milk. During lactation, the milk components are synthesized by the epithelial cells at the walls of the alveoli, stored in droplets in the cytoplasm and secreted into the luminal area. However, the accumulation of milk droplets in the cytoplasm of the epithelial cells in *Stim2*^{-/-} females at L2 suggest decreased secretion of milk into the luminal area (Fig. 16C, dark arrow).

Taken together, these results suggest that *Stim2*^{-/-} mammary gland developed faster during pregnancy as compared to wild-type controls but failed to develop further during delivery, impeding a complete expansion of alveoli and impairing the production of sufficient amounts of milk to feed their offspring. In contrast, the mammary gland of multiparous *Stim2*^{-/-} females showed better developed alveoli structure at L2 as compared with primiparous *Stim2*^{-/-} females, showing milk storage inside an almost completely expanded luminal area, indicating secretion of milk and better development of alveoli (Fig. 16D, yellow arrow). Thus, regarding the fact that multiparous *Stim2*^{-/-} females were also not able to feed their offspring, the reduced luminal area found in the alveoli in primiparous *Stim2*^{-/-} females can not explain itself impairment in offspring feeding. Therefore, this part of the analysis of *Stim2*^{-/-} mice will be continued further in the future.



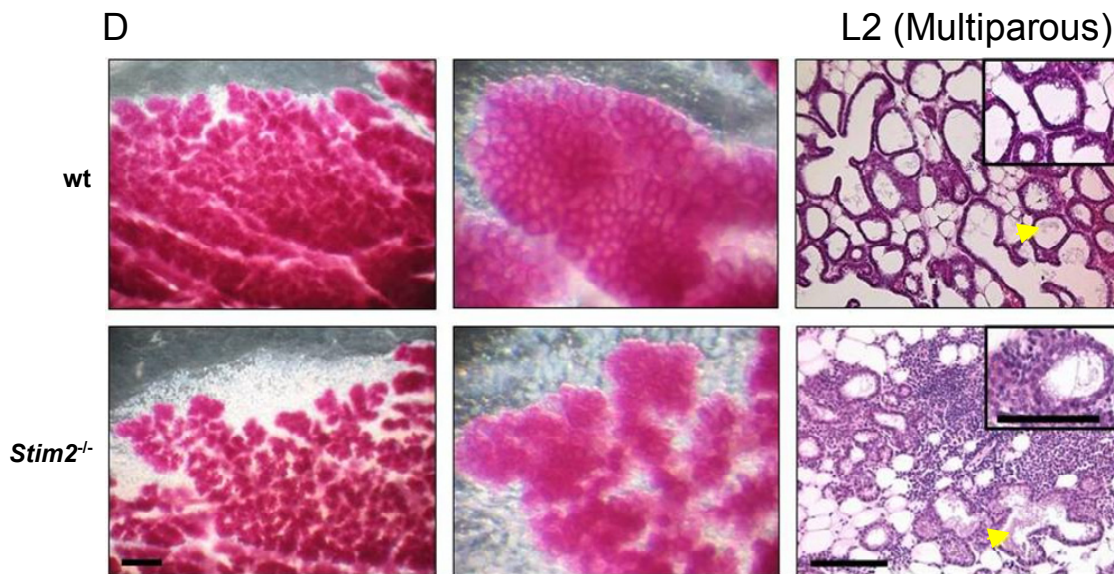


Figure 16. Histological analysis of female mammary glands at virgin, day 14 of pregnancy (P14) or day 2 of lactation (L2). Whole inguinal mammary glands were isolated from 8 weeks *Stim2*^{-/-} and wild-type females, fixed in 4 % PFA and stained with carmine (left and central panels) or cut in 7 µm paraffin sections and stained with H&E (right panels). (A) Mammary glands isolated from virgin, (B) primiparous at P14, (C) primiparous at L2 and (D) multiparous at L2 *Stim2*^{-/-} and wild-type females. Yellow arrows indicate presence of milk (pink colour) inside the luminal area, black arrows indicate droplets accumulated inside the secretory mammary endothelial cells. Scale bars are: left and middle panels: 100 µm, right panels: 50 µm; insets: 50 µm.

5.5. Analysis of STIM2-deficient platelets

5.5.1. STIM2-deficient platelets are normal in number, size and surface glycoprotein expression and display a normal life span *in vivo*

Analysis of protein expression by western blot showed that STIM2 is significantly expressed in wild-type platelets and is absent in STIM2 knockout platelets (Fig. 17A). Platelet size, counts and surface glycoprotein expression were analyzed in STIM2-deficient and wild-type platelets using Sysmex cell counter and flow cytometry, respectively (Fig. 17A-C). STIM2-deficient platelets were comparable in size, numbers and glycoprotein expression to wild-type controls (platelet size: 5.74 ± 0.23 fl in *Stim2*^{-/-}; 5.79 ± 0.23 fl in wt; n = 11; $p \geq 0.05$. platelet counts: 1000 ± 200 plt/ μ L in *Stim2*^{-/-}, 1000 ± 170 plt/ μ L in wt; n = 5; $p \geq 0.05$).

To study platelet life span in the blood stream *in vivo*, platelets were labeled by injection of a fluorescence-coupled antibody against GPIX surface protein

(Dylight-488 conjugated anti-GPIX Ig derivative) intravenously (i.v) in *Stim2*^{-/-} and wild-type mice (Fig. 17D). The antibody does not alter platelet function [132], and the percentage of labeled cells was assessed along 5 days by flow cytometry. After a single injection, *Stim2*^{-/-} mice showed normal platelet clearance from the blood stream as compared to wild-type controls, excluding preactivated STIM2-deficient platelets in resting conditions. Finally, H&E-stained paraffin sections of bone marrow and spleen did not show any alteration in macroscopic structure or in megakaryocyte numbers (Fig. 13C).

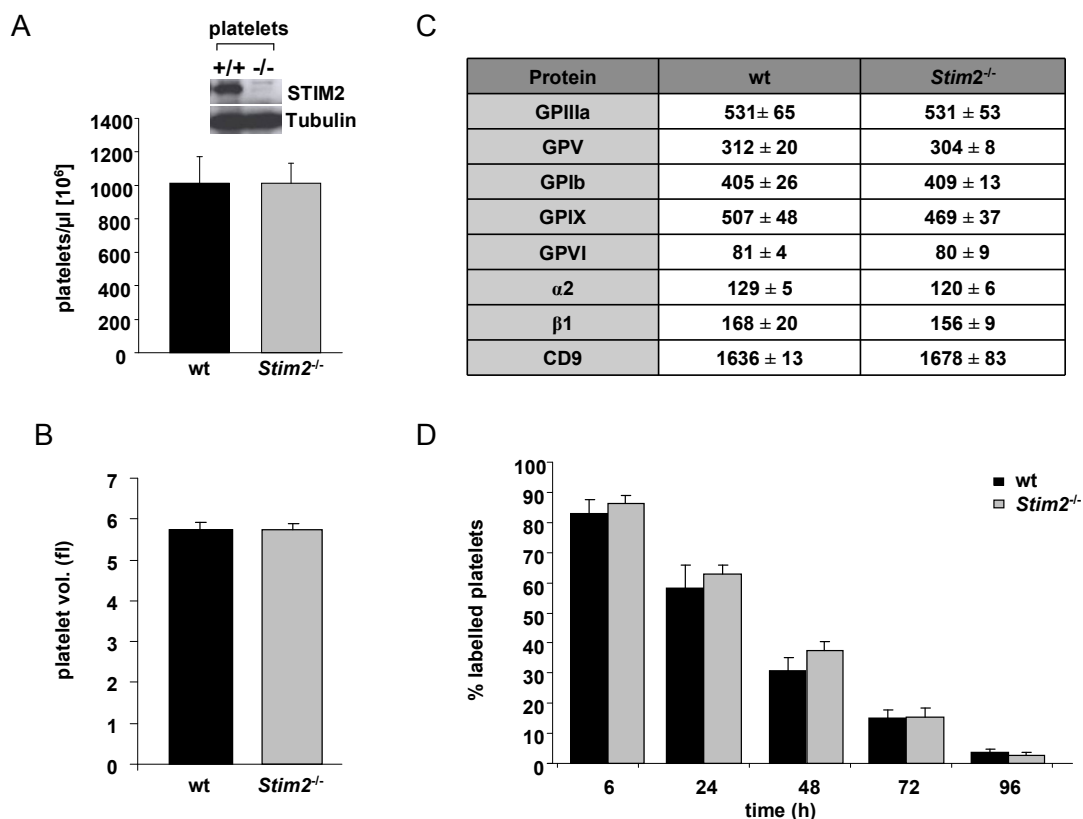


Figure 17. *Stim2*^{-/-} mice showed no alteration in platelet production and life span. **(A)** Western blot showing STIM2 expression in wild-type and absence in *Stim2*^{-/-} platelets. Platelet counts in wild-type (black bar) and *Stim2*^{-/-} (gray bar) determined by flow cytometry, represented as mean platelets ($\times 10^6$)/ μL blood \pm s.d. (n = 8). **(B)** Platelet volume determination by a SYSMEX cell counter in wild-type (black bar) and *Stim2*^{-/-} (gray bar) blood, represented as mean platelet volume (femtoliters) \pm s.d. (n = 8). **(C)** Expression level of prominent platelet surface receptors in resting platelets measured by flow cytometry, represented as mean relative fluorescence intensity \pm s.d. (n = 8). **(D)** Platelet life span determination in wild-type (black bar) and *Stim2*^{-/-} (gray bar) mice. Platelets were labeled *in vivo* by injection of 0.5 $\mu\text{g/g}$ mouse weight Dylight-488 conjugated anti-GPIX Ig derivative. The percentage of fluorescently-labeled platelets in whole blood was determined in 24 h intervals by flow cytometry. Data are represented as mean % of fluorescently labeled platelets \pm s.d. (n = 5). Differences were considered significant if $p < 0.05$ (Mann-Whitney U-test).

Taken together, these results indicate that STIM2 deletion does not affect the platelet formation and production from megakaryocytes.

5.5.2. Unaltered Ca²⁺ homeostasis in STIM2-deficient platelets

During my thesis work, STIM2 was proposed by Brandman *et al.* to function as a Ca²⁺ sensor in the ER, regulating basal [Ca²⁺]_i and ER Ca²⁺ levels [9]. Therefore, the effect of STIM2 deficiency on Ca²⁺ homeostasis was tested upon activation in platelets loaded with Fura-2, a fluorescent free-[Ca²⁺] indicator (Fig. 18). Under resting conditions, basal [Ca²⁺]_i was normal in Stim2-deficient platelets as compared to wild-type controls (wt: 48.25 ± 15.97 nM; *Stim2*^{-/-}: 56 ± 16.77 nM; n = 5; p > 0.05) (Fig. 18A). To assess SOCE, Ca²⁺ release from the ER Ca²⁺ store was induced by the sarco-/ER Ca²⁺ ATPase (SERCA) inhibitor TG (5 μM) in the absence of extracellular Ca²⁺ (Fig. 18A, B). Ten min after TG stimulation, Ca²⁺ release from ER was also similar in STIM2-deficient and wild-type platelets (wt: 114.75 ± 38.18 nM; *Stim2*^{-/-}: 129.50 ± 39.11 nM; n = 5; p > 0.05), indicating normal Ca²⁺ levels in ER Ca²⁺ stores in STIM2-deficient cells (Fig. 18A, B). After addition of 1 mM extracellular Ca²⁺, a second [Ca²⁺]_i peak indicated the presence of SOCE in STIM2-deficient platelets, which showed no differences in amplitude as compared to wild-type controls (wt: 1426.25 ± 703.77 nM; *Stim2*^{-/-}: 1262.14 ± 606.77 nM; n = 5; p > 0.05) (Fig. 18A, B). Thus, STIM2 deletion does not alter basal [Ca²⁺]_i, ER Ca²⁺ levels and SOCE in platelets.

Additionally, [Ca²⁺]_i changes were assessed in the presence of extracellular Ca²⁺ upon platelet stimulation with agonists activating G-protein-coupled signaling pathways, such as thrombin, ADP or the TxA₂ analogue U46619 (data not shown), as well as ITAM-coupled signaling pathways, such as the collagen related peptide (CRP) that stimulates the collagen receptor glycoprotein (GP)VI (Fig. 18A, B). After agonist addition, [Ca²⁺]_i raised exceeding the basal [Ca²⁺]_i level, indicating SOCE (Fig. 18A). In this case, comparable results were obtained in STIM2-deficient and wild-type control platelets with all agonist tested, indicating no altered Ca²⁺ homeostasis and SOCE after platelet stimulation through the main activation pathways (Fig. 18B). Thus, STIM2 does not seem to play a major role in regulation of basal [Ca²⁺]_i, ER Ca²⁺ levels, SOCE and Ca²⁺ signaling in response to all major agonists. A crucial role for STIM1, a homologue of STIM2, in SOCE in platelets has been described [6]. Western blot analysis of STIM expression revealed a dominant expression of STIM1 in platelets, although this method does not provide quantitative

information (Fig. 9B). Therefore, a possible hypothesis could be that STIM1 can compensate STIM2 deficiency indicating a redundant function of STIM2 in SOCE in platelets, at least under the tested conditions.

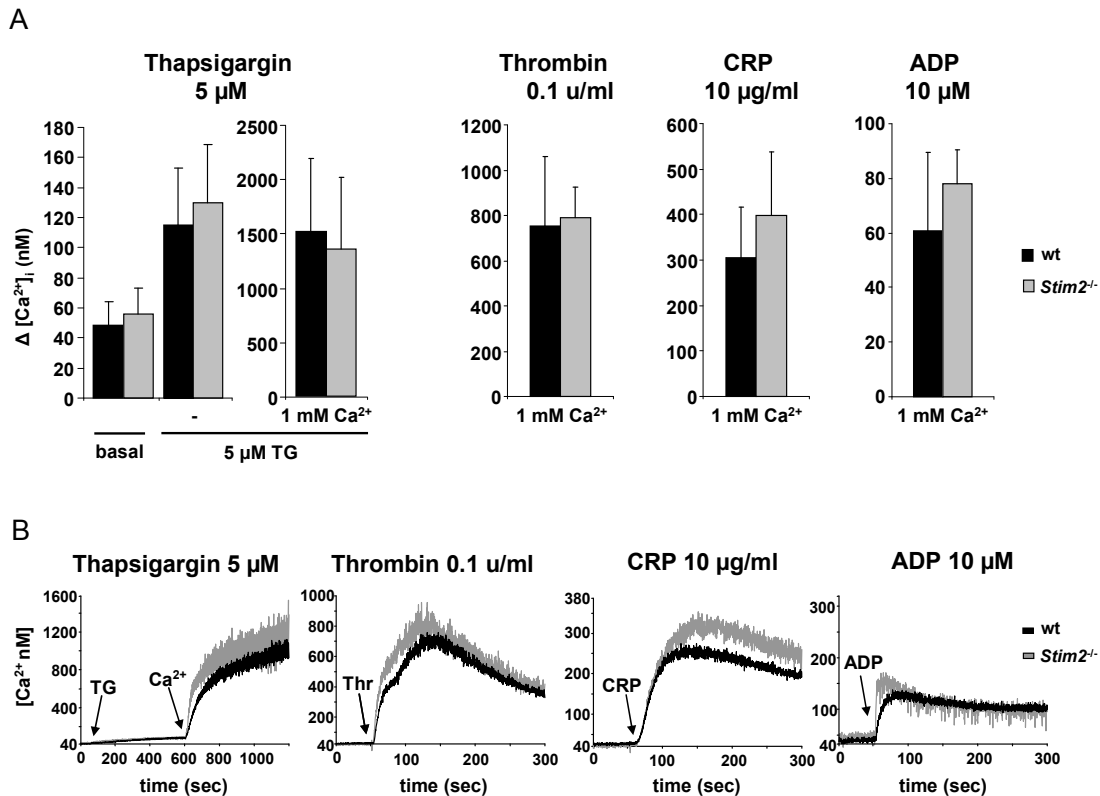


Figure 18. Normal Ca^{2+} homeostasis and SOCE in STIM2-deficient platelets upon agonist stimulation. Washed Fura-2 loaded platelets were stimulated with the indicated agonist in the presence or absence of 1 mM extracellular Ca^{2+} , and $[Ca^{2+}]_i$ was assessed using a Perkin-Elmer LS55 fluorimeter. **(A)** Bar graphs representation of maximal $[Ca^{2+}]_i$ changes after addition of the indicated agonists, given as mean increase of $[Ca^{2+}]_i$ ($\Delta[Ca^{2+}]_i$ (nM)) \pm s.d. **(B)** Representative Ca^{2+} measurements of the upper bar graphs. Values represented as mean $[Ca^{2+}]_i$ (nM) \pm s.d. ($n \geq 5$). Black arrows indicate the time points of agonist addition, TG = thapsigargin, Thr = thrombin. Differences considered significant if $p < 0.05$ (Mann-Whitney U-test).

5.5.3. Normal function of *Stim2*-deficient platelets *in vitro*

To test the functional consequences of STIM2 deficiency in platelets *in vitro*, activation studies were performed upon agonist stimulation using flow cytometry (Fig. 19) and aggregometry (Fig. 20). Flow cytometric studies of GPIIb/IIIa (integrin α IIb β 3) activation using the JON/A-PE antibody (preferentially binds to the high affinity conformation of mouse integrin α IIb β 3) [143], and of

degranulation-dependent P-selectin surface exposure after platelet activation showed that STIM2-deficient platelets become fully activated in response to thrombin, CRP, ADP+U46619, convulxin (CVX) or rhodocytin (Fig. 19). CVX and rhodocytin are platelet aggregators isolated from snake venom that bind to the receptor GPVI and Clec-2, respectively. Therefore, the loss of STIM2 does not impair integrin activation and degranulation in response to GPVI (ITAM signaling) as well as G-protein coupled agonist activation.

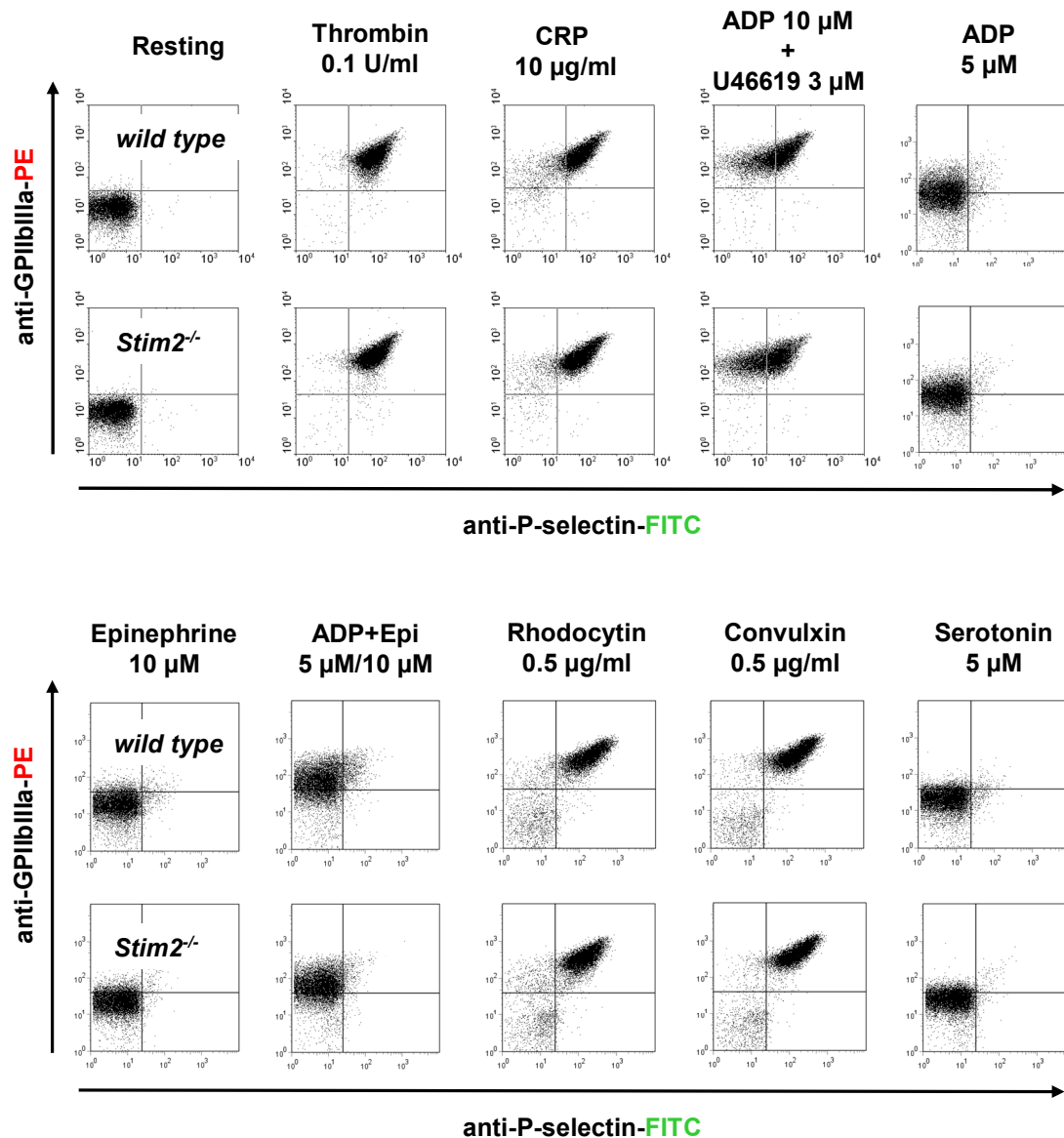
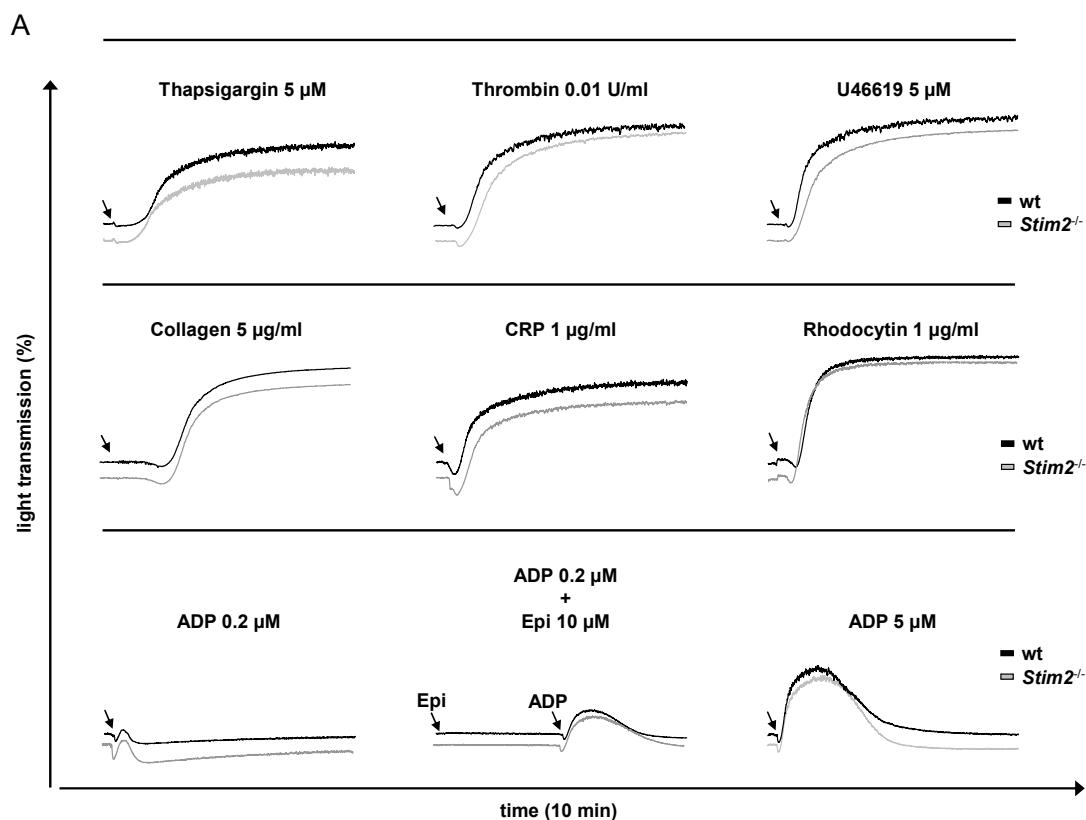


Figure 19. *Stim2*-deficient platelets are normally activated *in vitro*. Flow cytometric analysis of α IIb β 3 integrin activation and degranulation-dependent P-selectin exposure in response to the indicated agonists. Representative dot plots of wild-type and STIM2-deficient platelets (n = 8 per group). Epi = Epinephrine.

To study the effect of STIM2 deficiency on platelet aggregation *in vitro*, platelets were isolated from wild-type and *Stim2*^{-/-} mice and stimulated with different agonist in presence of 1 mM extracellular Ca²⁺ (Fig. 20).

Stimulation of wild-type platelets with 5 μ M TG induced platelet aggregation, indicating that passive Ca²⁺ depletion from the ER store is sufficient to produce normal aggregation in platelets, without additional stimulation of upstream activating pathways (Fig. 20A, upper lane left). Stimulation of STIM2-deficient platelets with 5 μ M TG produced the same effect as compared to wild-type controls (wt: 58.71 \pm 18.94 %; *Stim2*^{-/-}: 55.17 \pm 24.65 %; n = 6; p > 0.05) (Fig. 20B).

Furthermore, STIM2-deficient platelets aggregated normally and reached similar maximum aggregation rates as compared to wild-type controls in the presence of thrombin, collagen, CRP, ADP, U46619 or rhodocytin (Fig. 20A, B). Addition of 0.2 μ M ADP did not induce aggregation either in wild-type control or STIM2-deficient platelets (Fig. 20A, lower lane left). In contrast, 5 min incubation with 10 μ M epinephrine prior to platelet stimulation with 0.2 μ M ADP induced significant platelet aggregation (Fig. 20A, lower lane middle). Under these conditions, no differences in maximum aggregation rates were observed between STIM2-deficient platelets and wild-type control platelets (wt: 25.30 \pm 7.10 %; *Stim2*^{-/-}: 30.73 \pm 5.89 %; n = 4; p > 0.05) (Fig. 20B).



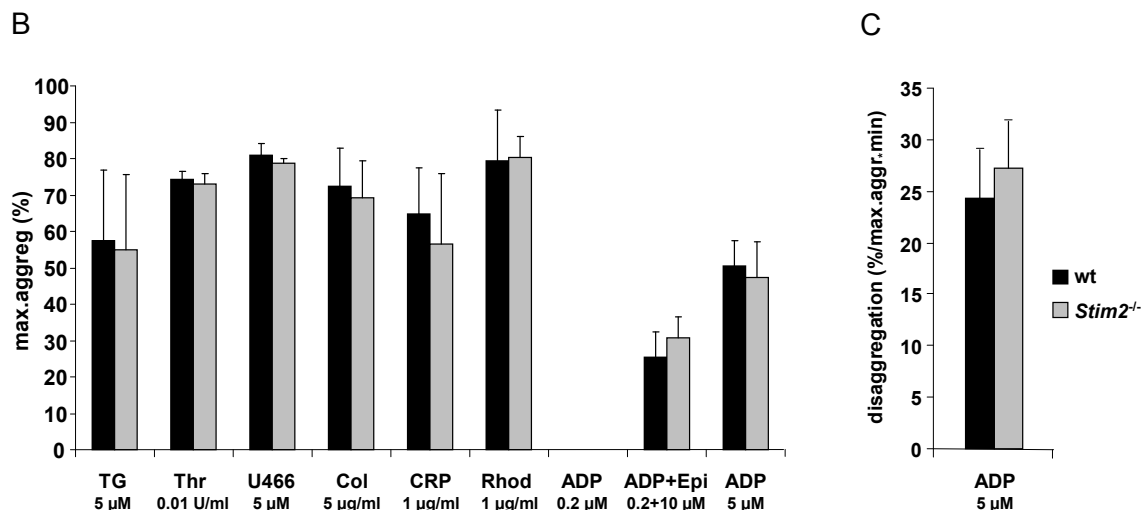


Figure 20. *Stim2*^{-/-} platelets aggregate normally *in vitro*. Wild-type or STIM2-deficient platelets were isolated, stimulated with the indicated agonist and the activity was assessed by recording light transmission in an aggregometer. TG = thapsigargin, Thr = thrombin, Col = collagen, Rhod = rhodocytin and Epi = epinephrine. **(A)** Representative aggregation measurements of platelets isolated from wild-type (black line) and *Stim2*^{-/-} mice (gray line), given as light transmission (%). Black arrows indicate the time points of agonist addition. **(B)** Bar graph representation of maximal platelet aggregation after stimulation with the indicated agonists on platelets isolated from wild-type (black line) and *Stim2*^{-/-} mice (gray line), given as mean Max. Aggregation (%) \pm s.d. ($n > 5$ per group). **(C)** Bar graph representation of disaggregation slopes after maximal aggregation induced by addition of 5 μ M ADP in platelet-rich-plasma (prp). Disaggregation was calculated as the difference on light transmission values after the maximal aggregation per minute, given as mean disaggregation (%/max.aggr.min) \pm s.d. ($n = 5$ per group). The higher is the value, the faster is the disaggregation. Differences were considered significant if $p < 0.05$ (Mann-Whitney U-test).

STIM2-deficient platelets showed a tendency (but no significant) to disaggregate faster as compared to wild-type control platelets when activated with 5 μ M ADP in prp (wt: 24.26 ± 6.15 %/max.aggr.min; *Stim2*^{-/-}: 27.17 ± 5.34 %/max.aggr.min; $n = 6$; $p > 0.05$) (Fig. 20C). The disaggregation was calculated as the difference on light transmission values after the maximal aggregation per minute.

Thus, despite this minor difference in disaggregation after ADP activation, the *in vitro* results indicate that the absence of STIM2 does not significantly affect platelet activation *in vitro*.

5.5.4. Tyrosine phosphorylation assay

To test a possible altered activation pathway in *Stim2*^{-/-} platelets, tyrosine phosphorylation of signaling proteins was analysed in washed platelets upon activation with a strong agonist (Fig. 21). Platelets were stimulated with 2.5 µg/mL CVX. Aliquots were collected at different time points from the same sample. For western blot analysis, the anti-phosphotyrosine IgG 4G10 was used to detect phosphorylated tyrosines in whole protein lysates. Wild-type platelets showed a band migrating at 35 kDa which decreased in intensity 60 sec after activation with 2.5 µg/mL CVX, indicating dephosphorylation activity. In contrast, this band decreased in intensity 120 sec after activation in *Stim2*^{-/-} platelets, indicating a delay in dephosphorylation. According to the molecular weight of the band LAT was proposed as candidate. However the importance of this delayed dephosphorylation observed in *Stim2*^{-/-} platelets is not clear.

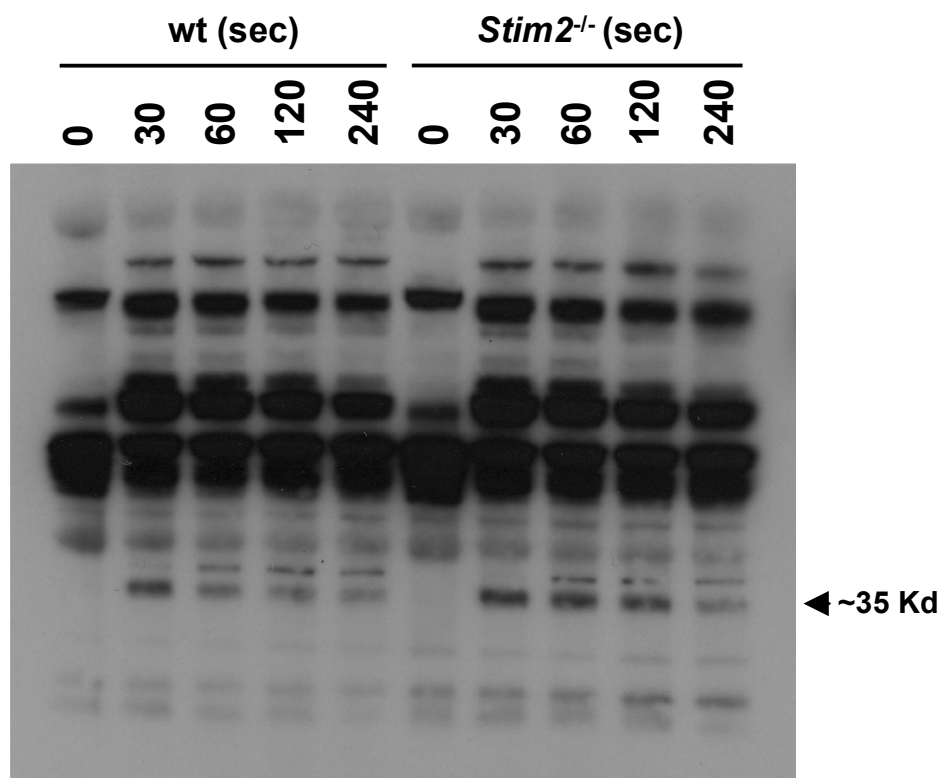


Figure 21. *Stim2*^{-/-} platelets showed a delayed dephosphorylation in a 35 kDa unidentified protein. Platelets isolated from *Stim2*^{-/-} or wt mice were incubated with constant stirring in Tyrode's buffer, supplemented with 0.5 M EDTA to avoid aggregation, and stimulated with 2.5 µg/mL CVX. Aliquots were collected at the indicated time points for western blot analysis using the anti-phosphotyrosine Ig 4G10 (n = 3). Black arrow indicates the size of the band.

5.5.5. Normal spreading and thrombus formation of *Stim2*^{-/-} platelets *ex vivo*

In vivo, platelet activation on the exposed ECM or a growing thrombus occur in flowing blood, where shear conditions, rheological characteristics of the blood stream and rapid clearance of produced soluble mediators play important roles for thrombus formation and stabilization. Under these conditions, *Stim2*^{-/-} platelets could potentially show different activity than during *in vitro* conditions. Therefore, the ability of *Stim2*^{-/-} platelets to form thrombi *ex vivo* on collagen-coated surfaces was analyzed in a whole blood perfusion system [130] under medium (1000 s⁻¹) or high shear conditions (1700 s⁻¹) (Fig. 22). As in the wild-type controls, *Stim2*^{-/-} platelets adhered to collagen fibers, formed aggregates within 3 min and grew into large thrombi within 5 min (Fig. 22B, D).

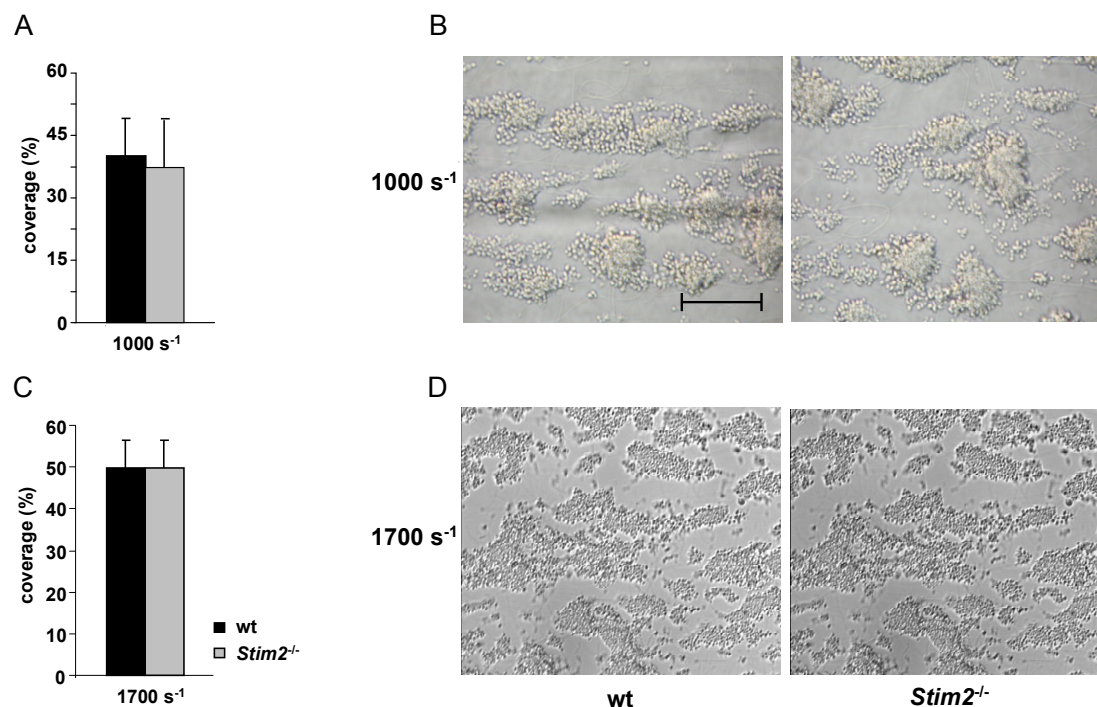


Figure 22. Normal thrombus formation in *Stim2*^{-/-} mice *ex vivo*. Wild-type and *Stim2*^{-/-} whole blood were perfused over a collagen-coated surface at a medium (1000 s⁻¹, upper) or high shear rate (1700 s⁻¹, lower) for 4 min. **(A, C)** Surface area covered by wild-type (black bar) or *Stim2*^{-/-} (gray bar) platelets/thrombi is given as a mean of 5 experiments \pm s.d. **(B, D)** Representative phase contrast images taken 4 min after washing at the end of the experiment. Scale bar, 100 μ m. Differences were considered significant if $p < 0.05$ (Mann-Whitney U-test).

As consequence, the surface area covered by platelets and the total thrombus volume were similar to wild-type controls at high (50 \pm 6 % for wt; 50 \pm 8 % for

Stim2^{-/-}; n = 5; p > 0.05) or medium (40 ± 8 % for wt; 38 ± 10 % for *Stim2*^{-/-} n = 5; p > 0.05) shear conditions (Fig. 22A, C). These findings indicate that STIM2 is not required for platelet activation on collagen, and on the surface of growing thrombi under conditions of medium or high shear *ex vivo*.

Finally, an *in vitro* spreading assay was performed on human fibrinogen-coated (100 µg/mL) slides to evaluate the effect of STIM2 absence on integrin-mediated adhesion and subsequent activation of “outside-inside” signaling pathways, platelet shape change and spreading (Fig. 23). Upon platelet activation in the presence of 0.05 U/mL thrombin, *Stim2*^{-/-} platelets could spread normally within the expected time of 20 min. Hence, no differences were observed as compared to wild-type control platelets. In conclusion, absence of STIM2 does not alter the ability of platelets to spread and to perform shape-change upon activation, indicating a normal activation of the “outside-in” signaling of the integrin α IIb β 3.

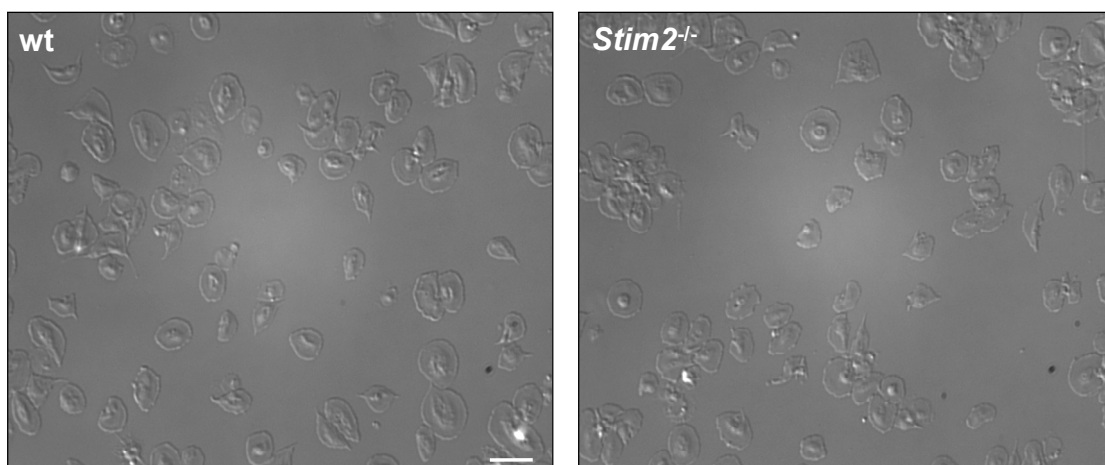


Figure 23. *Stim2*^{-/-} platelets spread normally on fibrinogen. Representative phase contrast images of wild-type (wt) or *Stim2*^{-/-} (*Stim2*^{-/-}) platelets activated with 0.05 U/mL thrombin on 100 µg/mL human fibrinogen-coated coverslips. Scale bar, 5 µm.

5.5.6. Normal function of *Stim2*^{-/-} platelets in murine *in vivo* models

As platelet aggregation may contribute to pathologic occlusive thrombus formation, the effects of STIM2 deficiency on ischemia and infarction were studied by *in vivo* fluorescence microscopy following ferric chloride-induced mesenteric arteriole injury. In all wild-type control mice, the formation of small aggregates was observed ~5 min after injury, increased in size after 10 min, with progression to complete vessel occlusion within 20 min (mean occlusion

time: 1110 ± 250 sec) (Fig. 24B, C). Similar results were obtained in *Stim2*^{-/-} mice, displaying no differences in thrombus formation as compared to wild-type control mice (n = 6 each).

An additional assay was performed to address the effect of STIM2 deletion in platelet hemostatic function: the tail bleeding time model (Fig. 24A). After cutting a 1 mm tail tip in anesthetized mice, wild-type control mice were able to stop bleeding within 300 sec. Similar results were obtained in *Stim2*^{-/-} mice (n = 12 each).

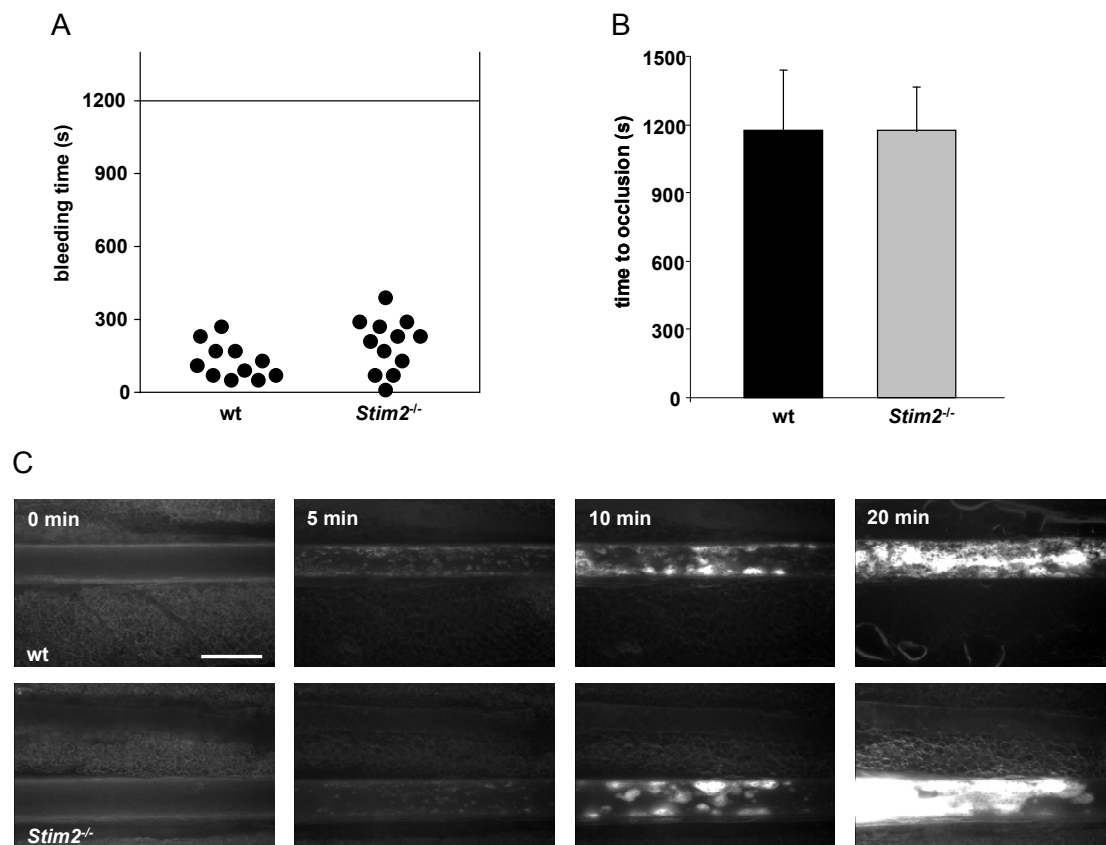


Figure 24. Normal bleeding time and thrombus formation in *Stim2*^{-/-} mice *in vivo*. (A) One mm tail tip was cut and individual tail bleeding times were monitored for 20 min. (B) Thrombosis was induced in mesenteric arterioles in wild-type (black bar) and *Stim2*^{-/-} (gray bar) mice by topical application of FeCl₃ and the time to complete occlusion was determined by Intravital microscopy. Mean occlusion time \pm s.d. (C) Representative pictures of one experiment. Occlusion occurred in both, the wild-type and *Stim2*^{-/-} mouse. Indicated time points represent minutes after FeCl₃-induced injury. Scale bar, 25 μ m. Differences were considered significant if $p < 0.05$ (Mann-Whitney U-test).

Thus, taken all platelet results together, the conclusion is that STIM2 deletion has no effect in platelet activity, thrombus formation and haemostasis neither *in vitro*, nor *in vivo*. This may be explained by a compensation of STIM2 function

by its homologue isoform STIM1, which shows stronger expression in platelets (Fig. 9 A, B).

5.6. Analysis of STIM2 deficiency in immune cells

In immune cells, the predominant pathway of Ca^{2+} entry is thought to involve IP_3R -mediated SOCE. Previous reports suggested a possible role of STIM2 in Jurkat T cells, and cells of the immune system [2,53]. Therefore, the effect of STIM2 deletion in the innate (mast cells and macrophages) and the adaptive (B and T cells) immune system was studied, together with my colleagues David Stergner and Timo Vögtle, respectively.

5.6.1. The effect of STIM2 deletion on the innate immune system: Mast cells

5.6.1.1. Stim2 deletion does not alter Ca^{2+} homeostasis and SOCE in mast cells

To analyze the effect of STIM2 deficiency on Ca^{2+} homeostasis and SOCE in mast cells, $[\text{Ca}^{2+}]_i$ changes were assessed in Fura-2-loaded peritoneal (PMC) and bone marrow *in vitro* differentiated (BMDC) mast cells (kindly produced by AG Huber, University of Freiburg) from *Stim2*^{-/-} and wild-type adult littermates (Fig. 25). Under resting conditions, no significant differences in basal $[\text{Ca}^{2+}]_i$ was observed in *Stim2*^{-/-} PMC (wt: 44.00 ± 7.42 nM; *Stim2*^{-/-}: 43.50 ± 29.03 nM; n = 5; p > 0.05) or BMDC (wt: 42.83 ± 17.26 nM; *Stim2*^{-/-}: 68.20 ± 32.62 nM; n = 6; p > 0.05) as compared to wild-type control mast cells (Fig. 25C). To assess SOCE, Ca^{2+} store release was induced by addition of 5 μM TG in the absence of extracellular Ca^{2+} . 10 min after TG stimulation, Ca^{2+} release from intracellular stores was also similar in BMDC (wt: 30.67 ± 15.58 nM; *Stim2*^{-/-}: 41.30 ± 21.86 nM; n = 6; p > 0.05) or PMC (wt: 21.67 ± 12.58 nM; *Stim2*^{-/-}: 12.33 ± 2.52 nM; n = 5; p > 0.05) and wild-type control mast cells, indicating normal Ca^{2+} levels in intracellular stores in *Stim2*^{-/-} cells (Fig. 25A, C). After addition of 1 mM extracellular Ca^{2+} , a second $[\text{Ca}^{2+}]_i$ peak indicated the presence of SOCE, which showed no significant differences in amplitude between *Stim2*^{-/-} PMC (wt: 88.33 ± 57.52 nM; *Stim2*^{-/-}: 57.67 ± 29.26 nM; n = 5 each; p > 0.05) or BMDC (wt: 86.75 ± 53.05 nM; *Stim2*^{-/-}: 48.00 ± 28.80 nM; n = 6; p > 0.05) and

wild-type control mast cells (Fig. 25C). Thus, STIM2 deletion does not alter basal $[Ca^{2+}]_i$, nor basal ER Ca^{2+} levels or SOCE in mast cells.

Mast cell activation mediated by the high-affinity receptors for IgE ($Fc\epsilon R_s$) is considered to be a key event in mast cell function for the allergic inflammatory response. This comprises secretion of inflammatory mediators, activation of transcription factors, and the elaboration of cytokines. LAT-mediated signals are initiated following activation and aggregation of $Fc\epsilon R_1$, resulting in the synergistic activation of $PLC\gamma_1$ and PKC. This leads to an increase in Ca^{2+} mobilization and degranulation [102].

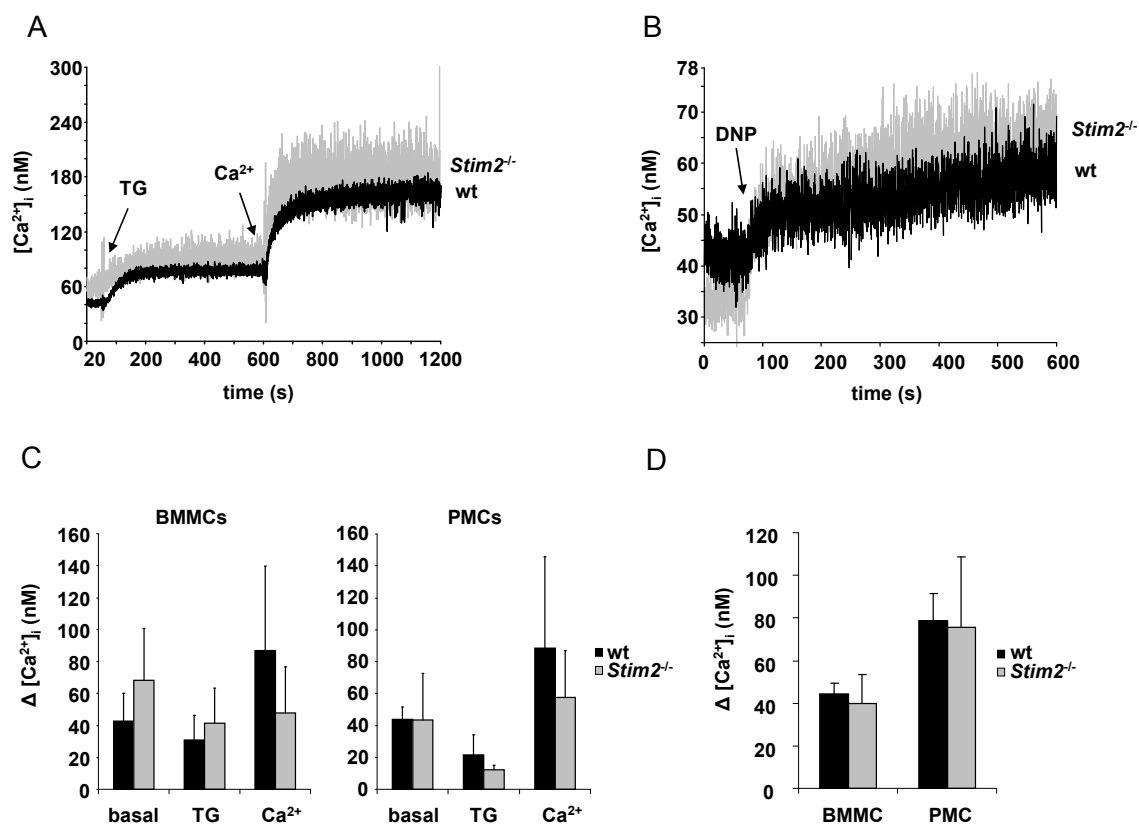


Figure 25. Normal Ca^{2+} homeostasis and SOCE in *Stim2*^{-/-} mast cells. Fura-2-loaded bone marrow (BMMC) or peritoneal (PMC) *in vitro* differentiated mast cells were stimulated with 5 μM TG for 10 min or IgE+DNP-HSA for 180 sec, in the absence or presence of 1 mM extracellular Ca^{2+} , respectively, and $[Ca^{2+}]_i$ was monitored. **(A, B)** Representative measurements of $[Ca^{2+}]_i$ in wild-type (black line) and *Stim2*^{-/-} mice (gray line), given as $[Ca^{2+}]_i$ (nM) \pm s.d. Black arrows indicate the time points of agonist addition. **(C)** Bar graph representation of basal $[Ca^{2+}]_i$ levels (basal), $[Ca^{2+}]_i$ increase after store depletion (TG) and maximal increase of $[Ca^{2+}]_i$ after extracellular Ca^{2+} addition (Ca^{2+}) compared to baseline levels (black bar for wild-type, gray bar for *Stim2*^{-/-} mice), given as mean $\Delta[Ca^{2+}]_i \pm$ s.d. ($n = 5$ per group). **(D)** Bar graph representation of maximal increase in $[Ca^{2+}]_i$ after addition of 20 ng/ μL DNP-HAS antigen in the presence of extracellular Ca^{2+} , compared to basal $[Ca^{2+}]_i$ levels (black bar for wild-type, gray bar for *Stim2*^{-/-} mice). Results given as mean $\Delta[Ca^{2+}]_i \pm$ s.d. ($n = 5$ per group). Differences were considered significant if $p < 0.05$ (Mann-Whitney U-test).

Experiments using Ca^{2+} -sensing fluorescent dyes and patch clamp suggest that $\text{Fc}\epsilon\text{R}$ -mediated Ca^{2+} influx in mast cells may occur by SOCE [144]. Therefore, Changes in $[\text{Ca}^{2+}]_i$ in response to $\text{Fc}\epsilon\text{R}$ stimulation via FcR crosslinking were also assessed using IgE antibodies directed against 2,4-Dinitrophenyl hapten conjugated to human serum albumin (DNP-HSA) as substrate in the absence of extracellular Ca^{2+} (Fig. 25B, D). Mast cells were incubated overnight with 150 ng/ μL anti-DNP-HSA IgE and the next day, the $[\text{Ca}^{2+}]_i$ was assessed in the presence 20 ng/ μL of the antigen DNP-HSA and 1 mM extracellular Ca^{2+} . Five min after stimulation with DNP-HSA, $[\text{Ca}^{2+}]_i$ increase was similar in *Stim2*^{-/-} mast cells (*Stim2*^{-/-} PMC: 75.63 ± 32.94 nM; *Stim2*^{-/-} BMMC: 40.00 ± 13.23 nM, n = 9; p > 0.05) as compared to wild-type control cells (wt PMC: 78.75 ± 12.50 nM; wt BMMC: 44.50 ± 5.07 nM; n = 10) indicating unaltered SOCE in STIM2-deficient mast cells (Fig. 25D). Thus, the Ca^{2+} measurements indicate that STIM2 deletion has no effect in $[\text{Ca}^{2+}]_i$ homeostasis and SOCE in mast cells after stimulation via store depletion by TG or IgE-mediated $\text{Fc}\epsilon\text{R}$ activation.

5.6.1.2. *Stim2*^{-/-} mice are protected against IgE-mediated anaphylaxis independently of mast cells

Mast cells play a central role in allergic inflammatory responses. The manifestations of mast-cell-driven allergic reactions, for instance anaphylaxis, are considered to be mainly due to the release of pro-inflammatory mediators following antigen-induced aggregation of $\text{Fc}\epsilon\text{R}$ s [102]. To test a possible effect of STIM2 deletion on mast cells function during inflammation, despite the fact that Ca^{2+} homeostasis was not affected, IgE-mediated response of mast cells was tested in systemic anaphylaxis murine *in vivo* model (Fig. 26). Mice received by intravenous injection (i.v.) a dosage of 30 μg anti-DNP IgE per mouse. 24 h later, 250 μg of DNP-HSA antigen was injected i.v. and the body temperature was subsequently measured every 10 min using a rectal probe. Wild-type mice showed a pronounced decrease in body temperature, reaching the minimum 40 min after injection (31.42 ± 0.95 °C; n = 6) (Fig. 26A). Surprisingly, *Stim2*^{-/-} mice showed a significant mild decrease in body temperature, reaching the minimum 20 min after injection (34.62 ± 1.09 °C; n = 6; p < 0.01). The differences in body temperature between wild-type and *Stim2*^{-/-} mice were significant at all time points tested. Thus, this result indicates that *Stim2*^{-/-} mice are protected from IgE-mediated systemic anaphylaxis. Since our previous results showed that Ca^{2+} homeostasis and SOCE are not

significantly altered in mast cells lacking STIM2, bone marrow chimeras were generated using wild-type mice transplanted with *Stim2*^{-/-} bone marrow (*Stim2*^{+/+}^{-/-}BM) to study the possible contribution of endothelial or other cells to the protective phenotype found in IgE-mediated systemic anaphylaxis (Fig. 26B). Wild-type platelets from host mice were effectively removed as most of the population in *Stim2*^{+/+}^{-/-}BM chimeras were STIM2-deficient platelets, derived from the donor *Stim2*^{-/-} bone marrow (Fig. 26C). *Stim2*^{+/+}^{-/-}BM chimeric mice did not show the protective observed in *Stim2*^{-/-} mice, and body temperature time course was similar to wild-type controls after IgE injection (n = 6) (Fig. 26B). Thus, the protective effect displayed by *Stim2*^{-/-} mice in IgE-mediated anaphylaxis model is independent of mast cells. Therefore, it is most likely due to an altered function in other cell types such as the endothelial cells of blood vessels. Despite the interest of these findings, our aim was more focused on the analysis of STIM2 deficiency in hematopoietic system. Since our data indicated that mast cells seem not to be altered, the study was not followed up in this work. However these questions will be addressed in further studies.

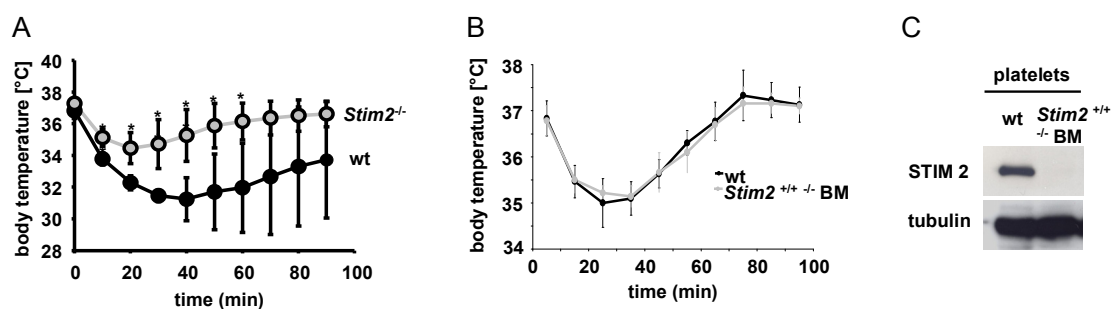


Figure 26. IgE-mediated anaphylaxis *in vivo* model. *Stim2*^{-/-}, wild-type or bone marrow chimeras (*Stim2*^{+/+}BM^{-/-}) were injected i.v. with 30 µg anti-DNP IgE per mouse 24 h before, and the next day the body temperature was measured every 10 min after injection of the DNP-HSA antigen (250 µg per mouse). **(A)** Graph representation of *Stim2*^{-/-} (gray line) and wild-type (black line) body temperature at the indicated time points after i.v. injection of IgE (n = 6). **(B)** Graph representation of *Stim2*^{+/+}BM^{-/-} (gray line) and wild-type (black line) body temperature at the indicated time points after i.v. injection of IgE (n = 6). **(C)** Representative western blot analysis of wild-type and STIM2-deficient platelets from wild-type control mice and *Stim2*^{+/+}^{-/-}BM chimeras, respectively. *p < 0.05, **p < 0.01. Differences were considered significant if p < 0.05 (Mann-Whitney U-test).

5.6.2. The effect of STIM2 deletion on the innate immune system: Macrophages

5.6.2.1. Stim2 deletion does not alter Ca^{2+} homeostasis and SOCE in macrophages

Although STIM1 seems to be strongly expressed in macrophages, western blot analysis showed a weak expression of STIM2 (Fig. 27A). Additionally, Oh-hora *et al.* showed that murine T cell activation leads to a substantial increase in STIM2 expression, nevertheless amounted to only a small proportion (3–10%) of total STIM protein [5]. Therefore, to analyze the role of STIM2 in Ca^{2+} homeostasis and SOCE in macrophages, $[\text{Ca}^{2+}]_i$ changes were assessed in Fura-2-loaded macrophages isolated by lavage of the peritoneal cavity from *Stim2*^{-/-} and wild-type adult mice (Fig. 27). Under resting conditions, *Stim2*^{-/-} macrophages showed slightly (but statistically not significant) elevated basal $[\text{Ca}^{2+}]_i$ as compared to controls (basal wt: 28.20 ± 14.18 nM; basal *Stim2*^{-/-}: 37.67 ± 15.08 nM; n = 5; p > 0.05), indicating normal basal $[\text{Ca}^{2+}]_i$ in the absence of STIM2 (Fig. 27C). To assess SOCE, Ca^{2+} store release was induced by addition of 5 μM TG in the absence of extracellular Ca^{2+} (Fig. 27B, C). Ten min after TG stimulation, Ca^{2+} release from the intracellular stores was also slightly higher in amplitude as compared to wild-type control mice but this difference was not significant (wt: 30.20 ± 6.72 nM; *Stim2*^{-/-}: 36.83 ± 17.99 nM; n = 5; p > 0.05), indicating normal Ca^{2+} content in the ER stores in *Stim2*^{-/-} macrophages (Fig. 27C). After addition of 1 mM extracellular Ca^{2+} , a second $[\text{Ca}^{2+}]_i$ peak was observed indicating the presence of SOCE in wild-type macrophages (Fig. 27B). Again, the increase in amplitude in *Stim2*^{-/-} cells was not significant as compared to wild-type control macrophages (wt: 91.60 ± 25.50 nM; *Stim2*^{-/-}: 118.83 ± 34.83 nM; n = 5; p > 0.05) (Fig. 27C). Thus, STIM2 deletion does not alter basal $[\text{Ca}^{2+}]_i$, Ca^{2+} content in the ER and SOCE in macrophages after stimulation of intracellular Ca^{2+} stores depletion.

Fc receptors for IgG (Fc γ Rs) control a wide variety of cellular responses in macrophages, such as antibody-dependent cell-mediated cytotoxicity, phagocytosis and release of inflammatory mediators. These responses are involved in cellular destruction and the amplification of normal and pathologic immune reactions *in vivo* [145]. Braun *et al.* found severely defective TG-induced SOCE and Fc γ Rs-triggered Ca^{2+} responses in *Stim1*^{-/-} macrophages, demonstrating for the first time that SOCE is the predominant mechanism of Ca^{2+} entry downstream of Fc γ Rs activation and that STIM1 is a critical mediator

of this process [173]. Therefore, changes in $[Ca^{2+}]_i$ in response to direct $Fc\gamma R$ activation were also assessed (Fig. 27E, F).

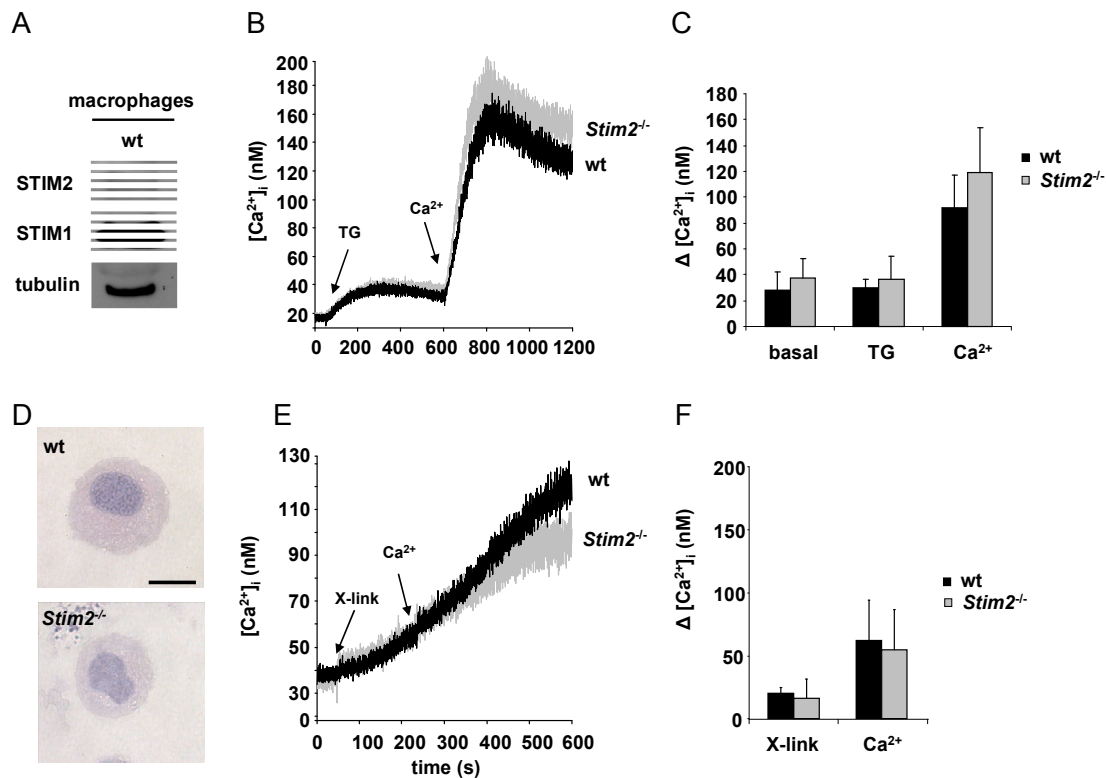


Figure 27. Normal Ca^{2+} homeostasis and SOCE in $Stim2^{-/-}$ macrophages. Fura-2-loaded peritoneal macrophages were stimulated for 10 min with 5 μM thapsigargin (TG) or for 180 sec with 2.4G2 (10 $\mu g/mL$) cross-linking (X-link) followed by addition of extracellular Ca^{2+} , and $[Ca^{2+}]_i$ was monitored. **(A)** Representative western blot analysis of STIM1 and STIM2 expression in cells isolated by peritoneal lavage of 2 month old wild-type mice. Tubulin expression was used as loading control ($n = 3$). **(B, E)** Representative measurements of $[Ca^{2+}]_i$ in wild-type (black line) and $Stim2^{-/-}$ (gray line) macrophages stimulated with TG or 2.4G2 Ig cross-linking, respectively ($n = 5$ per group). Black arrows indicate the time points of agonist addition. **(C)** Bar graphs representation of basal $[Ca^{2+}]_i$, increase after store depletion by TG (TG) and maximal increase in $[Ca^{2+}]_i$ compared to basal levels, given as mean $\Delta[Ca^{2+}]_i$ (nM) \pm s.d. ($n = 5$ per group), before and after addition of 1 mM extracellular Ca^{2+} . **(D)** H&E stainings of peritoneal resting wild-type and $Stim2^{-/-}$ macrophages. Bar scale: 10 μm . **(F)** Bar graphs representation of $[Ca^{2+}]_i$ increase after store depletion by 2.4G2 Ig plus cross-linking (x-link) and maximal increase in $[Ca^{2+}]_i$, given as mean $\Delta[Ca^{2+}]_i$ (nM) \pm s.d. ($n = 5$ per group), before and after addition of 1 mM extracellular Ca^{2+} . Differences were considered significant if $p < 0.05$ (Mann-Whitney U-test).

To assess SOCE, cells were incubated for 15 min with 10 $\mu g/mL$ 2.4G2 Ig, a monoclonal antibody against the extracellular homologous region of both $Fc\gamma RII$ and $Fc\gamma RIII$ [147], and Ca^{2+} store release was induced by 2.4G2 cross-linking

with a secondary Ig (10 µg/mL) in the absence of extracellular Ca²⁺ (Fig. 27E). 180 sec after cross-link stimulation, Ca²⁺ release from intracellular stores was similar in *Stim2*^{-/-} cells as compared to wild-type controls (wt: 20.00 ± 5.00 nM; *Stim2*^{-/-}: 20.75 ± 15.56 nM; n = 5; p > 0.05), indicating normal Ca²⁺ release from the ER Ca²⁺ store in *Stim2*^{-/-} macrophages (Fig. 27F). After addition of 1 mM extracellular Ca²⁺, no differences in SOCE were observed in *Stim2*^{-/-} cells as compared to wild-type controls (wt: 62.00 nM ± 32.13 nM; *Stim2*^{-/-}: 62.25 ± 30.05 nM; n = 5; p > 0.05) (Fig. 30F).

Finally, resting STIM2-deficient macrophages stained with H&E showed no obvious abnormalities in their cellular morphology (Fig. 27D).

Thus, STIM2-deletion does not alter SOCE in macrophages, neither after Ca²⁺ store release stimulation with 5 µM TG, nor by direct stimulation of FcγR.

5.6.2.2. Upregulated FcγR expression in *Stim2*^{-/-} macrophages

In mice, there are three different activating FcγRs; the high affinity receptor FcγRI, the low-affinity receptor FcγRIII, and the recently described FcγRIV [127], and one inhibitory receptor, the FcγRII.

To test the expression levels of FcγRs, flow cytometric analysis of resting peritoneal macrophages was performed using specific antibodies against FcγRI, FcγRIII, FcγRIV and the antibody 2.4G2 (used for assessment of [Ca²⁺]_i changes upon FcγR activation). The last one binds to FcγRII, III, and probably also IV (Fig. 28) [147]. Unexpectedly, apart from FcγRI, all activatory FcγRs were upregulated by 25 % in *Stim2*^{-/-} mice (FcγRIII: 617.40 ± 63.21; FcγRIV: 395.20 ± 36.21; 2.4G2: 139.00 ± 23.25; n = 5; p < 0.05) as compared to wild-type control mice (FcγRIII: 433.80 ± 29.00; FcγRIV: 395.20 ± 63.21; 2.4G2: 448.80 ± 58.47; n = 5). 2.4G2 Ig binds equally to FcγRII and FcγRIII. The observation that the 2.4G2 signal was increased to a smaller extent than the FcγRIII signal in *Stim2*^{-/-} macrophages might indicate that the inhibitory receptor FcγRII is expressed at similar level in STIM2-deficient and wild-type macrophages. Unfortunately, due to the absence of an anti-FcγRII Ig suitable for expression studies, this hypothesis could not be directly confirmed.

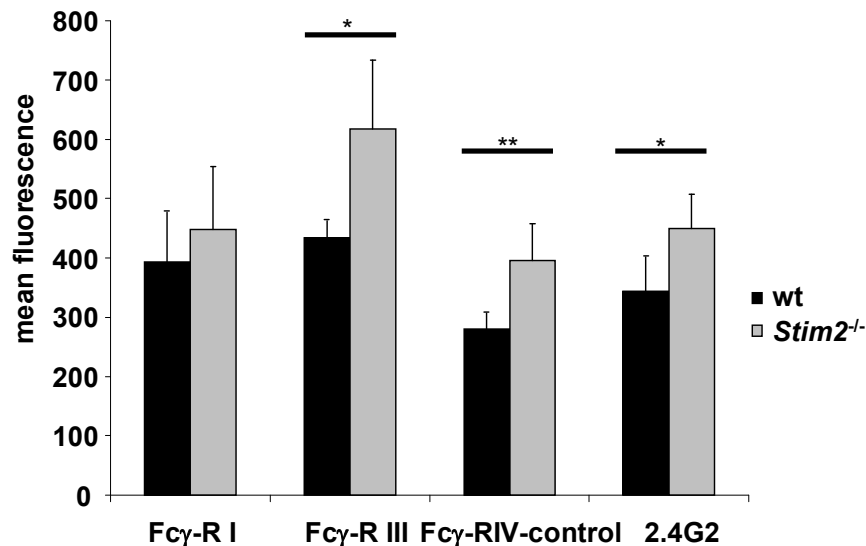


Figure 28. Surface Fc γ R expression in *Stim2*^{-/-} macrophages. Peritoneal macrophages were isolated and stained with Alexa 647–conjugated Fc γ R I, Fc γ R III, and Fc γ R IV-specific Igs at saturating concentrations for 15 min at RT and analyzed directly by flow cytometry. Macrophages were gated by FSC/SSC characteristics and PE-F4/80 expression, as a specific marker from macrophages and monocytes. Results are given as the mean fluorescence intensity \pm s.d. of 5 mice per group. * $p < 0.05$, ** $p < 0.01$, differences were considered significant if $p < 0.05$ using the Mann-Whitney U-test.

5.6.2.3. *Stim2*^{-/-} mice are protected in experimental thrombocytopenia and anaphylaxis

Immune thrombocytopenic purpura (ITP) is a rather common autoimmune disease in humans, characterized by the production of autoantibodies against platelet glycoproteins, resulting in an increased platelet clearance, normally accompanied by severe bleeding. Platelet surface glycoprotein IIb/IIIa (GPIIb/IIIa, α IIb β 3 integrin) is the most common antigenic target in ITP [148]. In mice, i.v. injection of anti-GPIIb/IIIa antibodies leads to a Fc γ R-dependent platelet clearance, mainly via macrophages located in the spleen and kupffer cells in the liver [132,149].

The *in vivo* relevance of STIM2 deficiency was tested in the murine model of IgG-induced ITP (Fig. 29). Fc γ R activation was induced by i.v. injection of the anti-GPIIb/IIIa antibodies JON3 (IgG₁ which induces ITP predominantly through Fc γ R III) or JON1 (IgG_{2b} which induces ITP predominantly through Fc γ R III and probably also Fc γ R IV) [132] in *Stim2*^{-/-} or wild-type mice. After i.v. injection of 4.7 or 11 μ g of JON or PBS as control, 50 μ L whole blood samples were collected at day 0, 1, 2 and 3 after and platelet counts were measured. Both

JON1 and JON3 induced profound thrombocytopenia in wild-type controls as expected, with a maximal reduction of 66.3 % in platelet counts (after injection of 11 μg JON, $n = 5$) and 56.5 % (after injection of 4 μg JON, $n = 5$) one day after injection (Fig. 29A). In contrast, *Stim2*^{-/-} mice showed significantly higher platelet counts as compared to wild-type controls, showing a maximal reduction of 10.9 % in platelet counts (after injection of 4 μg JON, $n = 5$) and 20.5 % (after injection of 7 μg JON, $n = 5$) 1 day after injection, respectively (Fig. 29A).

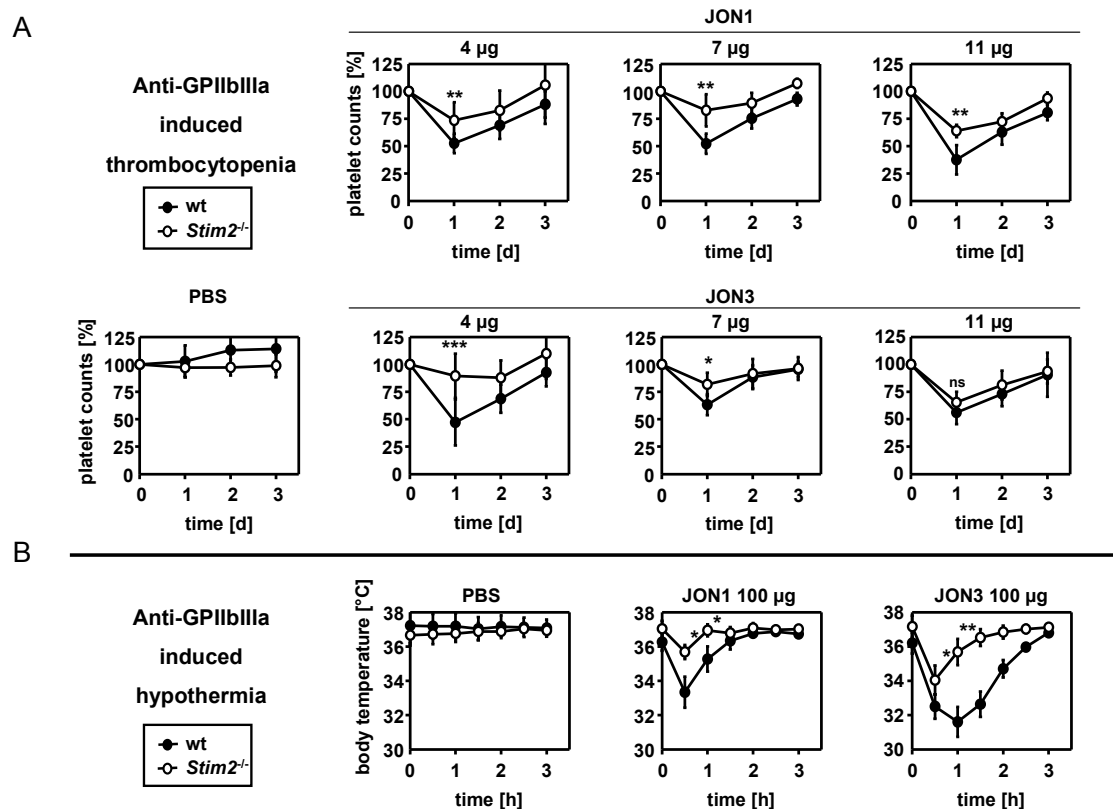


Figure 29. *Stim2*^{-/-} mice are protected from anti-GPIIb/IIIa IgG-induced thrombocytopenia and anaphylaxis. (A) Wild-type (black circles) or *Stim2*^{-/-} (open circles) mice received the indicated amounts of JON1, JON3 or vehicle and platelet counts were monitored ($n = 5$). **(B)** Wild-type or *Stim2*^{-/-} mice received vehicle or 100 μg of JON1 or JON3 and body temperature was measured using a rectal probe ($n = 5$). * $p < 0.05$, ** $p < 0.01$, *** $p < 0.001$, differences were considered significant if $p < 0.05$ (Mann-Whitney U-test).

However, no significant differences were observed in mice injected with 11 μg of JON 3 (Fig. 29A). To study the effect of STIM2 deficiency in anti-GPIIb/IIIa-induced anaphylaxis, a higher amount (100 $\mu\text{g}/\text{mL}$) of JON1 or JON3 was i.v. injected to *Stim2*^{-/-} or wild-type control mice, in order to activate the low-affinity receptor Fc γ RIII [132], and the body temperature was measured over time using a rectal probe (Fig. 29B). Both JON1 and JON3 induced strong hypothermia in wild-type control mice as expected, with a minimal body temperature of 33.5 °C

(0.5 h after JON 1 injection, n = 5) and 31.7 °C (1 h after JON 3 injection, n = 5), respectively (Fig. 29B). In contrast, *Stim2*^{-/-} mice showed significantly milder hypothermia as compared to wild-type control mice, with a minimal body temperature of 35.7 °C (0.5 h after JON 1 injection, n = 5) and 35.5 °C (1 h after JON 3 injection, n = 5), respectively (Fig. 29B).

These results indicate a protective effect to FcγRs-dependent immune thrombocytopenia in *Stim2*^{-/-} mice. Since previously, a normal surface glycoprotein expression was shown in *Stim2*^{-/-} platelets in this work (Fig. 17C), this protective effect is not based on a decrease of GPIIb/IIIa levels in platelets.

Taking all these results together, the connection between the unexpected upregulation of FcγRs, the normal Ca²⁺ influx mediated by FcγRs activation and the protective effect of STIM2 deletion in ITP model in mice is not clear. These results require further studies that are still ongoing.

5.6.3. Effect of STIM2 deletion on the adaptive immune system: T and B cells

5.6.3.1. Decreased SOCE in STIM2-deficient T cells

As previously shown, STIM2 is also expressed in lymph nodes, indicating a function in T cells (Fig. 9A, 11E). Previous reports indicated a potential role of STIM2 in Jurkat T cell Ca²⁺ homeostasis [2,9,53]. Therefore, the effect of STIM2 deficiency on Ca²⁺ homeostasis and SOCE was analyzed in Fura-2-loaded CD4⁺ T cells isolated from spleen and lymph nodes (Fig. 30). Deletion of STIM2 in lymphocytes did not alter STIM1 expression (Fig. 30A). In resting conditions no differences were observed in *Stim2*^{-/-} basal [Ca²⁺]_i as compared to wild-type control mice (wt: 27.00 ± 12.00 nM; *Stim2*^{-/-}: 37.00 ± 26.54 nM; n = 5; p ≥ 0.05) (Fig. 30B, C). Store-release upon TG treatment in *Stim2*^{-/-} (38.33 ± 11.87 nM; n = 6; p > 0.05) cells was also similar as compared to wild-type controls (28.90 ± 5.76 nM; n = 8) indicating normal Ca²⁺ levels in ER Ca²⁺ stores (Fig. 30B, C). After addition of 1 mM extracellular Ca²⁺, a second [Ca²⁺]_i peak indicated the presence of SOCE in *Stim2*^{-/-} CD4⁺ T cells, which showed 40 % decrease in amplitude as compared to wild-type control mice (297.83 ± 81.99 nM vs. 565.03 ± 65.56 nM in wt cells; p < 0.05) (Fig. 30B, C). Thus, STIM2 deficiency does not alter basal [Ca²⁺]_i and ER Ca²⁺ levels, but leads to a significant 40 % reduction in SOCE after TG-induced Ca²⁺ store depletion in CD4⁺ T cells.

Additionally, changes in $[Ca^{2+}]_i$ were assessed in response to direct T cell receptor (TCR) activation by the anti-CD3 IgG cross-linked by a secondary Ig (Fig. 30E, F). Stimulated CD3 receptor associates with the TCR and comprises the main activating pathway in T cells [25].

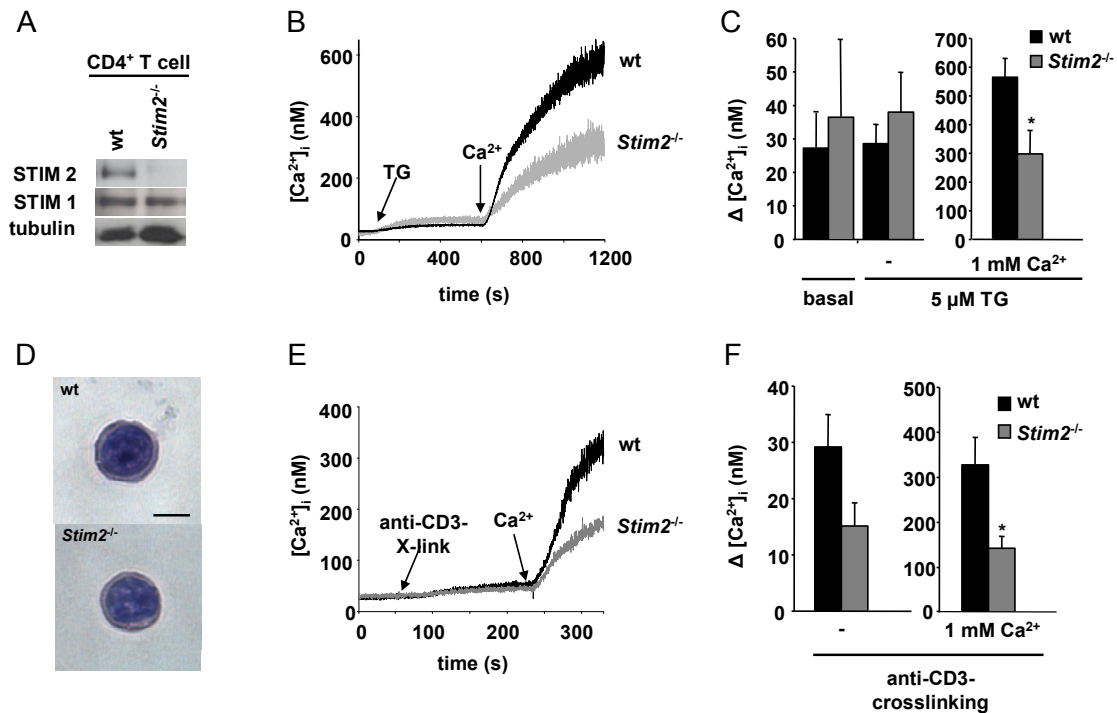


Figure 30. Reduced SOCE in *Stim2*^{-/-} CD4⁺ T cells. Fura-2-loaded CD4⁺ T cells isolated with MACS columns were stimulated for 10 min with 5 μM TG or for 180 sec 10 μg/mL anti-CD3 IgG cross-link, followed by addition of 1 mM extracellular Ca²⁺, and $[Ca^{2+}]_i$ was monitored. **(A)** Representative western blot analysis of STIM1 and STIM2 expression in lymph nodes of 8 weeks old wild-type or *Stim2*^{-/-} mice (n = 3). Tubulin expression was used as loading control. **(B, E)** Representative measurements of $[Ca^{2+}]_i$ in wild-type (Black line) and *Stim2*^{-/-} (gray line) CD4⁺ T cells. Black arrows indicate the time points of agonist addition, TG = thapsigargin. **(C, F)** Basal levels, increase after store depletion (-) and maximal increase in intracellular Ca²⁺ concentrations compared to baseline levels ($\Delta[Ca^{2+}]_i$) ± s.d. (n = 5 per group) before and after addition of 1 mM extracellular Ca²⁺ are shown. **(D)** Representative pictures of H&E stained CD4⁺ T cells. Scale bar: 5 μm. *p < 0.05. Differences were considered significant if p < 0.05 (Mann-Whitney U-test).

To assess SOCE, cells were incubated for 15 min with 10 μg/mL anti-CD3 and Ca²⁺ store release was induced by cross-linking the bound anti-CD3 IgG by a secondary Ig in the absence of extracellular Ca²⁺ (Fig. 30E, F). 180 sec after the cross-link stimulation, the Ca²⁺ release from intracellular stores in Stim2-deficient cells was similar as compared to wild-type controls (wt: 29.14 ± 5.78 nM; *Stim2*^{-/-}: 15.17 ± 4.09 nM; n = 6; p > 0.05), indicating normal Ca²⁺

release from ER Ca^{2+} stores in *Stim2*^{-/-} CD4⁺ T cells (Fig. 30E, F). After addition of 1 mM extracellular Ca^{2+} , SOCE was reduced by 60 % in *Stim2*^{-/-} T cells (142.00 ± 26.90 nM; $n = 6$; $p < 0.05$) as compared to wild-type controls (327.36 ± 61.81 nM; $n = 6$) (Fig. 30E, F).

Finally, resting STIM2-deficient CD4⁺ T cells stained with H&E showed no obvious abnormalities in morphology (Fig. 30D). Thus, STIM2 seems not to play a major role in regulation of basal $[\text{Ca}^{2+}]_i$, ER Ca^{2+} levels in CD4⁺ T cells, but STIM2 deficiency markedly reduces SOCE after intracellular Ca^{2+} stores depletion by TG or by direct TCR activation.

5.6.3.2. STIM2 deficiency does not alter CD3 and T cell receptor (TCR) expression in lymphocytes and splenocytes

Since STIM2 deletion reduced SOCE after Ca^{2+} store depletion by direct TCR activation, CD3 and TCR expression levels were studied in naive resting lymphocytes and splenocytes by flow cytometry (Fig. 31). *Stim2*^{-/-} CD4⁺ or CD8⁺ T cells from lymph node (Fig. 31A) or spleen (Fig. 31B) showed no differences in TCR expression levels and a non-significant decrease of CD3 expression in CD4⁺ (lymph node: 185.00 ± 56.76 in wt; 131.55 ± 43.08 in *Stim2*^{-/-}; spleen: 175.39 ± 69.70 in wt; 129.89 ± 45.95 in *Stim2*^{-/-}; $n = 5$; $p > 0.05$) or CD8⁺ (lymph node: 79.92 ± 26.62 in wt; 58.98 ± 20.51 in *Stim2*^{-/-}; spleen: 79.82 ± 30.80 in wt; 64.26 ± 17.82 in *Stim2*^{-/-}; $n = 5$; $p > 0.05$) T cells as compared to wild-type control mice.

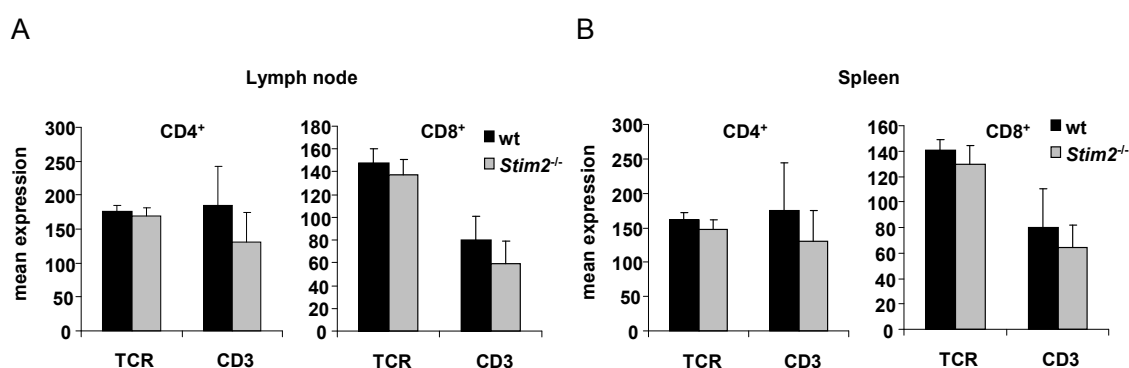


Figure 31. CD3 and TCR surface protein expression in CD4⁺ T or CD8⁺ cells. Analysis of CD3 and TCR expression by lymphocytes (**A**) and splenocytes (**B**) isolated from wild-type (black bar) or *Stim2*^{-/-} (gray bar) mice and assessed directly by flow cytometry. T cells were gated by FSC/SSC characteristics and CD4 or CD8 surface protein expression. Results are given as the mean fluorescence intensity \pm s.d. of 6 mice per group. Differences were considered significant if $p < 0.05$ (Mann-Whitney U-test).

This result indicates that STIM2 deficiency does not affect CD3 or TCR expression in T cells and the decreased SOCE seen after T cell stimulation through CD3 receptor is not due to a reduced expression of those surface molecules.

5.6.3.3. Normal cellularity and decreased CD8⁺ cells in primary and secondary lymphoid organs

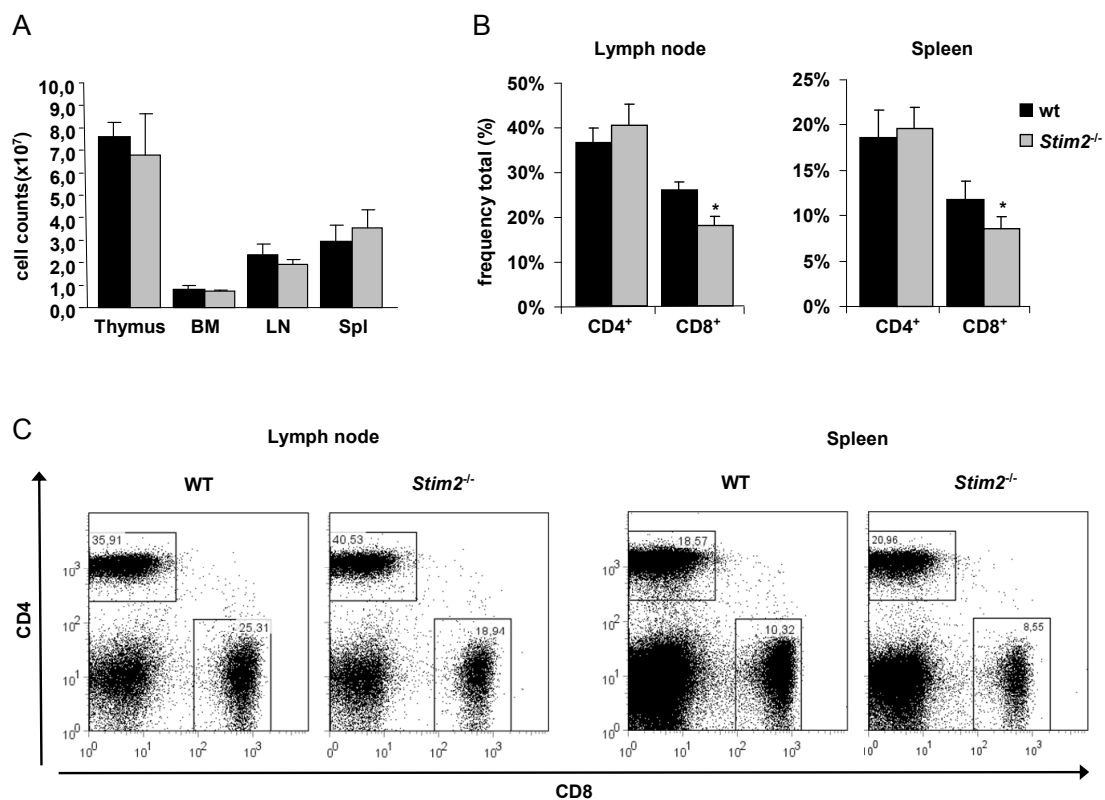


Figure 32. Normal cellularity in primary and secondary lymphoid organs. (A) Bar graph representation of thymocytes (thymus), bone marrow cells (BM), lymphocytes (LN) and splenocytes (Spl) isolated from wild-type (black bar) and *Stim2*^{-/-} (gray bar) mice and analyzed directly by flow cytometry. Cell counts given as mean (x10⁷) total cells ± s.d. (n = 3). (B) Bar graphs representation of CD4 and CD8 positive lymphocytes (left graph) and splenocytes (right graph) in wild-type (black bar) or *Stim2*^{-/-} (gray bar) mice, given as mean frequency (%) of the total ± s.d. (n = 3). (C) Representative dot plot of CD4 versus CD8 expression by lymphocytes (left) and splenocytes (right) in wild-type (left square) or *Stim2*^{-/-} (right square) mice measured by flow cytometry. *p < 0.05. Differences were considered significant if p < 0.05 (Mann-Whitney U-test).

Previously in this work it was shown that the major organs of *Stim2*^{-/-} mice exhibit no obvious abnormalities, including bone marrow, thymus and spleen (Fig. 13A-C). Furthermore, the effect of STIM2 deficiency on cellularity in

primary and secondary lymphoid organs was studied by flow cytometry. Naive *Stim2*^{-/-} mice displayed normal numbers of thymocytes, bone marrow cells, lymphocytes and splenocytes ($6.80 \times 10^7 \pm 1.82 \times 10^7$ cells; $7.17 \times 10^7 \pm 0.07 \times 10^7$ cells ; $1.93 \times 10^7 \pm 0.21 \times 10^7$ cells; $3.53 \times 10^7 \pm 0.83 \times 10^7$ cells, respectively; n = 4; p > 0.05) as compared to wild-type control mice ($7.60 \times 10^7 \pm 0.66 \times 10^7$ cells; $0.8 \times 10^7 \pm 0.17 \times 10^7$ cells ; $2.37 \times 10^7 \pm 0.45 \times 10^7$ cells; $2.93 \times 10^7 \pm 0.72 \times 10^7$ cells, respectively; n = 4; p > 0.05) (Fig. 32A). Further, the lymphocyte and splenocyte subset distribution was examined in *Stim2*^{-/-} mice and wild-type littermates by flow cytometry using anti-CD4 and anti-CD8 antibodies as markers (Fig. 32B-C). No significant differences were found in *Stim2*^{-/-} CD4⁺ lymphocytes (*Stim2*^{-/-}: 40.44 ± 4.43 %; wt: 36.58 ± 2.98 %; n = 6; p > 0.05) or splenocytes (*Stim2*^{-/-}: 19.62 ± 2.31 %; wt: 18.54 ± 3.13 %; n = 6; p > 0.05) as compared to wild-type control mice (Fig. 32B-C). In contrast, a mild significant decrease (28 %) in *Stim2*^{-/-} CD8⁺ lymphocytes (*Stim2*^{-/-}: 18.07 ± 2.07 %; wt: 25.83 ± 1.88 %; n = 6; p > 0.05) and splenocytes (*Stim2*^{-/-}: 8.62 ± 1.21 %; wt: 11.70 ± 2.12 %; n = 6; p > 0.05) was observed (Fig. 32B-C).

Thus, STIM2 deficiency leads to a reduced number of CD8⁺ T cells and splenocytes in mice, suggesting a possible role of STIM2 in CD8⁺ T cell maturation. However, analysis of thymocyte subset distribution showed no differences in *Stim2*^{-/-} mice as compared to wild-type control mice (Fig. 33A, B), indicating that CD8⁺ T cell maturation in thymus is normal. Therefore, such a reduced number of CD8⁺ lymphocytes and splenocytes can not be explained by an altered maturation of T cells in thymus.

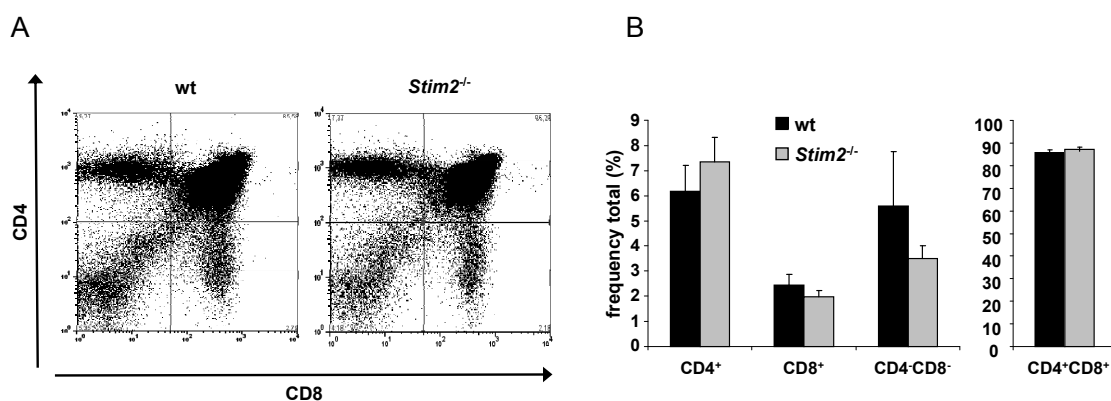


Figure 33. Normal CD4⁺ or CD8⁺ subset distribution in thymus. (A) Representative dot plot of CD4 versus CD8 expression by thymocytes in wild-type (left square) or *Stim2*^{-/-} (right square) mice measured by flow cytometry. (B) Bar graph representation of CD4 and CD8 positive thymocytes in wild-type (black bar) or *Stim2*^{-/-} (gray bar) mice, given as mean frequency (%) of the total ± s.d. (n = 5). Differences were considered significant if p < 0.05 (Mann-Whitney U-test).

To study the effect of STIM2 deficiency in naive and effector/memory cells distribution, the expression of CD44 and CD62L surface proteins by CD4⁺ and CD8⁺ lymphocytes or splenocytes was examined in *Stim2*^{-/-} mice and wild-type littermates using flow cytometry (Fig. 34) [150]. Naive T cells express a CD62L_{high}CD44_{low} expression profile, whereas effector memory T cells exhibit a CD62L_{low}CD44_{high} expression profile. Analysis of CD62L and CD44 expression in naive lymphocytes and splenocytes showed no differences in *Stim2*^{-/-} mice as compared to wild-type control mice (Fig. 34A, B).

Taken together, these results revealed a mild decrease of CD8⁺ in lymph node and spleen, suggesting a specific role of STIM2 in CD8⁺ T cell survival or maturation. Additional studies are currently ongoing to clarify the precise role of STIM2 in CD8⁺ T cell fate.

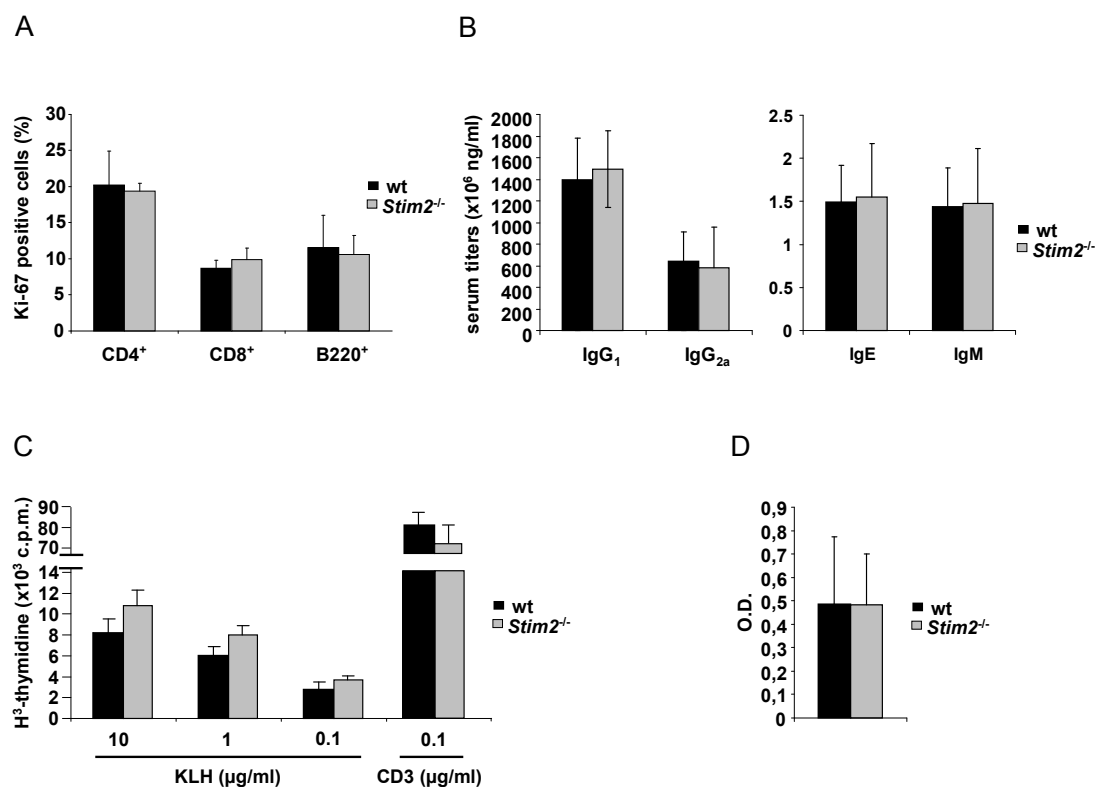


Figure 34. CD4⁺ T or CD8⁺ cell subset distribution in spleen and lymph nodes as assessed by flow cytometry for CD4, CD8, CD44 and CD62L surface protein expression. (A) Representative dot plots of CD62L versus CD44 expression by splenocytes (left) and lymphocytes (right) in wild-type (upper dot plots) or *Stim2*^{-/-} (lower dot plots) mice measured by flow cytometry. **(B)** Table showing the frequencies of the CD62L and CD44 immune subtypes in CD4⁺ and CD8⁺ lymphocytes or splenocytes in wild-type or *Stim2*^{-/-} mice, given as mean percentage ± s. d. Differences were considered significant if p < 0.05 (Mann-Whitney U-test).

5.6.3.4. Normal T cell proliferation in naive and normal immune response in Keyhole limpet hemocyanin (KLH)-immunized *Stim2*^{-/-} mice

To study the effect of STIM2 deficiency in splenocyte proliferation *ex vivo*, freshly isolated cells from naive *Stim2*^{-/-} and wild-type littermates were assessed by flow cytometry, using CD4, CD8 and B220 as markers of T and B cell respectively, and Ki-67 as a marker of proliferating cells (Fig. 35A). The Ki-67 protein is present during all active phases of the cell division (G1, S, G2, and mitosis), but is absent from resting cells (G0). No differences in numbers of Ki-67 positive cells were observed in *Stim2*^{-/-} mice (CD4⁺: 19.36 ± 1.10 %; CD8⁺: 9.87 ± 1.59 %; B220⁺: 10.60 ± 2.63 %; n = 6; p > 0.05) as compared to wild-type control mice (CD4⁺: 20.24 ± 4.66 %; CD8⁺: 8.66 ± 1.13 %; B220⁺: 11.56 ± 4.45 %; n = 6; p > 0.05). Thus, STIM2 deficiency does not alter proliferation in naive splenocytes.

To study the effect of STIM2 deficiency in B cell activity, the serum titers of IgG₁, IgG_{2a}, IgE and IgM antibodies were tested by isotype specific anti-Ig antibody-coated ELISA in naive mice (Fig. 35B). No differences were found in IgG₁ (*Stim2*^{-/-}: 1494x10⁶ ± 357.25 x10⁶ ng/mL ; wt: 1398x10⁶ ± 379.45x10⁶ ng/mL; n = 5; p > 0.05), IgG_{2a} (*Stim2*^{-/-}: 583.8x10⁶ ± 377.15x10⁶ ng/mL ; wt: 643.5x10⁶ ± 266.58x10⁶ ng/mL; n = 5; p > 0.05), IgE (*Stim2*^{-/-}: 1.55x10⁶ ± 0.62x10⁶ ng/mL ; wt: 1.49x10⁶ ± 0.43x10⁶ ng/mL; n = 5; p > 0.05) or IgM (*Stim2*^{-/-}: 1.48x10⁶ ± 0.63x10⁶ ng/mL ; wt: 1.44x10⁶ ± 0.45x10⁶ ng/mL; n = 5; p > 0.05) isotype titer in *Stim2*^{-/-} mice serum as compared to wild-type control serum.

To examine the effect of STIM2 deletion in adaptive immune response after antigen challenge, *Stim2*^{-/-} and wild-type control littermates were immunized with the T cell-dependent model antigen KLH, and the specific KLH-reactive T cell proliferation and IgG production by B cells were assessed (Fig. 35C, D). These experiments were performed in collaboration with Dr. Niklas Beyersdorf and Dr. Thomas Kerkau from the Immunology and Virology department, University of Würzburg. Mice were injected intraperitoneally (i.p.) with 25 µg of KLH antigen and after three weeks they were boosted with an additional injection of 25 µg of KLH antigen and 15 µL TiterMax adjuvant. Three weeks after CD4⁺ T cells were isolated from spleen, co-cultured with irradiated antigen presenting cells (APC) and re-stimulated for two days with 10 µg/mL of KLH antigen *in vitro*, in presence of radioactive H³-thymidine. T cell proliferation was assessed by radioactive H³-thymidine uptake, the so-called T cell recall assay. Specific KLH-reactive *Stim2*^{-/-} CD4⁺ T cells showed similar proliferation rates *in*

in vitro as compared to wild-type control T cells (wt: 8211 ± 1359 c.p.m.; *Stim2*^{-/-}: 10802 ± 1498 c.p.m.; n = 3; p > 0.05) (Fig. 35C).

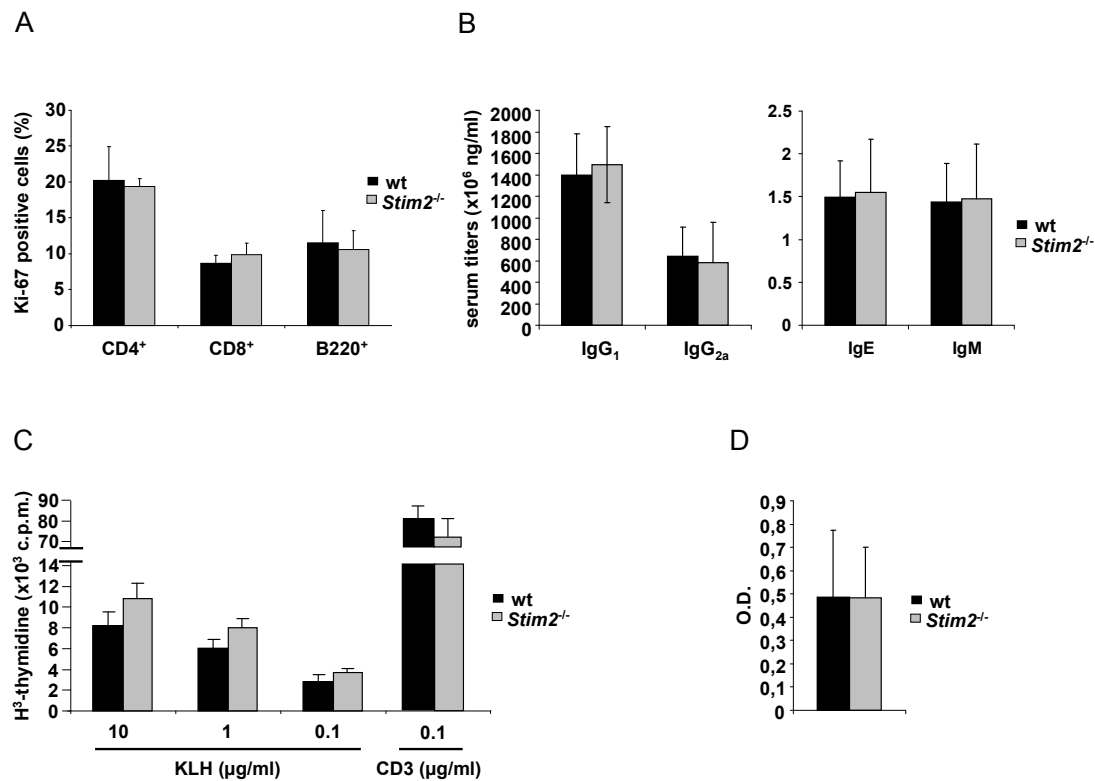


Figure 35. T cell proliferation in naive and normal immune response in KLH-immunized *Stim2*^{-/-} mice. (A) Bar graph representation of Ki-67 positive cells in *Stim2*^{-/-} (gray) and wild-type (black) splenocytes as assessed by flow cytometry, given as mean Ki-67 positive cells (%) ± s.d. **(B)** Bar graphs representation of Ig titers in naive *Stim2*^{-/-} (gray) and wild-type (black) mice blood serum assessed by isotype-specific anti-Ig antibody-coated ELISA, given as mean Ig concentration (x10⁶ ng/mL) ± s.d. **(C)** Bar graph representation of the proliferative response of *Stim2*^{-/-} (gray) and wild-type (black) KLH-reactive CD4⁺ T cells in presence of KLH antigen at the indicated concentrations, given as mean H³-thymidine counts per minute (c.p.m.) ± s.d. 0.5 μg/mL α-CD3 Ig stimulation was used as a positive control **(D)** Bar graph representation of KLH-specific IgG titers in *Stim2*^{-/-} (gray) and wild-type (black) mice blood serum three weeks after boosted immunization with the KLH antigen, given as mean optical density (O.D.) ± s. d.. Differences were considered significant if p < 0.05 (Mann-Whitney U-test).

In parallel, specific IgGs against KLH were measured in blood serum by KLH-coated ELISA (Fig. 35D). Again, mice were injected i.p. with 25 μg of KLH antigen and after three weeks they were boosted with an additional injection of 25 μg of KLH antigen and 15 μL TiterMax adjuvant. Three weeks after i.p. injection, comparable titers of specific IgG anti-KLH antibody were found in *Stim2*^{-/-} and wild-type control mice blood serum (*Stim2*^{-/-}: 0.481 ± 0.21 O.D.; wt: 0.485 ± 0.29 O.D.; n = 3; p > 0.05) (Fig. 35D). This result indicates that T cell-mediated antibody production in serum is not impaired in STIM2-deficient mice.

Taken together, these results indicate that STIM2 does not play a role in T cell proliferation, B cell antibody production in naive mice or in KLH-mediated adaptive immune response in mice.

5.6.3.5. Experimental autoimmune encephalomyelitis (EAE) is significantly ameliorated in STIM2-deficient mice

T cells are considered to orchestrate inflammation in Multiple sclerosis (MS), an inflammatory-demyelinating disorder of the central nervous system (CNS) [151,152]. Disturbed Ca^{2+} signaling and deregulation of the intracellular Ca^{2+} levels in T lymphocytes have been associated with inflammatory and autoimmune disorders, including MS [25]. Since it was previously shown in this work that STIM2-deficient T cells displayed a 40 % reduced SOCE after intracellular store depletion or CD3 cross-link stimulation (Fig. 30), it was hypothesized a possible role of STIM2 in autoimmune disorders in mice.

In an initial experiment in collaboration with Michael K. Schuhmann and Dr. Sven G. Meuth from the Department of Neurology, University of Würzburg, the role of STIM2 in myelin oligodendrocyte glycoprotein (MOG₃₅₋₅₅-peptide)-induced EAE as an *in vivo* model of autoimmune response was examined (Fig. 36) [153]. 13 days after MOG-peptide immunization *Stim2*^{-/-} mice showed a significantly reduced disease maximum (wt: day 13.8; score: 6.4 ± 0.8 ; *Stim2*^{-/-}: day 15.2; score: 4.6 ± 1.2 ; $p < 0.05$), while disease incidence, overall disease course and residual disease scores at day 50 were unaltered (Fig. 36A).

Consequences of STIM-deficiency for inhibiting EAE development were further analyzed by immunohistopathology (Fig. 36B and C). Since *Stim2*^{-/-} mice showed significant clinical differences only at the disease maximum, the lesion pattern in the spinal cord was investigated at this time point. H&E staining showed focal regions of T cell infiltration in *Stim2*^{-/-} and wild-type control mice (Fig. 36B, upper panels). *Stim2*^{-/-} mice showed a tendency to reduced demyelization in the white matter (neuronal axons) of the spinal cord (wt: 1.25 ± 0.18 %, *Stim2*^{-/-}: 0.97 ± 0.18 %, $p = 0.295$; $n = 3$ each) (Fig. 36B middle, C upper), but a comparable number of infiltrating T cells (Fig. 36B lower, C lower). Thus, *Stim2*^{-/-} mice developed an attenuated EAE, indicating a possible role of this STIM2 during early phase of EAE progression, more precisely during disease maximum onset.

These initial results gave rise to a fruitful collaboration to study the role of STIM2 in a murine EAE *in vivo* model (see publication list: Schuhmann, MK. *et al.* 2009, accepted manuscript, in press).

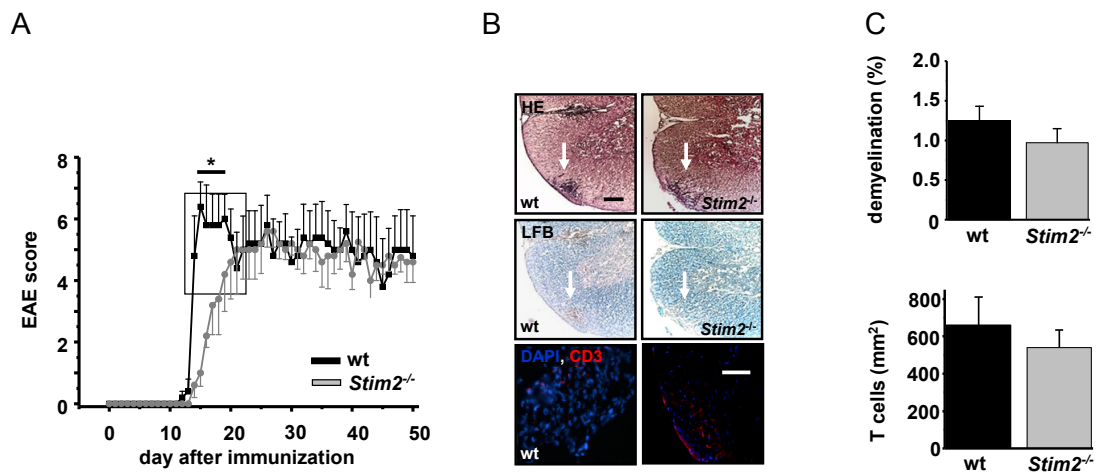


Figure 36. Mice lacking STIM2 show a significantly altered disease course and histopathology after EAE induction. (A) EAE was induced by MOG immunization (200 μ g) in 6-12 weeks old *Stim2*^{-/-} (grey line, n = 10) or wild-type (black line, n = 9/10) littermates. **(B)** (upper panels) Hematoxylin and eosin (HE) staining of spinal cord sections from wild-type (wt, n = 3) and *Stim2*^{-/-} mice (n = 3). (central panels) Luxol fast blue (LFB) staining of spinal cord myelin to study demyelination activity. (lower panels) Immunohistochemistry of spinal cord lesions using anti-CD3 IgG as marker of infiltrating T lymphocytes (n = 4). White arrows indicate the areas of T cell infiltration. Scale bar: 100 μ m for all images. **(C)** Bar graph representation of demyelination (upper graph) and number of infiltrated CD3⁺ (lower graph) as a marker for T cells, in wild-type and *Stim2*^{-/-} animals, given as mean demyelinated area (%) \pm s.d. and mean number T cells/mm² \pm s.d.. *p < 0.05. Differences were considered significant if p < 0.05 (student's t-test).

5.7. Analysis of STIM2 deficiency in neurons

5.7.1. STIM2 regulates SOCE and ischemia-induced Ca²⁺ accumulation in neurons

Previously in this work it was shown that STIM2 is the dominant isoform in brain (Fig. 9). To test the effect of STIM2 deficiency on neuronal Ca²⁺ homeostasis, Ca²⁺ imaging experiments were performed in neuronal cultures extracted from E19 embryonic cortical tissue (in collaboration with Prof. Jens Eilers, Carl-Ludwig-Institute for Physiology, University of Leipzig). To assess SOCE (referred to as CCE in neurons), Ca²⁺ store release was induced by the SERCA

pump inhibitor cyclopiazonic acid (CPA) in the absence of extracellular Ca^{2+} . This treatment caused a transient Ca^{2+} signal, followed by a second $[\text{Ca}^{2+}]_i$ increase after addition of external Ca^{2+} which exceeded the basal Ca^{2+} level, suggesting the presence of SOCE (Fig. 37A). Strikingly, SOCE was severely reduced in *Stim2*^{-/-} neurons compared to wild-type controls (*Stim2*^{-/-}: 27 ± 9 nM; wt: 82 ± 16 nM; $n = 7$ each representing the average signal from 20-35 cells; $p < 0.05$) (Fig. 37A). Thus, SOCE is regulated by STIM2 in cultured neurons.

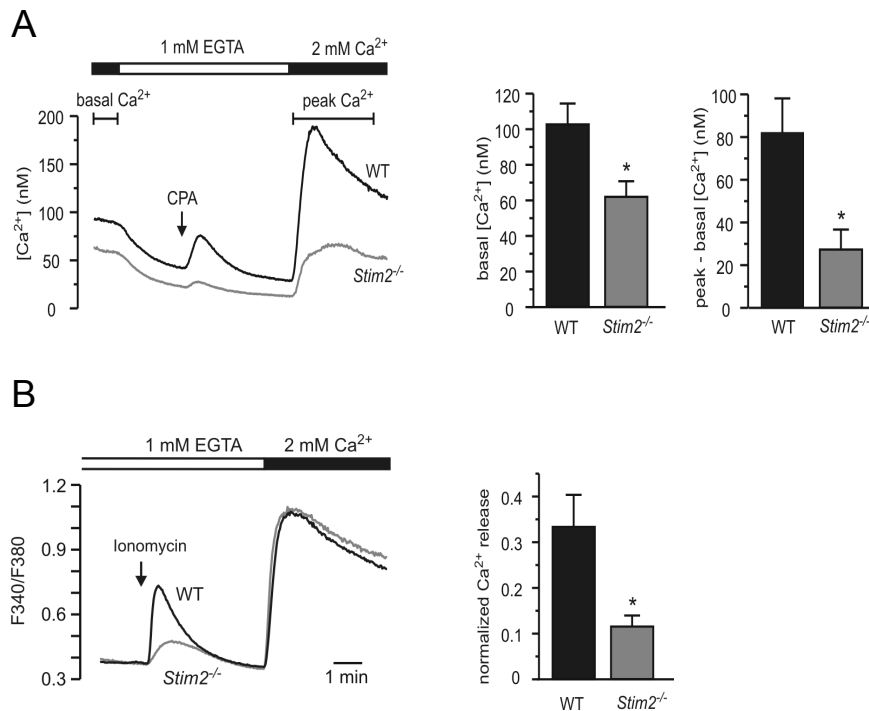


Figure 37. STIM2 regulates Ca^{2+} homeostasis in cortical neurons. Neuronal cultures [5 to 9 days *in vitro* (DIV 5-9)] were loaded with Fura-2 and averaged $[\text{Ca}^{2+}]_i$ responses in *Stim2*^{-/-} were compared to wild-type (WT) cells ($n = 5-7$ experiments per group, each representing the average signal from 20-35 cells). **(A)** Cells were stimulated with cyclopiazonic acid (CPA, 20 μM) followed by exchange of 1 mM EGTA for 2 mM Ca^{2+} . Basal and peak $[\text{Ca}^{2+}]_i$ were obtained during the time intervals indicated. **(B)** Ca^{2+} release from intracellular stores was monitored by addition of 5 μM ionomycin in the presence of EGTA. This Ca^{2+} release was normalized to the maximum response after exchange of 1 mM EGTA for 2 mM Ca^{2+} . All bars represent means of 5-7 experiments. Error bars indicate SEM. Asterisks indicate significant differences ($p < 0.05$, two-tailed Mann-Whitney U test).

As mentioned previously, Brandman *et al.* have shown that STIM2 regulates basal Ca^{2+} concentrations in the cytosol and the ER of different non-neuronal cell lines [9]. In line with this report, *Stim2*^{-/-} neurons displayed lower basal cytosolic Ca^{2+} levels than wild-type cells (*Stim2*^{-/-}: 62 ± 9 nM; wt: 103 ± 12 nM; $n = 7$; $p < 0.05$) (Fig. 37A). In order to evaluate the Ca^{2+} content of intracellular

stores, the release of free Ca^{2+} from this compartments was measured by application of the membrane permeant Ca^{2+} ionophore ionomycin in the absence of extracellular Ca^{2+} [9]. The amplitude of the relative Ca^{2+} peak was decreased in *Stim2*^{-/-} cells (*Stim2*^{-/-}: 0.12 ± 0.02 ; wt: 0.33 ± 0.07 ; n = 5; p < 0.05), whereas the subsequent Ca^{2+} entry induced by re-addition of extracellular Ca^{2+} was indistinguishable between *Stim2*^{-/-} and control neurons (Fig. 37B).

During brain ischemia, an excessive increase in $[\text{Ca}^{2+}]_i$ is thought to be a main activator of neuronal cell death [111]. To test a possible role of SOCE in this process, Ca^{2+} imaging experiments were performed on wild-type and *Stim2*^{-/-} neuronal cultures under conditions of oxygen-glucose deprivation (OGD) [154,155], optionally combined with a lowered pH [135], an established system for the examination of Ca^{2+} -dependent and Ca^{2+} -independent mechanisms in neuronal injury (Fig. 38A). OGD was reported to trigger cumulative increases in $[\text{Ca}^{2+}]_i$ that were mostly reversible when the duration of the insult was limited to 1 h [155]. A robust $[\text{Ca}^{2+}]_i$ rise could be confirmed in the wild-type cultures (131 ± 46 nM; n = 5) but found only a very small increase during a 1 h OGD in *Stim2*^{-/-} cells (11 ± 15 nM; n = 5; p < 0.05) (Fig. 38A). In *Stim2*^{-/-} cultures, a marked $[\text{Ca}^{2+}]_i$ increase was only visible when OGD was extended to 2 h.

Mitochondrial damage is one of the major features of ischemic cell death, as a result of the decreased available oxygen, and plays a role in the further development of the ischemic damage in the cell [111]. The inhibition of mitochondrial oxidative phosphorylation or significant uncoupling of the mitochondrial electron transport, which lower ATP levels in the cell, increase the production of mitochondrial free radicals, activate caspases and remove the Ca^{2+} buffering ability of the organelle. The disruption of the mitochondrial membrane and their increased permeation depletes the mitochondrial Ca^{2+} store, contributing further to the increased $[\text{Ca}^{2+}]_i$ in the cell [111]. Therefore, this phenomenon was mimicked using a mitochondrial uncoupling agent, carbonyl cyanide m-chlorophenylhydrazone (CCCP) (Fig. 38B). In the presence of CCCP, a rapid and excessive $[\text{Ca}^{2+}]_i$ increase was detectable in both wild-type and *Stim2*^{-/-} neurons (Fig. 38B). However, after 1 h washout of CCCP, the cytosolic Ca^{2+} level in *Stim2*^{-/-} cells declined more efficiently than in wild-type cells (89 ± 3 % vs. 72 ± 3 %; n = 5; p < 0.05) (Fig. 38B). Thus, ischemia-induced $[\text{Ca}^{2+}]_i$ increases develop slower and recover faster in *Stim2*^{-/-} neurons compared to wild-type which may in part be explained by the lower store content in these cells, which promotes a faster cytoplasm Ca^{2+} clearance by SERCA (explained in detail in the discussion part).

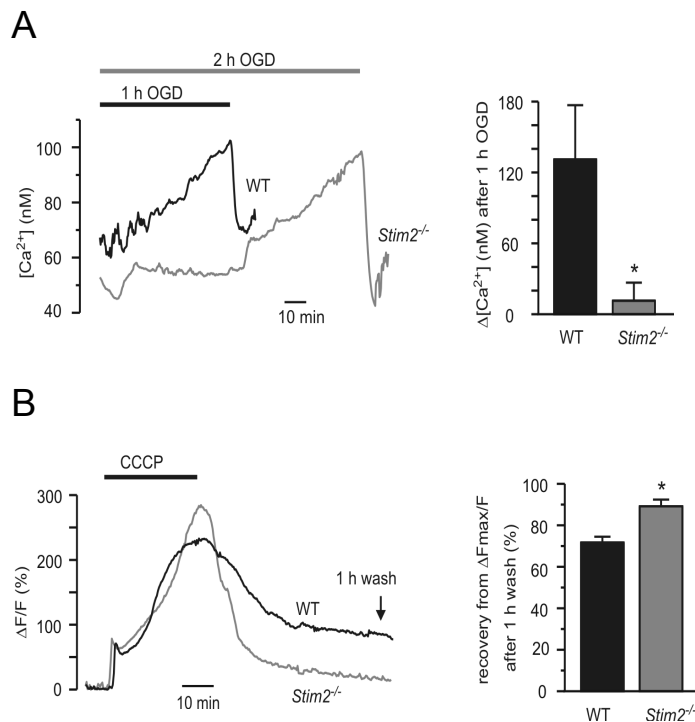


Figure 38. STIM2 regulates ischemia-induced Ca²⁺ accumulation in neurons. Neuronal cultures (DIV 5-9) were loaded with Fura-2 and averaged [Ca²⁺]_i responses in *Stim2*^{-/-} were compared to wild-type (WT) cells (n = 5-7 experiments per group, each representing the average signal from 20-35 cells). **(A)** Effect of combined oxygen-glucose deprivation (OGD) on [Ca²⁺]_i. Cultured neurons (DIV12-14) were exposed for 1 h (WT) or 2 h (*Stim2*^{-/-}) to a glucose-free bath solution continuously bubbled with N₂. **(B)** Chemical anoxia was induced in *Stim2*^{-/-} or WT cells by CCCP (2 μM, 30 min). Recovery from increases in [Ca²⁺]_i was obtained after wash-out of CCCP for 60 min. All bars represent means of 5-7 experiments. Error bars indicate SEM. Asterisks indicate significant differences (p < 0.05, two-tailed Mann-Whitney U test).

5.7.2. STIM2-defective neurons are protected from ischemia

The marked impairment of OGD-induced Ca²⁺ accumulation in *Stim2*^{-/-} neurons indicated a possible neuroprotective effect of STIM2 deficiency under ischemic conditions. To test this directly, cultured hippocampal neurons from E18 embryos were subjected to OGD (in collaboration with Michael K. Schuhmann and Dr. Sven G. Meuth from the Department of Neurology, University of Würzburg) (Fig. 39). After five to seven days under normal culture conditions, 80.6 ± 4.4 % (n = 5) wild-type neurons were viable in agreement with previous reports (Fig. 39B) [156]. Neurons prepared from *Stim2*^{-/-} mice showed increased viability (*Stim2*^{-/-}: 88.7 ± 2.6 %; wt: 52.4 ± 6.6 %; n = 3; p < 0.01) as compared to

wild-type controls. After 6 h under ischemic conditions (OGD, low glucose, N₂, pH 6.4) [135], *Stim2*^{-/-} neurons survived significantly better as compared to wild-type controls (*Stim2*^{-/-}: 72.9 ± 4.3 %; wt: 52.4 ± 6.6 %; n = 3, p < 0.001) (Fig. 39A, B). In the next set of experiments, the involvement of STIM2 in alternative cell death inducing pathways was assessed in cultured neurons. For this, the cells were treated with staurosporine, which is known to also modulate intracellular Ca²⁺ [157], or with N,N,N',N'-tetrakis(2-pyridylmethyl) ethylenediamine (TPEN), which induces protein synthesis-dependent caspase-11 mediated apoptosis that occurs largely Ca²⁺-independent (Fig. 40) [158].

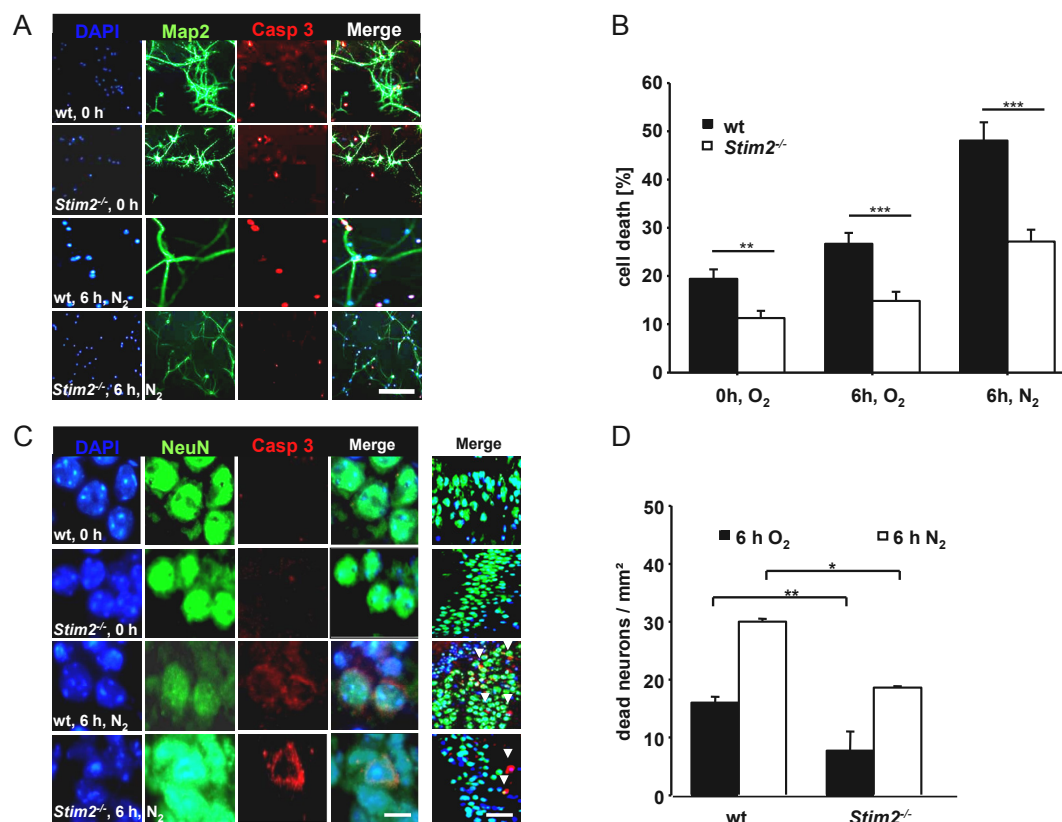


Figure 39. Lack of STIM2 is neuroprotective under ischemic conditions *in vitro* and *ex vivo*. (A) Representative images of apoptotic (Casp3, red) cultured hippocampal neurons (MAP2a/b, green) from wild type and *Stim2*^{-/-} E18 embryos under control (0 h, O₂) conditions and after *in vitro* ischemia (6 h, N₂). Scale bar represents 50 μm. (B) Bar graph representation of dead neurons (%) under the different experimental conditions. (C) Representative images of caspase3 (Casp3, red) positive hippocampal neurons (NeuN, green) under ischemic and control conditions in brain slices from 6-10 weeks old *Stim2*^{-/-} mice. DAPI counterstaining (DAPI, blue). Scale bars represent 10 (left panels) or 100 μm (right panel). (D) Bar graph representation of neuronal cell death (dead neurons/mm²) under normal (6 h, O₂ black columns) and ischemic conditions (6 h, N₂, grey columns) in brain slices from *Stim2*^{-/-} mice and control littermates. The results are presented as mean ± s.d.. *p < 0.05, **p < 0.01, *** p < 0.001, using a modified student's t-test.

These additional experiments clearly showed that *Stim2*^{-/-} neurons are protected from staurosporine (300 nM) induced cell death compared to wild-type neurons (Fig. 40A), while treatment with TPEN (2 μ M) induced apoptosis in wild-type and *Stim2*^{-/-} neurons to the same extent (Fig. 40B). These results suggested that *Stim2*^{-/-} neurons are less sensitive to Ca²⁺-related apoptotic mechanisms.

To study whether *Stim2*^{-/-} neurons display a protection to hypoxia in adult mice, neuronal death was also monitored in hemi-brain slices from 6-10 weeks old mice cultured under ischemia-like conditions (Fig. 39C, D). After 6 h, slices from wild-type mice kept under control conditions (normoglycemia, O₂, pH 7.25) showed 16.0 ± 1.7 dead neurons per mm² whereas this number was increased in consecutive slices that were kept under ischemic conditions (hypoglycemia, N₂, pH 6.4; 30 ± 0.9 ; n = 3, p < 0.01). In contrast, less dead neurons were found in slices from *Stim2*^{-/-} mice under control (7.7 ± 5.7 , n = 3, p < 0.05) and ischemic conditions (18.6 ± 0.4 , n = 3, p < 0.05) (Fig. 39C, D). Thus, *in vitro* results showed that STIM2-deficient neurons are protected from apoptosis during ischemic-like conditions (OGD, low glucose, N₂, pH 6.4) and to Ca²⁺-related apoptotic mechanisms.

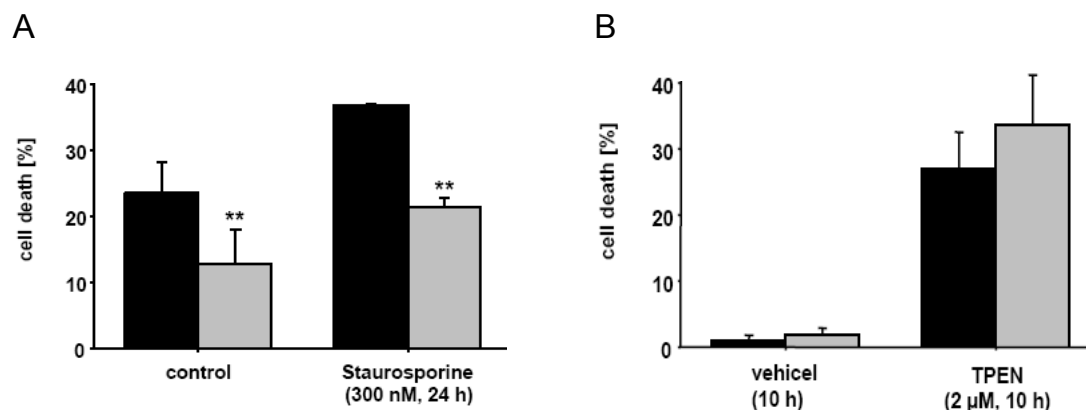


Figure 40. The neuroprotective effect of STIM2 deficiency is Ca²⁺-dependent. (A) Bar graph representation of dead neurons (%) under the different experimental conditions in wild-type and *Stim2*^{-/-} neurons. Staurosporine (300 nM) was used to induce an alternative Ca²⁺-dependent pathway leading to cell death. **(B)** N,N,N',N'-tetrakis(2-pyridylmethyl) ethylenediamine (TPEN; 2 μ M) or the vehicle (DMSO) was added to neuronal cell cultures for 10 h to induce mainly Ca²⁺-independent cell death. The results are presented as mean \pm s.d.. *p < 0.05, **p < 0.01, *** p < 0.001, using a modified student's t-test.

5.7.3. *Stim2*^{-/-} mice are protected from ischemic stroke

Cardiovascular diseases such as ischemic stroke are among the leading causes of death and disability in Western countries [159]. Microvascular integrity is disturbed during cerebral ischemia, and the involvement of platelets and intravascular thrombus formation after blood reperfusion is crucial for the development of a secondary ischemic area called “penumbra”, leading to a further increase of the ischemia [160]. To determine the effect of STIM2 deletion in this process, the development of neuronal damage was studied (in collaboration with Dr. Christoph Kleinschnitz and Prof. Guido Stoll from the Department of Neurology, University of Würzburg) in *Stim2*^{-/-} mice following transient cerebral ischemia in a model that depends on thrombus formation in microvessels downstream of a middle cerebral artery (MCA) occlusion (Fig. 41). This *in vivo* model is known as transient middle cerebral artery occlusion (tMCAO) [161]. Surprisingly, after 24 h, infarct volumes in *Stim2*^{-/-} mice were reduced to < 40 % compared to wild-type as assessed by 2,3,5-triphenyltetrazolium chloride (TTC) staining (18.6 ± 5.5 vs. 57.9 ± 13.1 mm³, $p < 0.01$) (Fig. 41A, B). Reductions in infarct size were functionally relevant, as the Bederson score assessing global neurological function (1.6 ± 0.8 vs 3.0 ± 1.0 , respectively; $p < 0.05$) and the grip test, which specifically measures motor function and coordination (2.0 ± 1.3 versus 4.1 ± 0.9 , respectively; $p < 0.05$), were significantly better in *Stim2*^{-/-} mice as compared to wild-type control mice (Fig. 41C, D).

Serial magnetic resonance imaging (MRI) on living mice up to day 5 after tMCAO showed that infarct volume did not increase over time in *Stim2*^{-/-} mice, indicating a sustained protective effect (Fig. 42). Because the severity of the brain damage, all wild-type mice were sacrificed for ethical reasons on day 1 and, therefore, not assessed by MRI on day 5. In line with this, histological analysis revealed that the infarctions were restricted to the basal ganglia in *Stim2*^{-/-} mice 24 h after tMCAO induction (Fig. 41E).

In order to analyse the role of *Stim2*^{-/-} blood cells or neuronal tissue in the protective phenotype, bone marrow chimeric mice were generated by transplantation of *Stim2*^{-/-} or wild-type bone marrow in lethally irradiated wild-type (*Stim2*^{+/+} ^{-/-}BM) or *Stim2*^{-/-} (*Stim2*^{-/-} ^{+/+}BM) donor mice, respectively. Twelve weeks after transplantation, chimeric mice were analyzed in the tMCAO model (Fig. 41A). *Stim2*^{+/+} ^{-/-}BM mice developed regular infarcts, while infarctions remained small in *Stim2*^{-/-} ^{+/+}BM mice (Fig. 41B). Additionally, *Stim2*^{-/-} ^{+/+}BM mice reached better scores in the Bederson score test and grip test as compared to *Stim2*^{+/+} ^{-/-}BM or wild-type control mice (Fig. 41C, D).

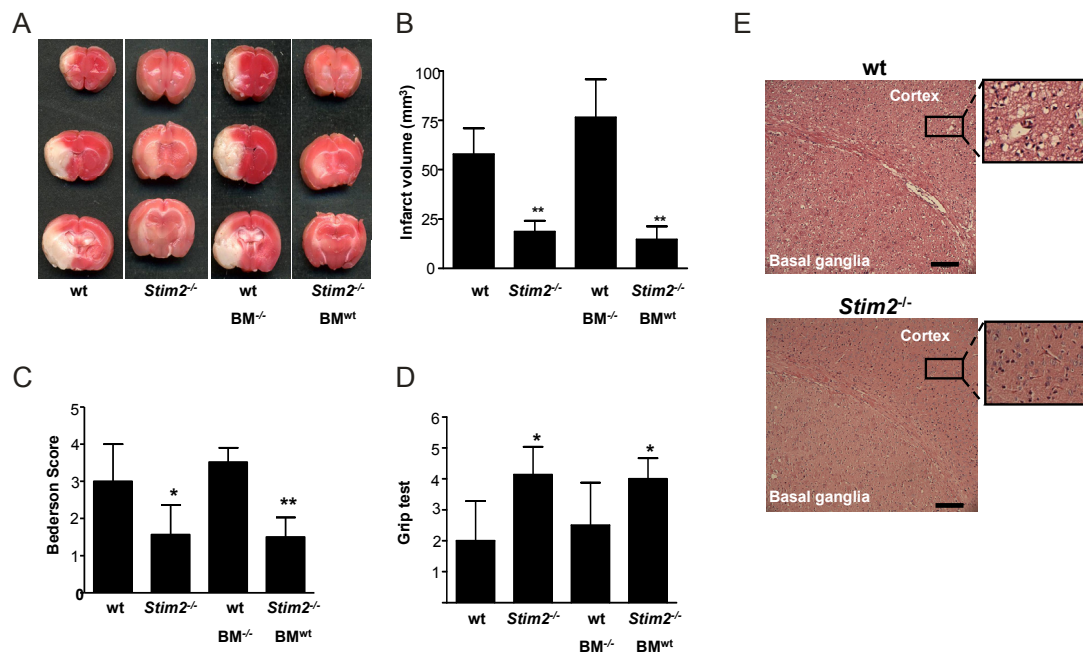


Figure 41. *Stim2*^{-/-} mice are protected from neuronal damage after cerebral ischemia. (A-C) Wild-type and *Stim2*^{-/-} mice were subjected to tMCAO and analysed after 24 h. In parallel, the experiments were performed with wild-type mice transplanted with *Stim2*^{-/-} bone marrow (*Stim2*^{+/+}BM^{-/-}) and *Stim2*^{-/-} mice transplanted with wild-type bone marrow (*Stim2*^{-/-} BM^{+/+}). (A) TTC stains of three coronal brain sections representative of each group. (B) Brain infarct volumes as measured by planimetry at day 1 after tMCAO (n = 8-10/group). (C) Neurological Bederson score and (D) grip test assessed at day 1 after tMCAO. Graphs plot mean ± s.d. (n = 8-10/group). *p < 0.05, **p < 0.01, Bonferroni-1-Way ANOVA tested against wild-type mice. (E) H&E stained sections in the ischemic hemispheres of wild-type and *Stim2*^{-/-} mice. Note that infarcts are restricted to the basal ganglia in *Stim2*^{-/-} mice, but consistently include the neocortex in the wild-type. Scale bars, 300 μm.

These results indicate that STIM2 deletion protects mice from ischemic neuronal damage independently of functional alterations within the hematopoietic system, and gave rise to a fruitful collaboration with Prof. Jens Eilers at the University of Leipzig to analyse the function of STIMs and Orai1 in Ca²⁺ homeostasis in neuronal cells (see publication list: Berna-Erro, A. *et al. Sci Signal.* 2009 Oct 20;2(93):ra67).

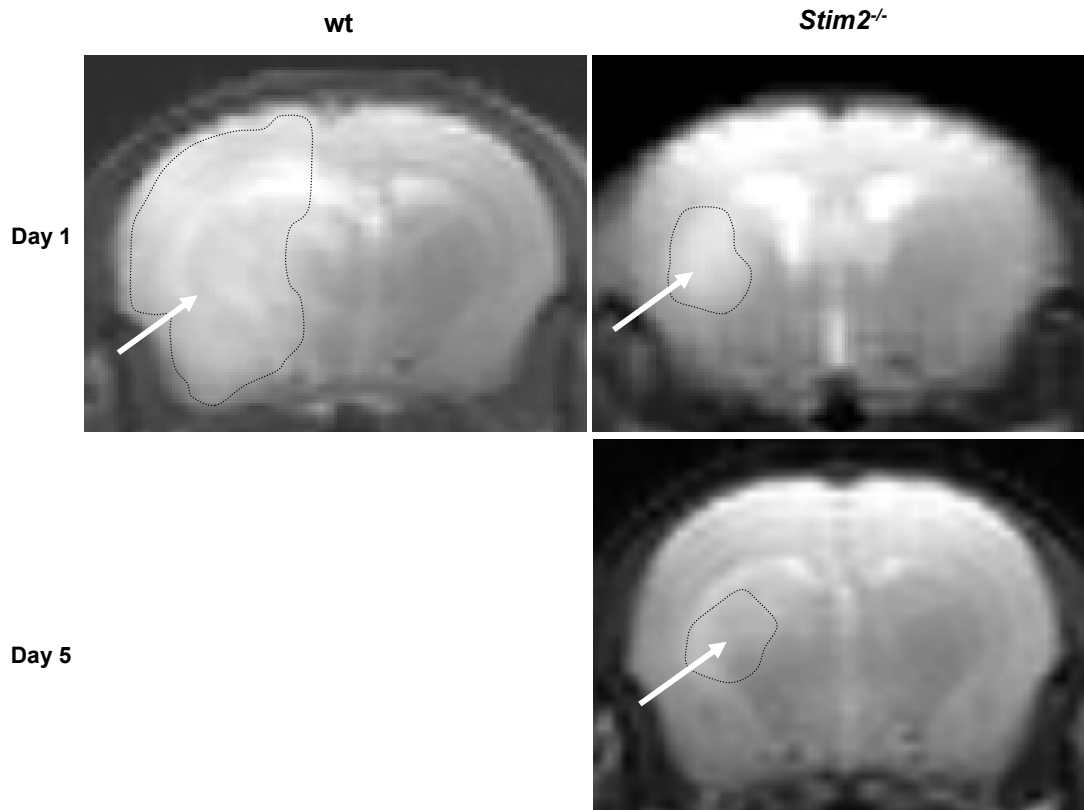


Figure 42 . Sustained neuroprotection after tMCAO in *Stim2*^{-/-} mice. Representative coronal T2-w MR brain images of wild-type or *Stim2*^{-/-} mice at day 1 and 5 after tMCAO. Infarcts are indicated by white arrows. Because the severity of the brain damage, all wild-type mice were sacrificed for ethical reasons on day 1 and were, therefore, not assessed by MRI on day 5.

6. DISCUSSION

Agonist-induced elevation of $[Ca^{2+}]_i$ is a central step during activation of cells of the immune system and platelets, but the underlying mechanisms are not fully understood. A major pathway for Ca^{2+} entry in electrically non-excitabile cells involves SOCE. In this mechanism it was clear that the activation of SOC channels in the PM is associated with a previous release of Ca^{2+} from intracellular stores. However, the molecular mechanisms, as well as the identity of the molecule/s that could link both processes were unknown for the past two decades, until the identification of the molecule STIM1. In 2001, *Stim1* and *Stim2* were identified as a gene family coding for a novel class of transmembrane proteins [44]. Most of the studies about STIM function performed by others were reported one year before and during the time period of the current thesis. In 2005, STIM1 was described as a Ca^{2+} sensor protein located in the ER of *Drosophila* S2 cells and in Jurkat T cell lines [2-4]. Additionally, Zhang et al. performed mutations leading to a single amino acid change in the EF-hand domain of STIM1 [4]. As a result, mutated STIM1 permanently opened SOC channels in the PM due to a disrupted Ca^{2+} binding of the mutated N terminus, demonstrating that STIM1 is a Ca^{2+} sensor essential for SOC channel activation and SOCE. The function of STIM2 instead, was completely unknown.

The elevation of $[Ca^{2+}]_i$ as a central step in platelet activation was clear at that time [162]. RT-PCR performed in our lab, together with The Platelet Proteosome Project performed by Prof. Albert Stickman's group at the University of Würzburg, showed strong expression of STIM molecules in human and mouse platelets. Later, the expression of STIM1 and STIM2 was confirmed in platelets by western blot (Fig. 9). Therefore, I started my PhD project in June 2006 to understand the function of STIM2 in Ca^{2+} homeostasis in murine platelets using the mouse knock-out technology.

6.1. General description of the STIM2-deficient mouse

Mice heterozygous for the STIM2-null allele were apparently healthy and had a normal life expectancy. *Stim2*^{-/-} mice were born at the expected Mendelian ratio, developed normally in size and weight to adulthood and were fertile (Fig. 12). Western blot analysis showed that STIM1 expression levels were unaltered in *Stim2*^{-/-} mice (Fig. 11E). However, a pronounced sudden death in *Stim2*^{-/-} mice

was observed, starting at the age of 8 weeks after birth (Fig. 12C). In humans, sudden death has been observed in cases of cardio-vascular alterations such as heart hypertrophy and arrhythmia, genetic malformations of the heart as well as epileptic episodes and seizures in the brain [139,163]. Alterations in intracellular Ca^{2+} release channels located in the ER, for instance IP_3R and RyR, have been associated with seizures in brain and heart arrhythmias in mice [164-166], events which in many cases led to sudden death. The analysis of heart physiology by electrocardiography (ECG) revealed a normal heart function (data not shown), indicating that sudden death in *Stim2*^{-/-} mice is not based on abnormal ECG records. However, these results do not completely rule out a possible cardiac origin, since transient short heart alterations or other alterations were not predictable and therefore hardly detectable by ECG.

Stim2^{-/-} mice also showed normal levels of different parameters in blood serum (Fig. 14), used extensively as indicators to detect possible alterations in the physiology and metabolism and therefore in organ's function. Histological examination of major organs showed no obvious abnormalities (Fig. 13). Thus, sudden death in *Stim2*^{-/-} mice is neither based on alterations in the tested blood parameters, nor on macroscopic alterations in the structure of the main organs, and it is most likely not related to heart dysfunction. Since episodes of sudden death related to altered neuronal functions have been described in humans [163,167], a possible hypothesis could be that sudden death in *Stim2*^{-/-} mice is related to brain dysfunction, although the mechanism remains unclear. It has been reported that PLC β 1 null mice suffered from epileptic seizures which finally led to the sudden death of the mice [123]. This evidence suggests that an altered SOCE in neuronal cells might also contribute to sudden death.

Early death has also been observed in *Stim1*^{-/-} mice generated in our lab [6]. Approximately, 70 % of mice lacking STIM1 died within a few hours after birth. Marked cyanosis was noted before death, suggesting a cardiopulmonary defect. Surviving *Stim1*^{-/-} mice exhibited marked growth retardation, achieving ~50 % of the weight of wild-type littermates at 3 and 7 weeks of age. Such higher and earlier mortality in the *Stim1*^{-/-} mice compared to *Stim2*^{-/-} mice indicates a more relevant function of STIM1 in murine development.

Finally, spontaneous death of *Stim2*^{-/-} mice was also reported by others during the last year of my PhD [5], although it occurred before adulthood (4-5 weeks after birth), which may be related to the variability in the genetic background between the two *Stim2*^{-/-} mouse strains. In that report, the reason of the spontaneous death was also unknown.

Furthermore, *Stim2*^{-/-} females were not able to feed their offspring (Fig. 15B, C), probably due to a mammary gland dysfunction, and such alteration could be

partially rescued in further pregnancies (Fig. 15B, C). Macroscopic histological analysis suggested that during pregnancy the mammary gland developed faster in *Stim2*^{-/-} mice as compared to wild-type controls but failed to develop further during delivery, impeding a complete expansion of alveoli and impairing the production of a sufficient amount of milk to feed the litters (Fig. 16). Such a phenotype has been reported before in other knockout mice, however, the respective proteins were not related to SOCE. For instance, local overexpression of prolactin (PRL) in mouse mammary gland induced increased development of the alveoli at early stages of pregnancy and the glands tended to be less developed during lactation. In addition, half of the PRL mutant females exhibited lactation defects, leading to significantly increased mortality of their offspring [168].

Stat5 is a transcription factor essential for milk protein gene expression in mammary epithelial cells and it is activated by PRL. Over-expression of a constitutively activated Stat5 mutant in mice led to a similar phenotype to that observed in *Stim2*^{-/-} and in the over-expressed PRL mutant mammary gland [169]. However, impaired lactation or offspring mortality were not reported. This study identified Stat5 also as a regulator of mammary cell proliferation.

Socs5 has been shown to be an inhibitor of IL-4/IL-13 signaling. This last signaling pathway activate the transcription factor Stat6, and it is primarily expressed in Th₁ cells of the immune system. Interestingly, it has been reported that *Socs5*^{-/-} mice had accelerated mammary gland development compared to controls, and showed increased number of alveoli [170]. This suggests that enhanced IL-4/IL-13 signaling, and therefore increased activation of Stat6 in the mammary epithelium of *Socs5*^{-/-} mice, results in accelerated mammary gland development. In the same study Khaled *et al.* reported that *IL-4/IL-13* double knockout and *Stat6*^{-/-} mice exhibited delayed mammary gland development, confirming the unexpected importance of these signaling pathways related to the immune system in mammary gland. It would be interesting, therefore, to study the expression of hormones and different important factors during mammary gland development in *Stim2*^{-/-} mice, specially stat5, stat6 and gata-3. Moreover, regarding the observation that multiparous *Stim2*^{-/-} females were also not able to feed their offspring (Fig. 15B), the reduced luminal area found in the alveoli in primiparous *Stim2*^{-/-} females can not explain itself the impairment in offspring feeding. Therefore, measurements of milk volumes in *Stim2*^{-/-} lactating mice will be performed, as well as the determination of fat and protein content, in order to study possible alterations in milk composition. Transplantation experiments of newborn *Stim2*^{-/-} or wild-type mammary epithelial cells in wild-type or *Stim2*^{-/-} mammary pads are planned, in order to find out whether the

altered mammary function and development is dependent on mammary epithelial cells or other external tissues.

6.2. Analysis of STIM2-deficient platelets

Since our lab is interested in functional mechanisms in platelets, the effect of STIM2 deficiency in these cells was studied. Western blot assay demonstrated that STIM2 is expressed in these cells and that the protein is completely absent in *Stim2*^{-/-} platelets (Fig. 17A). Surprisingly, no alteration in Ca²⁺ homeostasis or function could be detected in these cells in the absence of STIM2. A deep analysis was performed in order to detect possible specialized functions of this isoform in platelet function but all our results suggested that STIM2 does not play any detectable role in platelets.

In 2006, Soboloff *et al.* suggested that STIM2 is an inhibitor of STIM1-mediated store-operated Ca²⁺ entry [53]. One year later, our group reported that a constitutively active STIM1 mutant causes premature platelet activation and bleeding in mice [56]. The mouse line was named “Saxcoburggotski” (Sax). This STIM1 mutant molecule bears a point mutation in the EF-hand motif that impairs Ca²⁺ binding, mimicking the depletion of the intracellular Ca²⁺ stored in the ER. As a result, Sax mutant platelets were preactivated under non-stimulating conditions and the mice showed increased platelet consumption in the bloodstream and suffered from macrothrombocytopenia and an associated bleeding disorder [56]. Therefore, one would expect a similar phenotype in *Stim2*^{-/-} and Sax mice according to Soboloff’s hypothesis. However, STIM2-deficient platelets were not preactivated and *Stim2*^{-/-} mice showed normal platelet clearance from the blood stream (Fig. 17D). Additionally, flow cytometric studies of GPIIb/IIIa (integrin α IIb β 3) activation and of degranulation-dependent P-selectin surface exposure under resting conditions confirmed that STIM2-deficient platelets were not pre-activated (Fig. 19).

Later in the course of the current project, a study by Brandman *et al.* proposed STIM2 as a Ca²⁺ sensor in the ER, regulating basal [Ca²⁺]_i and ER Ca²⁺ levels in HeLa, HUVEC, and HEK293T cells [9]. The effect of STIM2 deficiency on Ca²⁺ homeostasis was tested in platelets (Fig. 18). In contrast to the proposed function of STIM2 by Brandman *et al.*, STIM2-deficient platelets showed unaltered basal [Ca²⁺]_i and normal Ca²⁺ concentration in the ER. Additionally, despite robust expression of STIM2 in platelets, lack of the protein did not alter SOCE upon different agonist activation (Fig. 18). Moreover, STIM2-deficient platelets were normally activable (Fig. 19) and aggregated normally *ex vivo*

(Fig. 24), indicating a non-essential function of STIM2 in platelet's, Ca^{2+} homeostasis and activation. In the course of the current project, a parallel study for STIM1 function in platelets was performed in our lab. Varga-Szabó *et al.* reported that STIM1 is not essential for megakaryopoiesis or platelet production in *Stim1*^{-/-} mice [6]. However, $[\text{Ca}^{2+}]_i$ measurements on *Stim1*^{-/-} platelets showed severely defective Ca^{2+} responses to all major agonists. Unexpectedly, the ER Ca^{2+} concentration was significantly decreased, as one would expect in STIM2-deficient platelets [9]. In addition, analysis of platelets lacking the STIM1-regulated Ca^{2+} channel, Orai1, revealed defective SOCE, but unaltered ER Ca^{2+} content [36]. These results suggest that STIM1 rather than STIM2 regulates the Ca^{2+} store content in platelets and indicate that this function does not require Orai1. A possible explanation for these contradictory results with the study by Brandman *et al.* is that the relevance of the STIM isoform function in Ca^{2+} homeostasis regulation strongly depends on the cell type.

Previous studies reported that STIM2 also interacts with the Orai1 channel and the co-expression of both molecules increases SOCE in cell lines [63,65]. A very interesting study would be to test for competition mechanisms between both STIM isoforms and the Orai1 channel in platelets. Such an experiment could also explain in part the unaltered function and Ca^{2+} homeostasis in STIM2-deficient platelets by the existence of compensatory mechanisms between both STIM isoforms. However, STIM1-deficient platelets showed severely defective responses to all major agonists [6], indicating that STIM2 can not take over the function of STIM1 thereby questioning this idea. Interestingly, these mutant cells showed a residual Ca^{2+} influx, suggesting that other molecules may regulate SOC influx to a minor extent. One candidate molecule could be STIM2, and this residual Ca^{2+} influx could be explained by a partial compensation, possibly due to the lower expression of STIM2 in platelets as compared to STIM1 (Fig. 9) or/and a partial but not completely overlapping function of both isoforms. Supporting this idea, Oh-hora *et al.* overexpressed STIM2 in STIM1-deficient mouse embryonic fibroblasts (MEFs), isolated from conditional STIM1 knock-out mice (*Stim1*^{-/-}) [5]. They found that STIM2 partially restored SOCE in the STIM1-deficient background, indicating a partial overlap of the STIM function in these cells.

6.3. Analysis of STIM2 deficiency in immune cells

In immune cells, the predominant pathway of Ca^{2+} entry is thought to involve IP_3R -mediated SOCE. Therefore, the effect of STIM2 deletion in the innate (mast cells and macrophages) and the adaptive (B and T cells) immune system was also studied.

6.3.1. The effect of STIM2 deletion on the innate immune system: Mast cells

The analysis of Ca^{2+} homeostasis and SOCE in PMC and BMMC *in vitro* differentiated mast cells showed that STIM2 deletion does not alter the basal $[\text{Ca}^{2+}]_i$, nor the basal ER Ca^{2+} levels in these cells, nor SOCE after stimulation via store depletion or IgE-mediated $\text{Fc}\epsilon\text{R}$ activation (Fig. 25). Surprisingly, *Stim2*^{-/-} mice were protected from IgE-mediated systemic anaphylaxis (Fig. 26A). In contrast, *Stim2*^{+/+} ^{-/-}BM chimeric mice did not show such a protective effect to anaphylaxis, indicating that STIM2-deficient blood cells were not involved in the phenotype (Fig. 26B). In the IgE-mediated anaphylaxis model, the mast cell activity was assessed indirectly by measuring the body temperature. The histamine released by mast cells is primarily responsible for the development of the hypothermia, while platelet-activating factor (PAF) is responsible for the increased vascular permeation and hypotension (for review, see [171]). This released histamine during the systemic anaphylaxis seems to act in the brain, presumably by binding to histamine receptors in the hypothalamus, which is known to be involved in body thermoregulation [172]. Thus, in conclusion the protective effect in *Stim2*^{-/-} mice in IgE-mediated anaphylaxis model is independent of mast cells and is most likely due to an altered function in other STIM2-deficient cell types such as certain neuronal circuits of the hypothalamus or the endothelial cells of blood vessels. An essential function of Stim1 in mast cell activation and anaphylactic responses has been described previously [146]. STIM1-deficient mast cells showed impaired SOCE after $\text{Fc}\epsilon\text{RI}$ -mediated stimulation and abolished activation of the transcription factors NF- κB and NFAT. Mast cells lacking STIM1 also displayed much less degranulation and cytokine production and *Stim1*^{-/-} mice were less sensitive to immunoglobulin E-mediated immediate-phase anaphylactic responses *in vivo*. These results support the idea that the relevance of STIM function is strongly dependent of the cell type.

6.3.2. The effect of STIM2 deletion on the innate immune system: Macrophages

Ca²⁺ homeostasis and SOCE was also analyzed in *Stim2*^{-/-} macrophages. STIM2 deletion did not alter SOCE in these cells, neither after stimulation of Ca²⁺ store release with 5 μM TG, nor by direct stimulation through FcγR activation (Fig. 27). However, the expression of the activating receptors FcγRIII and IV was increased by 25 % in *Stim2*^{-/-} macrophages (Fig. 28). It can be speculated that this rather mild increase could not have a significant effect on SOCE, or that there is a compensatory mechanism during macrophage maturation in order to re-establish normal Ca²⁺ homeostasis. Unfortunately, there is no good anti-FcγRII antibody commercially available to study whether the expression of the inhibitory receptor is increased as well, which might indicate compensation mechanisms to the increased expression of FcγRIII and FcγRIV. Strikingly, *Stim2*^{-/-} mice were protected to FcγR-mediated ITP after i.v. injection of anti-GPIIb/IIIa antibodies (Fig. 29). Since surface glycoprotein expression is normal in *Stim2*^{-/-} platelets (Fig. 17C), the protective effect can not be associated to an alteration in the described glycoproteins. Our lab found that STIM1 is also essential for FcγR activation and autoimmune inflammation [173]. This could be explained by an abolishment of SOCE after FcγR activation in the absence of STIM1, indicating that SOCE is an important mechanism for FcγR-dependent activation in macrophages. The protective effect of *Stim2*^{-/-} mice in ITP is however, not easy to explain, since SOCE is not altered in these cells. Therefore, a possible hypothesis is that this protective phenotype could be due to another STIM2-deficient cells.

The apparent contradiction between the unexpected upregulation of FcγRs, the normal Ca²⁺ influx after FcγR activation and the protective effect of *Stim2*^{-/-} mice in the ITP model remains to be clarified. These results require further studies that are still ongoing. It is necessary to perform the same experiments using bone marrow chimeras, in order to study whether the upregulation of FcγR and the protective phenotype seen in the ITP model is dependent on the STIM2 deficiency in blood cells or in other cells. In mice, i.v. injection of anti-GPIIb/IIIa antibodies leads to FcγR-dependent platelet clearance, mainly via macrophages located in the spleen [132,149]. Therefore, it is also important to study the platelet clearance occurring in the spleen in this model.

6.3.3. Effect of STIM2 deletion on the adaptive immune system: T and B cells

In this study, it was shown that STIM2 is also expressed in lymph nodes, suggesting a function in T cells (Fig. 9A, 11E). Previous reports indicated a potential role of STIM2 in T cell Ca^{2+} homeostasis [2,53]. Therefore, the effect of STIM2 deficiency on Ca^{2+} homeostasis and SOCE in CD4^+ T cells isolated from spleen and lymph nodes was analyzed. STIM2 deficiency did not play a role in the regulation of basal $[\text{Ca}^{2+}]_i$ and the ER Ca^{2+} levels in CD4^+ T cells. However, SOCE was markedly reduced after Ca^{2+} store depletion by TG or direct TCR activation (Fig. 30), but it was independent of altered CD3 or TCR expression in the cells (Fig. 31). In contrast to the proposed function of STIM2 by Brandman *et al.*[9], basal $[\text{Ca}^{2+}]_i$ and the ER Ca^{2+} concentration was unaltered in STIM2-deficient CD4^+ T cells. However, in contrast to the results obtained in platelets, mast cells or macrophages, STIM2 deficiency significantly altered SOCE in T cells, suggesting again that the relevance of the respective STIM isoform function strongly depends on the cell type. In 2008, Oh-hora *et al.* generated conditional knock-out mice for STIM1 and STIM2 and showed that T cells and fibroblasts lacking STIM1 had severely impaired store-operated Ca^{2+} influx, whereas deficiency in STIM2 had a small or even no effect [5]. They showed that naive CD4^+ T cells had almost no expression of STIM2, while T cell activation led to a substantial increase in STIM2 expression up to 3–10 % of total STIM protein. They proposed this as a possible explanation for this discrepancy. In our study, in contrast to Oh-hora's model, wild-type naive CD4^+ T cells substantially expressed STIM2 (Fig. 30A), which may be related to the variability in the genetic background between the two *Stim2*^{-/-} mouse strains, and deletion of STIM2 led to a 50 % decrease of SOCE in these cells (Fig. 30B, C, D, F).

A mild decrease in the number of CD8^+ lymphocytes and splenocytes was also found in naive *Stim2*^{-/-} mice (Fig. 32B, C). Although SOCE has been implicated in negative selection of thymic T cell precursors [174], *Stim2*^{-/-} mice had a normal composition of thymocyte subsets (Fig. 33). Analysis of the splenocyte proliferation *ex vivo* from naive *Stim2*^{-/-} mice revealed no differences in proliferation as compared to control cells (Fig. 35A), indicating that this mild decrease in the numbers of CD8^+ T cells can not be explained by an abnormal maturation of T cells in the thymus or by an altered turnover in spleen. I can be speculated that this mild decrease could be the consequence of many alterations that are too small to be statistically significant. For instance, the CD4^+ thymocyte subset showed a slightly increase in numbers in *Stim2*^{-/-} mice,

while the CD8⁺ thymocyte subset showed a decrease in numbers (Fig. 33), but these differences were statistically non-significant. Similar results were obtained in lymph nodes and spleen, where the CD4⁺ T subset was slightly increased in numbers, but this difference was again statistically non-significant (Fig. 32B, C). Thus, such small differences could have an additive effect that at the end could significantly influence the percentages of CD4⁺ T and CD8⁺ cells in the secondary lymphoid organs (lymph nodes and spleen). Additional processes not studied in this work that might be altered, such as apoptosis or migration could also influence the cellularity in lymphoid organs.

Furthermore, the adaptive immune response in *Stim2*^{-/-} mice was examined after immunization with the T cell-dependent model antigen KLH (Fig. 35C, D), but no differences were found compared to wild-type controls, indicating that STIM2 does not play a role in T cell proliferation or B cell antibody production in this model (Fig. 35C, D). Beyersdorf *et al.* reported that *Stim1*^{-/-} mice were able to drive a normal humoral immune response after vaccination despite the fact that SOCE was virtually absent in isolated STIM1-deficient T cells [7]. Additionally *Stim1*^{-/-} mice developed a lymphoproliferative disease, characterized by a hyper-proliferation of CD4⁺ T cells, despite normal thymic T cell maturation [5,7]. Our results, together with these results obtained in *Stim1*^{-/-} mice, suggest that the STIM family is involved in homeostatic T cell proliferation, but it is much less important for thymic T cell differentiation or humoral T cell-dependent responses.

Finally, the effect of STIM2 deficiency in an *in vivo* model of autoimmune response was tested in collaboration with Michael K. Schuhmann and Dr. Sven G. Meuth from the Department of Neurology, University of Würzburg, referred to as myelin oligodendrocyte glycoprotein (MOG₃₅₋₅₅-peptide)-induced EAE (Fig. 36). Strikingly, *Stim2*^{-/-} mice showed a significantly reduced disease maximum (Fig. 36A) while the disease incidence, overall disease course and residual disease scores at day 50 were unaltered. Additionally, *Stim2*^{-/-} mice showed a tendency to reduced demyelination in spinal cord white matter (neuronal axons) at disease maximum (Fig. 36B middle, C upper), but a comparable number of infiltrating T cells (Fig. 36B lower, C lower). Thus, in contrast to the T cell-dependent model antigen KLH of adaptive immune response, where *Stim2*^{-/-} mice did not show an altered response (Fig. 35C, D), these mice developed an attenuated EAE, indicating a possible role of STIM2 during the early phase of EAE progression. The reason why *Stim2*^{-/-} mice showed an attenuated disease progression in the EAE model but a normal adaptive immune response in the KLH-antigen model is not clear. KLH is a very strong exogenous antigen, transiently present in blood, that elicits T cell-

dependent anti-KLH antibody production (humoral immune response) and a memory T cell response [175,176]. An altered level of anti-KLH antibodies in blood serum is indicative of alterations in antigen presenting T-B cell function, T cell proliferation or B cell antibody production.

EAE is a complex model for autoimmune diseases where many factors and cell types are involved, and where an auto-antigen (MOG) elicits a chronic immune response against a component of the myelin, in other words, the antigen is always present during the disease. The role of B cells and autoantibodies in the pathogenesis of EAE remains controversial. Mice immunized against mouse MOG produce autoantibodies directed against conformation-dependent epitopes of the extracellular domain of the native protein expressed at the cell surface, and these autoantibodies play a major role in the immunopathogenesis of demyelination in EAE. However, these autoantibodies generated after MOG-immunization do not recognize the native protein in mouse strains with the haplotype H-2^b, for instance in C57Bl/6 mice [177,178]. Since the genetically engineered *Stim2* chimeras were backcrossed with the C57BL/6 background to obtain *Stim2*^{-/-} mice, and murine MOG was used to immunize them, the resulting auto-antibodies should not play an important role in the EAE progression in our study.

It is very important to point out that in the EAE model the disease progression in mice was monitored daily (Fig. 36A), while the titer of the anti-KLH antibody in blood serum of KLH-injected mice was measured at only one time point, at week 6 after immunization, where according to the standard protocol the antibodies show the maximum levels in blood serum (Fig. 35D). *Stim2*^{-/-} mice showed differences in the EAE scores only at early stages of the disease progression. However, there is no information about the antibody titer at earlier stages after KLH immunization and therefore, data from both models can not be contrasted. It is not known whether the KLH autoantibody production is attenuated in *Stim2*^{-/-} mice at early time points after immunization or not. Regarding this consideration, the results obtained in both models would not contradict each other and it is clear that further studies must be performed to investigate the role of STIM2 in humoral responses and EAE progression. Such studies are currently ongoing (see publications list: Schuhmann, MK. *et al. J Immunol*, 2009, accepted manuscript).

6.4. Analysis of STIM2 deficiency in neurons

In brain, the absence of STIM2 had a greater impact on Ca^{2+} homeostasis and it correlated with the finding that STIM2 is the dominant isoform in this organ (Fig. 9). The existence of SOCE (referred to as CCE in neurons) in wild-type neurons was confirmed using the agent CPA (Fig. 37A). The analysis of Ca^{2+} homeostasis in E19 embryonic cultured neurons showed that STIM2 deletion lowered the basal $[\text{Ca}^{2+}]_i$ and the basal ER Ca^{2+} levels in these cells (Fig. 37), indicating that STIM2 is a regulator that stabilizes basal cytosolic and ER Ca^{2+} levels in neurons, which is in agreement to previous results reported by Brandman *et al.* [9]. Strikingly, SOCE was severely reduced in *Stim2*^{-/-} neurons compared to wild-type controls, indicating that STIM2 is also essential for SOCE in neurons (Fig. 37A). This finding is in line with the notion that STIM2 regulates store refilling as well as the basal cytosolic Ca^{2+} concentration in neurons by sensing the ER Ca^{2+} content and, if it is too low, activating SOCE, possibly via Orai channels [63,179]. The resulting Ca^{2+} influx is used to refill Ca^{2+} stores in the wild-type cell [27]. Correspondingly, due to the severely decreased SOCE in *Stim2*^{-/-} neurons, the ER Ca^{2+} content and the $[\text{Ca}^{2+}]_i$ are reduced. For pathophysiological conditions such as ischemia, our study assigned a key role to STIM2 and SOCE in Ca^{2+} -dependent cell death (Fig. 38-40), which evolves from and/or into glutamate-mediated neurotoxicity [114]. The existing literature describes that anoxia reduces SERCA activity in neurons [180,181], but also appears to involve active Ca^{2+} release mediated by the IP₃R and RyR channels located in the ER, as evidenced by protection of neurons against excitotoxic injury through blockade of IP₃R or RyR [182,183]. Together, these events lead to Ca^{2+} accumulation in the cytosol and a corresponding store depletion, the latter inducing an additional Ca^{2+} load via SOCE. In turn, SOCE may trigger a further Ca^{2+} influx by increasing the release of glutamate and the subsequent activation of ionotropic glutamate receptors [114]. Both, SOCE and glutamatergic Ca^{2+} entry, then rapidly push the cytosolic Ca^{2+} concentration to damaging levels. Our results showed that *Stim2*^{-/-} neurons subjected to a longer period of OGD were less sensitive to apoptosis (Fig. 39) because they did not undergo SOCE (Fig. 37A) and had a lower Ca^{2+} content in the intracellular stores (Fig. 37B), which critically depends on a functional SOCE [27]. The decreased store content limits the initial Ca^{2+} release (Fig. 37B) and helps to better utilize the remaining Ca^{2+} sequestration capacity during the ischemic challenge (Fig. 38). This protective phenotype was observed only in Ca^{2+} -related apoptotic mechanisms (Fig. 40A), since treatment with TPEN, an

apoptotic agent that does not alter $[Ca^{2+}]_i$, induced apoptosis in wild-type and *Stim2*^{-/-} neurons to the same extent (Fig. 40B).

Finally, the *in vivo* implication of these findings was studied using a model of cerebral ischemia, referred to as tMCAO (Fig. 41). Surprisingly, STIM2 deficiency significantly protected mice from ischemic neuronal damage independently of functional alterations within blood cells (Fig. 41A, B), presumably since STIM2 deficiency in platelets did not alter platelet function. This is the first evidence for the involvement of SOCE in ischemic neuronal damage. Varga-Szabó *et al.* demonstrated that STIM1 is also an essential mediator of ischemic brain infarction [6]. However, in contrast to *Stim2*^{+/+} *-/-* BM chimeric mice, which developed regular infarcts, *Stim1*^{+/+} *-/-* BM chimeric mice were protected from neuronal damage following transient cerebral ischemia, displaying a 30 % reduction in the infarct volume. This result indicated that the absence of STIM1 in platelets conferred the protective effect to neuronal damage to *Stim1*^{-/-} mice. Interestingly, densitometric analysis of STIM proteins performed in this thesis revealed a dominant expression of STIM2 in brain compared to platelets and to other organs, where STIM1 seems to be the most abundant isoform (Fig. 9B). It is presently not clear why neurons use STIM2 but not STIM1 to regulate SOCE, but our data suggest that the relevance of the STIM isoform function strongly depends on the cell type and correlates with their relative cellular expression. At the beginning of the current project, there was no report in the literature about the possible role of SOCE in ischemic processes, and few studies about its role in other neuronal processes have been reported. However, different knockout models for proteins related with IP₃-mediated intracellular Ca²⁺ release suggested an important role of this mechanism in neuronal functions. For instance, the absence of PLCβ1 led to epileptic-type seizures in mice [123], which indicated an involvement of PLCβ1 in the development and control of brain inhibitory pathways. IP₃R type I null mice exhibited severe neurological symptoms, including ataxia and epilepsy [124]. These evidences, together with our results in neurons, suggest an unexpectedly important role of SOCE in diverse functions in electrically excitable cells such as neurons. Clearly, further studies are required to draw a full picture of i) the role that STIM2 plays under physiological conditions in neurons, ii) which molecular partners interact with STIM2 (e.g., Orai/CRACM and/or TRP channels [27,63] iii) which neuronal activity triggers SOCE (e.g., burst firing or high frequency discharges of excitatory inputs), and iv) whether STIM2-deficiency affects synaptic activity and plasticity.

In summary, the studies shown here provide new insights into the *in vivo* function of STIM2 in mice. The presented data strongly suggest that STIM2 is a functional ER Ca^{2+} sensor *in vivo* and plays an important role in brain, mammary gland and T cells. The presented results could not provide a comprehensive molecular explanation of the phenotypes found in *Stim2*^{-/-} mice but they were the starting point for three ongoing parallel studies.

STIM2 seems to be not relevant for the function of platelets, at least under the experimental conditions tested. Furthermore, STIM2 seems to be involved in mammary gland development during pregnancy and essential for mammary gland function during lactation.

In T cells, STIM2 is involved in SOCE as a positive regulator of Ca^{2+} signaling rather than being an inhibitor of STIM1, as was proposed before [53]. Additionally, our data suggest that the function of STIM2 is very specific in the immune system, involved in EAE at the early stages of disease progression.

In brain, our results evidenced that STIM2 participates in mechanisms of neuronal damage after ischemic events. This is the first time that the involvement of SOCE in ischemic neuronal damage has been reported, but further analysis of these processes will be necessary. These findings may serve as a basis for the development of novel neuroprotective agents for the treatment of ischemic stroke but possibly also other neurodegenerative disorders in which disturbances in cellular Ca^{2+} homeostasis are considered a major pathophysiological component [112,113].

Most of the reports published during my thesis suggested that STIM2 has a minor function in Ca^{2+} homeostasis compared to STIM1. In contrast, the data presented in this work suggest that the relevance of the STIM function is strongly dependent on the cell type and correlates with the relative isoform expression in the studied cell type.

7. REFERENCES

1. Hoth, M., and R. Penner. 1992. Depletion of intracellular calcium stores activates a calcium current in mast cells. *Nature* 355:353.
2. Liou, J., M. L. Kim, W. D. Heo, J. T. Jones, J. W. Myers, J. E. Ferrell, Jr., and T. Meyer. 2005. STIM is a Ca^{2+} sensor essential for Ca^{2+} -store-depletion-triggered Ca^{2+} influx. *Curr. Biol.* 15:1235.
3. Roos, J., P. J. DiGregorio, A. V. Yeromin, K. Ohlsen, M. Lioudyno, S. Zhang, O. Safrina, J. A. Kozak, S. L. Wagner, M. D. Cahalan, G. Velicelebi, and K. A. Stauderman. 2005. STIM1, an essential and conserved component of store-operated Ca^{2+} channel function. *J. Cell Biol.* 169:435.
4. Zhang, S. L., Y. Yu, J. Roos, J. A. Kozak, T. J. Deerinck, M. H. Ellisman, K. A. Stauderman, and M. D. Cahalan. 2005. STIM1 is a Ca^{2+} sensor that activates CRAC channels and migrates from the Ca^{2+} store to the plasma membrane. *Nature* 437:902.
5. Oh-hora, M., M. Yamashita, P. G. Hogan, S. Sharma, E. Lamperti, W. Chung, M. Prakriya, S. Feske, and A. Rao. 2008. Dual functions for the endoplasmic reticulum calcium sensors STIM1 and STIM2 in T cell activation and tolerance. *Nat. Immunol.* 9:432.
6. Varga-Szabo, D., A. Braun, C. Kleinschnitz, M. Bender, I. Pleines, M. Pham, T. Renne, G. Stoll, and B. Nieswandt. 2008. The calcium sensor STIM1 is an essential mediator of arterial thrombosis and ischemic brain infarction. *J. Exp. Med.* 205:1583.
7. Beyersdorf, N., A. Braun, T. Vogtle, D. Varga-Szabo, R. R. Galdos, S. Kissler, T. Kerkau, and B. Nieswandt. 2009. STIM1-independent T cell development and effector function in vivo. *J. Immunol.* 182:3390.
8. Peinelt, C., M. Vig, D. L. Koomoa, A. Beck, M. J. Nadler, M. Koblan-Huberson, A. Lis, A. Fleig, R. Penner, and J. P. Kinet. 2006. Amplification of CRAC current by STIM1 and CRACM1 (Orai1). *Nat. Cell Biol.* 8:771.
9. Brandman, O., J. Liou, W. S. Park, and T. Meyer. 2007. STIM2 is a feedback regulator that stabilizes basal cytosolic and endoplasmic reticulum Ca^{2+} levels. *Cell* 131:1327.
10. Byron, K. L., G. Babnigg, and M. L. Villereal. 1992. Bradykinin-induced Ca^{2+} entry, release, and refilling of intracellular Ca^{2+} stores. Relationships revealed by image analysis of individual human fibroblasts. *J. Biol. Chem.* 267:108.
11. Berridge, M. J., M. D. Bootman, and H. L. Roderick. 2003. Calcium signalling: dynamics, homeostasis and remodelling. *Nat. Rev. Mol. Cell Biol.* 4:517.
12. Parekh, A. B. 2008. Ca^{2+} microdomains near plasma membrane Ca^{2+} channels: impact on cell function. *J. Physiol* 586:3043.

13. Strehler, E. E., A. J. Caride, A. G. Filoteo, Y. Xiong, J. T. Penniston, and A. Enyedi. 2007. Plasma membrane Ca^{2+} ATPases as dynamic regulators of cellular calcium handling. *Ann. N. Y. Acad. Sci.* 1099:226.
14. Guerini, D., L. Coletto, and E. Carafoli. 2005. Exporting calcium from cells. *Cell Calcium* 38:281.
15. Philipson, K. D., D. A. Nicoll, M. Ottolia, B. D. Quednau, H. Reuter, S. John, and Z. Qiu. 2002. The $\text{Na}^+/\text{Ca}^{2+}$ exchange molecule: an overview. *Ann. N. Y. Acad. Sci.* 976:1.
16. Periasamy, M., and A. Kalyanasundaram. 2007. SERCA pump isoforms: their role in calcium transport and disease. *Muscle Nerve* 35:430.
17. Bird, G. S., O. Aziz, J. P. Lievremont, B. J. Wedel, M. Trebak, G. Vazquez, and J. W. Putney, Jr. 2004. Mechanisms of phospholipase C-regulated calcium entry. *Curr. Mol. Med.* 4:291.
18. Suh, P. G., J. I. Park, L. Manzoli, L. Cocco, J. C. Peak, M. Katan, K. Fukami, T. Kataoka, S. Yun, and S. H. Ryu. 2008. Multiple roles of phosphoinositide-specific phospholipase C isozymes. *BMB. Rep.* 41:415.
19. Demaurex, N., and M. Frieden. 2003. Measurements of the free luminal ER $\text{Ca}(2+)$ concentration with targeted "cameleon" fluorescent proteins. *Cell Calcium* 34:109.
20. Barrero, M. J., M. Montero, and J. Alvarez. 1997. Dynamics of $[\text{Ca}^{2+}]$ in the endoplasmic reticulum and cytoplasm of intact HeLa cells. A comparative study. *J. Biol. Chem.* 272:27694.
21. Jardin, I., J. J. Lopez, J. A. Pariente, G. M. Salido, and J. A. Rosado. 2008. Intracellular calcium release from human platelets: different messengers for multiple stores. *Trends Cardiovasc. Med.* 18:57.
22. Patterson, R. L., D. Boehning, and S. H. Snyder. 2004. Inositol 1,4,5-trisphosphate receptors as signal integrators. *Annu. Rev. Biochem.* 73:437.
23. Nakagawa, T., H. Okano, T. Furuichi, J. Aruga, and K. Mikoshiba. 1991. The subtypes of the mouse inositol 1,4,5-trisphosphate receptor are expressed in a tissue-specific and developmentally specific manner. *Proc. Natl. Acad. Sci. U. S. A* 88:6244.
24. Wojcikiewicz, R. J., and S. G. Luo. 1998. Differences among type I, II, and III inositol-1,4,5-trisphosphate receptors in ligand-binding affinity influence the sensitivity of calcium stores to inositol-1,4,5-trisphosphate. *Mol. Pharmacol.* 53:656.
25. Feske, S. 2007. Calcium signalling in lymphocyte activation and disease. *Nat. Rev. Immunol.* 7:690.
26. Carafoli, E., L. Santella, D. Branca, and M. Brini. 2001. Generation, control, and processing of cellular calcium signals. *Crit Rev. Biochem. Mol. Biol.* 36:107.
27. Parekh, A. B., and J. W. Putney, Jr. 2005. Store-operated calcium channels. *Physiol Rev.* 85:757.

28. Minke, B. 2006. TRP channels and Ca²⁺ signaling. *Cell Calcium* 40:261.
29. Vig, M., A. Beck, J. M. Billingsley, A. Lis, S. Parvez, C. Peinelt, D. L. Koomoa, J. Soboloff, D. L. Gill, A. Fleig, J. P. Kinet, and R. Penner. 2006. CRACM1 multimers form the ion-selective pore of the CRAC channel. *Curr. Biol.* 16:2073.
30. Mignen, O., J. L. Thompson, and T. J. Shuttleworth. 2008. Both Orai1 and Orai3 are essential components of the arachidonate-regulated Ca²⁺-selective (ARC) channels. *J. Physiol* 586:185.
31. Lis, A., C. Peinelt, A. Beck, S. Parvez, M. Monteilh-Zoller, A. Fleig, and R. Penner. 2007. CRACM1, CRACM2, and CRACM3 are store-operated Ca²⁺ channels with distinct functional properties. *Curr. Biol.* 17:794.
32. Mercer, J. C., W. I. DeHaven, J. T. Smyth, B. Wedel, R. R. Boyles, G. S. Bird, and J. W. Putney, Jr. 2006. Large store-operated calcium selective currents due to co-expression of Orai1 or Orai2 with the intracellular calcium sensor, Stim1. *J. Biol. Chem.* 281:24979.
33. Gwack, Y., S. Srikanth, S. Feske, F. Cruz-Guilloty, M. Oh-hora, D. S. Neems, P. G. Hogan, and A. Rao. 2007. Biochemical and functional characterization of Orai proteins. *J. Biol. Chem.* 282:16232.
34. Feske, S., Y. Gwack, M. Prakriya, S. Srikanth, S. H. Puppel, B. Tanasa, P. G. Hogan, R. S. Lewis, M. Daly, and A. Rao. 2006. A mutation in Orai1 causes immune deficiency by abrogating CRAC channel function. *Nature* 441:179.
35. Gross, S. A., U. Wissenbach, S. E. Philipp, M. Freichel, A. Cavalie, and V. Flockerzi. 2007. Murine ORAI2 splice variants form functional Ca²⁺ release-activated Ca²⁺ (CRAC) channels. *J. Biol. Chem.* 282:19375.
36. Braun, A., D. Varga-Szabo, C. Kleinschnitz, I. Pleines, M. Bender, M. Austinat, M. Bosl, G. Stoll, and B. Nieswandt. 2009. Orai1 (CRACM1) is the platelet SOC channel and essential for pathological thrombus formation. *Blood* 113:2056.
37. Vig, M., W. I. DeHaven, G. S. Bird, J. M. Billingsley, H. Wang, P. E. Rao, A. B. Hutchings, M. H. Jouvin, J. W. Putney, and J. P. Kinet. 2008. Defective mast cell effector functions in mice lacking the CRACM1 pore subunit of store-operated calcium release-activated calcium channels. *Nat. Immunol.* 9:89.
38. Gwack, Y., S. Srikanth, M. Oh-hora, P. G. Hogan, E. D. Lamperti, M. Yamashita, C. Gelinis, D. S. Neems, Y. Sasaki, S. Feske, M. Prakriya, K. Rajewsky, and A. Rao. 2008. Hair loss and defective T- and B-cell function in mice lacking ORAI1. *Mol. Cell Biol.* 28:5209.
39. Yue, L., J. B. Peng, M. A. Hediger, and D. E. Clapham. 2001. CaT1 manifests the pore properties of the calcium-release-activated calcium channel. *Nature* 410:705.
40. Pigozzi, D., T. Ducret, N. Tajeddine, J. L. Gala, B. Tombal, and P. Gailly. 2006. Calcium store contents control the expression of TRPC1, TRPC3 and TRPV6 proteins in LNCaP prostate cancer cell line. *Cell Calcium* 39:401.

41. Varga-Szabo, D., K. S. Authi, A. Braun, M. Bender, A. Ambily, S. R. Hassock, T. Gudermann, A. Dietrich, and B. Nieswandt. 2008. Store-operated Ca(2+) entry in platelets occurs independently of transient receptor potential (TRP) C1. *Pflugers Arch.* 457:377.
42. Liu, X., K. T. Cheng, B. C. Bandyopadhyay, B. Pani, A. Dietrich, B. C. Paria, W. D. Swaim, D. Beech, E. Yildirim, B. B. Singh, L. Birnbaumer, and I. S. Ambudkar. 2007. Attenuation of store-operated Ca²⁺ current impairs salivary gland fluid secretion in TRPC1(-/-) mice. *Proc. Natl. Acad. Sci. U. S. A* 104:17542.
43. Liao, Y., C. Erxleben, E. Yildirim, J. Abramowitz, D. L. Armstrong, and L. Birnbaumer. 2007. Orai proteins interact with TRPC channels and confer responsiveness to store depletion. *Proc. Natl. Acad. Sci. U. S. A* 104:4682.
44. Williams, R. T., S. S. Manji, N. J. Parker, M. S. Hancock, S. L. Van, J. P. Eid, P. V. Senior, J. S. Kazenwadel, T. Shandala, R. Saint, P. J. Smith, and M. A. Dziadek. 2001. Identification and characterization of the STIM (stromal interaction molecule) gene family: coding for a novel class of transmembrane proteins. *Biochem. J.* 357:673.
45. Zheng, L., P. B. Stathopoulos, G. Y. Li, and M. Ikura. 2008. Biophysical characterization of the EF-hand and SAM domain containing Ca²⁺ sensory region of STIM1 and STIM2. *Biochem. Biophys. Res. Commun.* 369:240.
46. Stathopoulos, P. B., L. Zheng, G. Y. Li, M. J. Plevin, and M. Ikura. 2008. Structural and mechanistic insights into STIM1-mediated initiation of store-operated calcium entry. *Cell* 135:110.
47. Stathopoulos, P. B., L. Zheng, and M. Ikura. 2009. Stromal interaction molecule (STIM) 1 and STIM2 calcium sensing regions exhibit distinct unfolding and oligomerization kinetics. *J. Biol. Chem.* 284:728.
48. Kim, C. A., and J. U. Bowie. 2003. SAM domains: uniform structure, diversity of function. *Trends Biochem. Sci.* 28:625.
49. Qiao, F., and J. U. Bowie. 2005. The many faces of SAM. *Sci. STKE.* 2005:re7.
50. Schultz, J., C. P. Ponting, K. Hofmann, and P. Bork. 1997. SAM as a protein interaction domain involved in developmental regulation. *Protein Sci.* 6:249.
51. Parry, D. A., R. D. Fraser, and J. M. Squire. 2008. Fifty years of coiled-coils and alpha-helical bundles: a close relationship between sequence and structure. *J. Struct. Biol.* 163:258.
52. Williams, R. T., P. V. Senior, S. L. Van, J. E. Layton, P. J. Smith, and M. A. Dziadek. 2002. Stromal interaction molecule 1 (STIM1), a transmembrane protein with growth suppressor activity, contains an extracellular SAM domain modified by N-linked glycosylation. *Biochim. Biophys. Acta* 1596:131.
53. Soboloff, J., M. A. Spassova, T. Hewavitharana, L. P. He, W. Xu, L. S. Johnstone, M. A. Dziadek, and D. L. Gill. 2006. STIM2 is an inhibitor of STIM1-mediated store-operated Ca²⁺ Entry. *Curr. Biol.* 16:1465.

54. Li, Z., J. Lu, P. Xu, X. Xie, L. Chen, and T. Xu. 2007. Mapping the interacting domains of STIM1 and Orai1 in Ca²⁺ release-activated Ca²⁺ channel activation. *J. Biol. Chem.* 282:29448.
55. Zhang, S. L., A. V. Yeromin, X. H. Zhang, Y. Yu, O. Safrina, A. Penna, J. Roos, K. A. Stauderman, and M. D. Cahalan. 2006. Genome-wide RNAi screen of Ca(2+) influx identifies genes that regulate Ca(2+) release-activated Ca(2+) channel activity. *Proc. Natl. Acad. Sci. U. S. A* 103:9357.
56. Grosse, J., A. Braun, D. Varga-Szabo, N. Beyersdorf, B. Schneider, L. Zeitlmann, P. Hanke, P. Schropp, S. Muhlstedt, C. Zorn, M. Huber, C. Schmittwolf, W. Jagla, P. Yu, T. Kerkau, H. Schulze, M. Nehls, and B. Nieswandt. 2007. An EF hand mutation in Stim1 causes premature platelet activation and bleeding in mice. *J. Clin. Invest* 117:3540.
57. Baba, Y., K. Hayashi, Y. Fujii, A. Mizushima, H. Watarai, M. Wakamori, T. Numaga, Y. Mori, M. Iino, M. Hikida, and T. Kurosaki. 2006. Coupling of STIM1 to store-operated Ca²⁺ entry through its constitutive and inducible movement in the endoplasmic reticulum. *Proc. Natl. Acad. Sci. U. S. A* 103:16704.
58. Stathopoulos, P. B., G. Y. Li, M. J. Plevin, J. B. Ames, and M. Ikura. 2006. Stored Ca²⁺ depletion-induced oligomerization of stromal interaction molecule 1 (STIM1) via the EF-SAM region: An initiation mechanism for capacitive Ca²⁺ entry. *J. Biol. Chem.* 281:35855.
59. Huang, G. N., W. Zeng, J. Y. Kim, J. P. Yuan, L. Han, S. Muallem, and P. F. Worley. 2006. STIM1 carboxyl-terminus activates native SOC, I(crac) and TRPC1 channels. *Nat. Cell Biol.* 8:1003.
60. Bauer, M. C., D. O'Connell, D. J. Cahill, and S. Linse. 2008. Calmodulin binding to the polybasic C-termini of STIM proteins involved in store-operated calcium entry. *Biochemistry* 47:6089.
61. Ong, H. L., K. T. Cheng, X. Liu, B. C. Bandyopadhyay, B. C. Paria, J. Soboloff, B. Pani, Y. Gwack, S. Srikanth, B. B. Singh, D. L. Gill, and I. S. Ambudkar. 2007. Dynamic assembly of TRPC1-STIM1-Orai1 ternary complex is involved in store-operated calcium influx. Evidence for similarities in store-operated and calcium release-activated calcium channel components. *J. Biol. Chem.* 282:9105.
62. Yuan, J. P., W. Zeng, G. N. Huang, P. F. Worley, and S. Muallem. 2007. STIM1 heteromultimerizes TRPC channels to determine their function as store-operated channels. *Nat. Cell Biol.* 9:636.
63. Parvez, S., A. Beck, C. Peinelt, J. Soboloff, A. Lis, M. Monteilh-Zoller, D. L. Gill, A. Fleig, and R. Penner. 2008. STIM2 protein mediates distinct store-dependent and store-independent modes of CRAC channel activation. *FASEB J.* 22:752.
64. Spassova, M. A., J. Soboloff, L. P. He, W. Xu, M. A. Dziadek, and D. L. Gill. 2006. STIM1 has a plasma membrane role in the activation of store-operated Ca(2+) channels. *Proc. Natl. Acad. Sci. U. S. A* 103:4040.
65. Soboloff, J., M. A. Spassova, X. D. Tang, T. Hewavitharana, W. Xu, and D. L. Gill. 2006. Orai1 and STIM reconstitute store-operated calcium channel function. *J. Biol. Chem.* 281:20661.

66. Zarbock, A., R. K. Polanowska-Grabowska, and K. Ley. 2007. Platelet-neutrophil-interactions: linking hemostasis and inflammation. *Blood Rev.* 21:99.
67. Deckmyn, H., K. Vanhoorelbeke, H. Ulrichts, A. Schoolmeester, S. Staelens, and S. De Meyer. 2003. Amplification loops and signal transduction pathways. eds. Leuven university Press, pp. 75.
68. Willoughby, S., A. Holmes, and J. Loscalzo. 2002. Platelets and cardiovascular disease. *Eur. J. Cardiovasc. Nurs.* 1:273.
69. Sachs, U. J., and B. Nieswandt. 2007. In vivo thrombus formation in murine models. *Circ. Res.* 100:979.
70. Schmitt, A., J. Guichard, J. M. Masse, N. Debili, and E. M. Cramer. 2001. Of mice and men: comparison of the ultrastructure of megakaryocytes and platelets. *Exp. Hematol.* 29:1295.
71. Jirouskova, M., A. S. Shet, and G. J. Johnson. 2007. A guide to murine platelet structure, function, assays, and genetic alterations. *J. Thromb. Haemost.* 5:661.
72. Savage, B., F. mus-Jacobs, and Z. M. Ruggeri. 1998. Specific synergy of multiple substrate-receptor interactions in platelet thrombus formation under flow. *Cell* 94:657.
73. Nieswandt, B., and S. P. Watson. 2003. Platelet-collagen interaction: is GPVI the central receptor? *Blood* 102:449.
74. Watson, S. P., J. M. Auger, O. J. McCarty, and A. C. Pearce. 2005. GPVI and integrin alphaIIb beta3 signaling in platelets. *J. Thromb. Haemost.* 3:1752.
75. Offermanns, S. 2006. Activation of platelet function through G protein-coupled receptors. *Circ. Res.* 99:1293.
76. Furie, B., and B. C. Furie. 2007. In vivo thrombus formation. *J. Thromb. Haemost.* 5 Suppl 1:12.
77. Bergmeier, W., C. L. Piffath, T. Goerge, S. M. Cifuni, Z. M. Ruggeri, J. Ware, and D. D. Wagner. 2006. The role of platelet adhesion receptor GPIIb/IIIa far exceeds that of its main ligand, von Willebrand factor, in arterial thrombosis. *Proc. Natl. Acad. Sci. U. S. A* 103:16900.
78. Ambudkar, I. S., B. C. Bandyopadhyay, X. Liu, T. P. Lockwich, B. Paria, and H. L. Ong. 2006. Functional organization of TRPC-Ca²⁺ channels and regulation of calcium microdomains. *Cell Calcium* 40:495.
79. Lian, L., Y. Wang, J. Draznin, D. Eslin, J. S. Bennett, M. Poncz, D. Wu, and C. S. Abrams. 2005. The relative role of PLCbeta and PI3Kgamma in platelet activation. *Blood* 106:110.
80. Suzuki-Inoue, K., O. Inoue, J. Frampton, and S. P. Watson. 2003. Murine GPVI stimulates weak integrin activation in PLCgamma2^{-/-} platelets: involvement of PLCgamma1 and PI3-kinase. *Blood* 102:1367.
81. Rameh, L. E., S. G. Rhee, K. Spokes, A. Kazlauskas, L. C. Cantley, and L. G. Cantley. 1998. Phosphoinositide 3-kinase regulates phospholipase Cgamma-mediated calcium signaling. *J. Biol. Chem.* 273:23750.

82. O'Callaghan, C. A. 2009. Thrombomodulation via CLEC-2 targeting. *Curr. Opin. Pharmacol.* 9:90.
83. Gibbins, J. M. 2004. Platelet adhesion signalling and the regulation of thrombus formation. *J. Cell Sci.* 117:3415.
84. Blake, R. A., J. Asselin, T. Walker, and S. P. Watson. 1994. Fc gamma receptor II stimulated formation of inositol phosphates in human platelets is blocked by tyrosine kinase inhibitors and associated with tyrosine phosphorylation of the receptor. *FEBS Lett.* 342:15.
85. Suzuki-Inoue, K., G. L. Fuller, A. Garcia, J. A. Eble, S. Pohlmann, O. Inoue, T. K. Gartner, S. C. Hughan, A. C. Pearce, G. D. Laing, R. D. Theakston, E. Schweighoffer, N. Zitzmann, T. Morita, V. L. Tybulewicz, Y. Ozaki, and S. P. Watson. 2006. A novel Syk-dependent mechanism of platelet activation by the C-type lectin receptor CLEC-2. *Blood* 107:542.
86. Levy-Toledano, S. 1999. Platelet signal transduction pathways: could we organize them into a 'hierarchy'? *Haemostasis* 29:4.
87. Brune, B., and V. Ullrich. 1991. Different calcium pools in human platelets and their role in thromboxane A₂ formation. *J. Biol. Chem.* 266:19232.
88. Cavallini, L., M. Coassin, and A. Alexandre. 1995. Two classes of agonist-sensitive Ca²⁺ stores in platelets, as identified by their differential sensitivity to 2,5-di-(tert-butyl)-1,4-benzohydroquinone and thapsigargin. *Biochem. J.* 310 (Pt 2):449.
89. Papp, B., A. Enyedi, T. Kovacs, B. Sarkadi, F. Wuytack, O. Thastrup, G. Gardos, R. Bredoux, S. Levy-Toledano, and J. Enouf. 1991. Demonstration of two forms of calcium pumps by thapsigargin inhibition and radioimmunoblotting in platelet membrane vesicles. *J. Biol. Chem.* 266:14593.
90. Gohla, A., S. Offermanns, T. M. Wilkie, and G. Schultz. 1999. Differential involvement of Galpha12 and Galpha13 in receptor-mediated stress fiber formation. *J. Biol. Chem.* 274:17901.
91. Klages, B., U. Brandt, M. I. Simon, G. Schultz, and S. Offermanns. 1999. Activation of G12/G13 results in shape change and Rho/Rho-kinase-mediated myosin light chain phosphorylation in mouse platelets. *J. Cell Biol.* 144:745.
92. Crittenden, J. R., W. Bergmeier, Y. Zhang, C. L. Piffath, Y. Liang, D. D. Wagner, D. E. Housman, and A. M. Graybiel. 2004. CalDAG-GEFI integrates signaling for platelet aggregation and thrombus formation. *Nat. Med.* 10:982.
93. Chrzanowska-Wodnicka, M., S. S. Smyth, S. M. Schoenwaelder, T. H. Fischer, and G. C. White. 2005. Rap1b is required for normal platelet function and hemostasis in mice. *J. Clin. Invest* 115:680.
94. Hogan, P. G., L. Chen, J. Nardone, and A. Rao. 2003. Transcriptional regulation by calcium, calcineurin, and NFAT. *Genes Dev.* 17:2205.
95. Feske, S., M. Prakriya, A. Rao, and R. S. Lewis. 2005. A severe defect in CRAC Ca²⁺ channel activation and altered K⁺ channel gating in T cells from immunodeficient patients. *J. Exp. Med.* 202:651.

96. Le, D. F., C. Hivroz, M. Partiseti, C. Thomas, H. A. Buc, M. Oleastro, B. Belohradsky, D. Choquet, and A. Fischer. 1995. A primary T-cell immunodeficiency associated with defective transmembrane calcium influx. *Blood* 85:1053.
97. Partiseti, M., D. F. Le, C. Hivroz, A. Fischer, H. Korn, and D. Choquet. 1994. The calcium current activated by T cell receptor and store depletion in human lymphocytes is absent in a primary immunodeficiency. *J. Biol. Chem.* 269:32327.
98. Scharenberg, A. M., L. A. Humphries, and D. J. Rawlings. 2007. Calcium signalling and cell-fate choice in B cells. *Nat. Rev. Immunol.* 7:778.
99. Vig, M., and J. P. Kinet. 2009. Calcium signaling in immune cells. *Nat. Immunol.* 10:21.
100. Turner, H., and J. P. Kinet. 1999. Signalling through the high-affinity IgE receptor Fc epsilonRI. *Nature* 402:B24-B30.
101. Huang, Y., and R. L. Wange. 2004. T cell receptor signaling: beyond complex complexes. *J. Biol. Chem.* 279:28827.
102. Gilfillan, A. M., and C. Tkaczyk. 2006. Integrated signalling pathways for mast-cell activation. *Nat. Rev. Immunol.* 6:218.
103. Galli, S. J., M. Tsai, and A. M. Piliponsky. 2008. The development of allergic inflammation. *Nature* 454:445.
104. Ravetch, J. V., and S. Bolland. 2001. IgG Fc receptors. *Annu. Rev. Immunol.* 19:275.
105. Schulze-Luehrmann, J., and S. Ghosh. 2006. Antigen-receptor signaling to nuclear factor kappa B. *Immunity.* 25:701.
106. Bivona, T. G., d. C. Perez, I, I. M. Ahearn, T. M. Grana, V. K. Chiu, P. J. Lockyer, P. J. Cullen, A. Pellicer, A. D. Cox, and M. R. Philips. 2003. Phospholipase Cgamma activates Ras on the Golgi apparatus by means of RasGRP1. *Nature* 424:694.
107. Priatel, J. J., S. J. Teh, N. A. Dower, J. C. Stone, and H. S. Teh. 2002. RasGRP1 transduces low-grade TCR signals which are critical for T cell development, homeostasis, and differentiation. *Immunity.* 17:617.
108. Gallo, E. M., M. M. Winslow, K. Cante-Barrett, A. N. Radermacher, L. Ho, L. McGinnis, B. Iritani, J. R. Neilson, and G. R. Crabtree. 2007. Calcineurin sets the bandwidth for discrimination of signals during thymocyte development. *Nature* 450:731.
109. Karin, M., and E. Gallagher. 2005. From JNK to pay dirt: jun kinases, their biochemistry, physiology and clinical importance. *IUBMB. Life* 57:283.
110. Macian, F. 2005. NFAT proteins: key regulators of T-cell development and function. *Nat. Rev. Immunol.* 5:472.

111. Lipton, P. 1999. Ischemic cell death in brain neurons. *Physiol Rev.* 79:1431.
112. Wojda, U., E. Salinska, and J. Kuznicki. 2008. Calcium ions in neuronal degeneration. *IUBMB. Life* 60:575.
113. Mattson, M. P. 2007. Calcium and neurodegeneration. *Aging Cell* 6:337.
114. Arundine, M., and M. Tymianski. 2004. Molecular mechanisms of glutamate-dependent neurodegeneration in ischemia and traumatic brain injury. *Cell Mol. Life Sci.* 61:657.
115. Rao, V. R., and S. Finkbeiner. 2007. NMDA and AMPA receptors: old channels, new tricks. *Trends Neurosci.* 30:284.
116. Burnashev, N., and A. Rozov. 2005. Presynaptic Ca²⁺ dynamics, Ca²⁺ buffers and synaptic efficacy. *Cell Calcium* 37:489.
117. Burgoyne, R. D. 2007. Neuronal calcium sensor proteins: generating diversity in neuronal Ca²⁺ signalling. *Nat. Rev. Neurosci.* 8:182.
118. Haeseleer, F., Y. Imanishi, I. Sokal, S. Filipek, and K. Palczewski. 2002. Calcium-binding proteins: intracellular sensors from the calmodulin superfamily. *Biochem. Biophys. Res. Commun.* 290:615.
119. Hidalgo, C. 2005. Cross talk between Ca²⁺ and redox signalling cascades in muscle and neurons through the combined activation of ryanodine receptors/Ca²⁺ release channels. *Philos. Trans. R. Soc. Lond B Biol. Sci.* 360:2237.
120. Zalk, R., S. E. Lehnart, and A. R. Marks. 2007. Modulation of the ryanodine receptor and intracellular calcium. *Annu. Rev. Biochem.* 76:367.
121. Danoff, S. K., and C. A. Ross. 1994. The inositol trisphosphate receptor gene family: implications for normal and abnormal brain function. *Prog. Neuropsychopharmacol. Biol. Psychiatry* 18:1.
122. Putney, J. W., Jr. 2003. Capacitative calcium entry in the nervous system. *Cell Calcium* 34:339.
123. Kim, D., K. S. Jun, S. B. Lee, N. G. Kang, D. S. Min, Y. H. Kim, S. H. Ryu, P. G. Suh, and H. S. Shin. 1997. Phospholipase C isozymes selectively couple to specific neurotransmitter receptors. *Nature* 389:290.
124. Matsumoto, M., and E. Nagata. 1999. Type 1 inositol 1,4,5-trisphosphate receptor knock-out mice: their phenotypes and their meaning in neuroscience and clinical practice. *J. Mol. Med.* 77:406.
125. Knight, C. G., L. F. Morton, D. J. Onley, A. R. Peachey, T. Ichinohe, M. Okuma, R. W. Farndale, and M. J. Barnes. 1999. Collagen-platelet interaction: Gly-Pro-Hyp is uniquely specific for platelet Gp VI and mediates platelet activation by collagen. *Cardiovasc. Res.* 41:450.

126. Bergmeier, W., D. Bouvard, J. A. Eble, R. Mokhtari-Nejad, V. Schulte, H. Zirngibl, C. Brakebusch, R. Fassler, and B. Nieswandt. 2001. Rhodocytin (aggrexin) activates platelets lacking alpha(2)beta(1) integrin, glycoprotein VI, and the ligand-binding domain of glycoprotein Ibalpha. *J. Biol. Chem.* 276:25121.
127. Nimmerjahn, F., P. Bruhns, K. Horiuchi, and J. V. Ravetch. 2005. FcγRIV: a novel FcR with distinct IgG subclass specificity. *Immunity.* 23:41.
128. Fassler, R., K. Martin, E. Forsberg, T. Litzemberger, and A. Iglesias. 1995. Knockout mice: how to make them and why. The immunological approach. *Int. Arch. Allergy Immunol.* 106:323.
129. Fassler, R., P. N. Schnegelsberg, J. Dausman, T. Shinya, Y. Muragaki, M. T. McCarthy, B. R. Olsen, and R. Jaenisch. 1994. Mice lacking alpha 1 (IX) collagen develop noninflammatory degenerative joint disease. *Proc. Natl. Acad. Sci. U. S. A* 91:5070.
130. Nieswandt, B., C. Brakebusch, W. Bergmeier, V. Schulte, D. Bouvard, R. Mokhtari-Nejad, T. Lindhout, J. W. Heemskerk, H. Zirngibl, and R. Fassler. 2001. Glycoprotein VI but not alpha2beta1 integrin is essential for platelet interaction with collagen. *EMBO J.* 20:2120.
131. Lessmann, E., G. Grochow, L. Weingarten, T. Giesemann, K. Aktories, M. Leitges, G. Krystal, and M. Huber. 2006. Insulin and insulin-like growth factor-1 promote mast cell survival via activation of the phosphatidylinositol-3-kinase pathway. *Exp. Hematol.* 34:1532.
132. Nieswandt, B., W. Bergmeier, K. Rackebrandt, J. E. Gessner, and H. Zirngibl. 2000. Identification of critical antigen-specific mechanisms in the development of immune thrombocytopenic purpura in mice. *Blood* 96:2520.
133. Meuth, S. G., O. J. Simon, A. Grimm, N. Melzer, A. M. Herrmann, P. Spitzer, P. Landgraf, and H. Wiendl. 2008. CNS inflammation and neuronal degeneration is aggravated by impaired CD200-CD200R-mediated macrophage silencing. *J. Neuroimmunol.* 194:62.
134. Meuth, S. G., T. Budde, T. Kanyshkova, T. Broicher, T. Munsch, and H. C. Pape. 2003. Contribution of TWIK-related acid-sensitive K⁺ channel 1 (TASK1) and TASK3 channels to the control of activity modes in thalamocortical neurons. *J. Neurosci.* 23:6460.
135. Plant, L. D., P. J. Kemp, C. Peers, Z. Henderson, and H. A. Pearson. 2002. Hypoxic depolarization of cerebellar granule neurons by specific inhibition of TASK-1. *Stroke* 33:2324.
136. Grynkiewicz, G., M. Poenie, and R. Y. Tsien. 1985. A new generation of Ca²⁺ indicators with greatly improved fluorescence properties. *J. Biol. Chem.* 260:3440.
137. Dirnagl, U. 2006. Bench to bedside: the quest for quality in experimental stroke research. *J. Cereb. Blood Flow Metab* 26:1465.

138. Kleinschnitz, C., M. Pozgajova, M. Pham, M. Bendszus, B. Nieswandt, and G. Stoll. 2007. Targeting platelets in acute experimental stroke: impact of glycoprotein Ib, VI, and IIb/IIIa blockade on infarct size, functional outcome, and intracranial bleeding. *Circulation* 115:2323.
139. Sen-Chowdhry, S., and W. J. McKenna. 2006. Sudden cardiac death in the young: a strategy for prevention by targeted evaluation. *Cardiology* 105:196.
140. Hyun, C., and L. J. Filippich. 2006. Molecular genetics of sudden cardiac death in small animals - a review. *Vet. J.* 171:39.
141. Reginato, M. J., and S. K. Muthuswamy. 2006. Illuminating the center: mechanisms regulating lumen formation and maintenance in mammary morphogenesis. *J. Mammary. Gland. Biol. Neoplasia.* 11:205.
142. Hennighausen, L., and G. W. Robinson. 1998. Think globally, act locally: the making of a mouse mammary gland. *Genes Dev.* 12:449.
143. Bergmeier, W., V. Schulte, G. Brockhoff, U. Bier, H. Zirngibl, and B. Nieswandt. 2002. Flow cytometric detection of activated mouse integrin alphaIIb beta3 with a novel monoclonal antibody. *Cytometry* 48:80.
144. McCloskey, M. A. 1999. New perspectives on Ca²⁺ influx in mast cells. In *Signal Transduction in Mast Cells and Basophils*. R. J. e. In Razin E., ed. Springer-Verlag, New York, pp. 227.
145. Takai, T. 2002. Roles of Fc receptors in autoimmunity. *Nat. Rev. Immunol.* 2:580.
146. Baba, Y., K. Nishida, Y. Fujii, T. Hirano, M. Hikida, and T. Kurosaki. 2008. Essential function for the calcium sensor STIM1 in mast cell activation and anaphylactic responses. *Nat. Immunol.* 9:81.
147. Hirano, M., R. S. Davis, W. D. Fine, S. Nakamura, K. Shimizu, H. Yagi, K. Kato, R. P. Stephan, and M. D. Cooper. 2007. IgE_b immune complexes activate macrophages through Fc gamma RIV binding. *Nat. Immunol.* 8:762.
148. Woods, V. L., Jr., and R. McMillan. 1984. Platelet autoantigens in chronic ITP. *Br. J. Haematol.* 57:1.
149. Kuwana, M., Y. Okazaki, and Y. Ikeda. 2009. Splenic macrophages maintain the anti-platelet autoimmune response via uptake of opsonized platelets in patients with immune thrombocytopenic purpura. *J. Thromb. Haemost.* 7:322.
150. Sallusto, F., J. Geginat, and A. Lanzavecchia. 2004. Central memory and effector memory T cell subsets: function, generation, and maintenance. *Annu. Rev. Immunol.* 22:745.
151. Sospedra, M., and R. Martin. 2005. Immunology of multiple sclerosis. *Annu. Rev. Immunol.* 23:683.
152. Frohman, E. M., M. K. Racke, and C. S. Raine. 2006. Multiple sclerosis--the plaque and its pathogenesis. *N. Engl. J. Med.* 354:942.

153. Gold, R., C. Linington, and H. Lassmann. 2006. Understanding pathogenesis and therapy of multiple sclerosis via animal models: 70 years of merits and culprits in experimental autoimmune encephalomyelitis research. *Brain* 129:1953.
154. Goldberg, M. P., and D. W. Choi. 1993. Combined oxygen and glucose deprivation in cortical cell culture: calcium-dependent and calcium-independent mechanisms of neuronal injury. *J. Neurosci.* 13:3510.
155. Aarts, M., K. Iihara, W. L. Wei, Z. G. Xiong, M. Arundine, W. Cerwinski, J. F. MacDonald, and M. Tymianski. 2003. A key role for TRPM7 channels in anoxic neuronal death. *Cell* 115:863.
156. Kim, H. J., K. A. Martemyanov, and S. A. Thayer. 2008. Human immunodeficiency virus protein Tat induces synapse loss via a reversible process that is distinct from cell death. *J. Neurosci.* 28:12604.
157. Jantas, D., M. Szymanska, B. Budziszewska, and W. Lason. 2009. An involvement of BDNF and PI3-K/Akt in the anti-apoptotic effect of memantine on staurosporine-evoked cell death in primary cortical neurons. *Apoptosis.* 14:900.
158. Lee, J. M., Y. J. Kim, H. Ra, S. J. Kang, S. Han, J. Y. Koh, and Y. H. Kim. 2008. The involvement of caspase-11 in TPEN-induced apoptosis. *FEBS Lett.* 582:1871.
159. Murray, C. J., and A. D. Lopez. 1997. Mortality by cause for eight regions of the world: Global Burden of Disease Study. *Lancet* 349:1269.
160. Zhang, Z. G., L. Zhang, W. Tsang, A. Goussev, C. Powers, K. L. Ho, D. Morris, S. S. Smyth, B. S. Coller, and M. Chopp. 2001. Dynamic platelet accumulation at the site of the occluded middle cerebral artery and in downstream microvessels is associated with loss of microvascular integrity after embolic middle cerebral artery occlusion. *Brain Res.* 912:181.
161. Choudhri, T. F., B. L. Hoh, H. G. Zerwes, C. J. Prestigiacomo, S. C. Kim, E. S. Connolly, Jr., G. Kottirsch, and D. J. Pinsky. 1998. Reduced microvascular thrombosis and improved outcome in acute murine stroke by inhibiting GP IIb/IIIa receptor-mediated platelet aggregation. *J. Clin. Invest* 102:1301.
162. Detwiler, T. C., I. F. Charo, and R. D. Feinman. 1978. Evidence that calcium regulates platelet function. *Thromb. Haemost.* 40:207.
163. Tomson, T., L. Nashef, and P. Ryvlin. 2008. Sudden unexpected death in epilepsy: current knowledge and future directions. *Lancet Neurol.* 7:1021.
164. Lehnart, S. E., M. Mongillo, A. Bellinger, N. Lindegger, B. X. Chen, W. Hsueh, S. Reiken, A. Wronska, L. J. Drew, C. W. Ward, W. J. Lederer, R. S. Kass, G. Morley, and A. R. Marks. 2008. Leaky Ca²⁺ release channel/ryanodine receptor 2 causes seizures and sudden cardiac death in mice. *J. Clin. Invest* 118:2230.
165. Ai, X., J. W. Curran, T. R. Shannon, D. M. Bers, and S. M. Pogwizd. 2005. Ca²⁺/calmodulin-dependent protein kinase modulates cardiac ryanodine receptor phosphorylation and sarcoplasmic reticulum Ca²⁺ leak in heart failure. *Circ. Res.* 97:1314.

166. Mohler, P. J., J. J. Schott, A. O. Gramolini, K. W. Dilly, S. Guatimosim, W. H. duBell, L. S. Song, K. Haurogne, F. Kyndt, M. E. Ali, T. B. Rogers, W. J. Lederer, D. Escande, M. H. Le, and V. Bennett. 2003. Ankyrin-B mutation causes type 4 long-QT cardiac arrhythmia and sudden cardiac death. *Nature* 421:634.
167. Kinney, H. C. 2009. Brainstem mechanisms underlying the sudden infant death syndrome: evidence from human pathologic studies. *Dev. Psychobiol.* 51:223.
168. Manhes, C., C. Kayser, P. Bertheau, B. Kelder, J. J. Kopchick, P. A. Kelly, P. Touraine, and V. Goffin. 2006. Local over-expression of prolactin in differentiating mouse mammary gland induces functional defects and benign lesions, but no carcinoma. *J. Endocrinol.* 190:271.
169. Iavnilovitch, E., B. Groner, and I. Barash. 2002. Overexpression and forced activation of stat5 in mammary gland of transgenic mice promotes cellular proliferation, enhances differentiation, and delays postlactational apoptosis. *Mol. Cancer Res.* 1:32.
170. Khaled, W. T., E. K. Read, S. E. Nicholson, F. O. Baxter, A. J. Brennan, P. J. Came, N. Sprigg, A. N. McKenzie, and C. J. Watson. 2007. The IL-4/IL-13/Stat6 signalling pathway promotes luminal mammary epithelial cell development. *Development* 134:2739.
171. Finkelman, F. D. 2007. Anaphylaxis: lessons from mouse models. *J. Allergy Clin. Immunol.* 120:506.
172. Sakata, T., H. Yoshimatsu, and M. Kurokawa. 1997. Thermoregulation modulated by hypothalamic histamine in rats. *Inflamm. Res.* 46 Suppl 1:S35-S36.
173. Braun, A., J. E. Gessner, D. Varga-Szabo, S. N. Syed, S. Konrad, D. Stegner, T. Vogtle, R. E. Schmidt, and B. Nieswandt. 2009. STIM1 is essential for Fcγ receptor activation and autoimmune inflammation. *Blood* 113:1097.
174. Cante-Barrett, K., E. M. Gallo, M. M. Winslow, and G. R. Crabtree. 2006. Thymocyte negative selection is mediated by protein kinase C- and Ca²⁺-dependent transcriptional induction of bim [corrected]. *J. Immunol.* 176:2299.
175. Smith, A., U. Vollmer-Conna, B. Bennett, D. Wakefield, I. Hickie, and A. Lloyd. 2004. The relationship between distress and the development of a primary immune response to a novel antigen. *Brain Behav. Immun.* 18:65.
176. Smith, T. P., S. L. Kennedy, and M. Fleshner. 2004. Influence of age and physical activity on the primary in vivo antibody and T cell-mediated responses in men. *J. Appl. Physiol* 97:491.
177. Bourquin, C., A. Schubart, S. Tobollik, I. Mather, S. Ogg, R. Liblau, and C. Lington. 2003. Selective unresponsiveness to conformational B cell epitopes of the myelin oligodendrocyte glycoprotein in H-2b mice. *J. Immunol.* 171:455.
178. Oliver, A. R., G. M. Lyon, and N. H. Ruddle. 2003. Rat and human myelin oligodendrocyte glycoproteins induce experimental autoimmune encephalomyelitis by different mechanisms in C57BL/6 mice. *J. Immunol.* 171:462.

179. Varnai, P., L. Hunyady, and T. Balla. 2009. STIM and Orai: the long-awaited constituents of store-operated calcium entry. *Trends Pharmacol. Sci.* 30:118.
180. Larsen, G. A., H. K. Skjellegrind, M. C. Moe, M. L. Vinje, and J. Berg-Johnsen. 2005. Endoplasmic reticulum dysfunction and Ca²⁺ deregulation in isolated CA1 neurons during oxygen and glucose deprivation. *Neurochem. Res.* 30:651.
181. Henrich, M., and K. J. Buckler. 2008. Effects of anoxia and aglycemia on cytosolic calcium regulation in rat sensory neurons. *J. Neurophysiol.* 100:456.
182. Frandsen, A., and A. Schousboe. 1991. Dantrolene prevents glutamate cytotoxicity and Ca²⁺ release from intracellular stores in cultured cerebral cortical neurons. *J. Neurochem.* 56:1075.
183. Mattson, M. P., H. Zhu, J. Yu, and M. S. Kindy. 2000. Presenilin-1 mutation increases neuronal vulnerability to focal ischemia in vivo and to hypoxia and glucose deprivation in cell culture: involvement of perturbed calcium homeostasis. *J. Neurosci.* 20:1358.

8. ACKNOWLEDGEMENTS

During my PhD work many people helped and supported me. Now is time to thank them:

My supervisor, Prof. Dr. Bernhard Nieswandt, at the Rudolf Virchow Center for Experimental Medicine of the University of Würzburg, where I have performed most of the experiments discussed in this work. He allowed me to work in his lab, financed my project and helped me with his great ideas. I would like to thank him as well for his patient with me and for allow me to develop risky ideas.

I also would like to thank the formal members of the supervisory comity Prof. Dr. Thomas Dandekar and Prof. Dr. Med. Ulrich Walter for their various suggestions during the annual meetings of the Graduate School for Life Sciences (GSLs) program.

My friend and colleague, Dr. Attila Braun, for his support throughout my work and for carefully reading my thesis.

I thank a lot David Stegner, Timo Voegtle and David Varga-Szabó for the help and the close work together in the lab.

Sylvia Hengst for her great help when I was desperately busy.

People from my lab, with an especial mention to Frauke May, for help me with the corrections and editing of my “spanglish” in this manuscript.

Especially my friend and colleague Irina Pleines for her charming personality and her support, as well as all the members of the lab for the good atmosphere and the useful discussions during my stay. I would like to thank them as well for teaching me and introduce me to the different methodology available in our lab.

All external collaboration partners for teach me and help me with the experimental methodology that was not available in our lab.

Last but not less important, to my friends Dr. Ingrid Teßmer and Dr. Daniel Bouvard for their suggestions and constructive critics to my thesis manuscript.

9. CURRICULUM VITAE

Name Alejandro Berna-Erro
Nationality Spanish
Date/Place of birth 24-07-1975, Paris, France
Status Single

Education

1993 Bachelor degree, San Vicente del Raspeig High school, Alicante (Spain).
1997 Master degree in Biology, grade in Biotechnology, University of Alicante, Alicante (Spain).

Research Experience

Sept. 1997 / Jul. 2002 “*Generation and analysis of profilin1 null and conditional Knockout mice*”. Doctoral thesis (started but not achieved). Thesis Supervisors: Dr. Mercedes Costell i Rossellò, Prof. Dr. Reinhard Fässler. Institution: Universidad de Valencia, Valencia (Spain). Lunds Universitet, Lund (Sweden), Dpt. of Molecular Medicine. Max-Planck-Institut für Biochemie, München, (Germany).

Oct. 2004 / Mar. 2006 “Derivation, characterization and *in vitro* expansion of human embryonic stem (hES) cell lines, clinical grade”. Project, Technical Assistant Team Leader. Director: Carlos Simón. Institution: Centro de Investigación Principe Felipe (CIPF), Valencia (Spain).

Since Jun. 2006

“Generation and Characterization of Stromal Interaction Molecule 2 (STIM2)-deficient Mice”. Doctoral thesis.

Thesis Supervisor: Prof. Dr. Bernhard Nieswandt.

Institution: Rudolf-Virchow-Zentrum, Julius-Maximilians-Universität, Würzburg (Germany).

10. LIST OF PUBLICATIONS

Schuhmann MK, Stegner D, **Berna-Erro A**, Bittner S, Braun A, Kleinschnitz Ch, Stoll G, Wiendl H, Meuth SG and Nieswandt B. Modulation of store operated calcium entry (SOCE) in T lymphocytes ameliorates autoimmune inflammation in an animal model of multiple sclerosis. *J Immunol*. 2009 (accepted manuscript, in press).

Berna-Erro A, Braun A, Kraft R, Kleinschnitz Ch, Schuhmann MK, Stegner D, Wultsch T, Eilers J, Meuth SG, Stoll G and Nieswandt B. STIM2 regulates capacitive Ca²⁺ entry in neurons and plays a key role in hypoxic neuronal cell death. *Sci Signal*. 2009 Oct 20;2(93):ra67.

Böttcher RT, Wiesner S, Braun A, Wimmer R, **Berna A**, Elad N, Medalia O, Pfeifer A, Aszódi A, Costell M, Fässler R. Profilin1 is required for abscission during late cytokinesis of chondrocytes. *EMBO J*. 2009 Apr 22;28 (8):1157-69.

Braun A, Aszodi A, Hellebrand H, **Berna A**, Fassler R, Brandau O. Genomic organization of profilin-III and evidence for a transcript expressed exclusively in testis. *Gene*. 2002 Jan 23;283(1-2):219-25.

Bouvard D, Brakebusch C, Gustafsson E, Aszódi A, Bengtsson T, **Berna A**, Fässler R. Functional Consequences of Integrin Gene Mutations in Mice. Review. *Circ Res*. 2001;89:211-223.

AFFIDAVIT (Eidesstattliche Erklärung)

I hereby declare that my thesis entitled: **“Generation and Characterization of Stromal Interaction Molecule 2 (STIM2)-deficient Mice”**

is the result of my own work. I did not receive any help or support from commercial consultants. All sources and / or materials applied are listed and specified in the thesis.

Furthermore, I verify that this thesis has not yet been submitted as part of another examination process neither in identical nor in similar form.

Würzburg.....

Date

Signature

Alejandro Berna-Erro

